

AN EXPERIMENTAL AND THEORETICAL STUDY OF OLIGO- AND
POLYELECTROLYTE ADSORPTION

BIBLIOTHEEK
LANDBOUWUNIVERSITEIT
WAGENINGEN

Promotor: Dr. J. Lyklema,
hoogleraar in de fysische en kolloïdchemie

H.A. van der Schee

AN EXPERIMENTAL AND THEORETICAL STUDY OF
OLIGO- AND POLYELECTROLYTE ADSORPTION

Proefschrift

ter verkrijging van de graad van
doctor in de landbouwwetenschappen,
op gezag van de rector magnificus,
dr. C.C. Oosterlee,
hoogleraar in de veeteeltwetenschap,
in het openbaar te verdedigen
op vrijdag 23 maart 1984
des namiddags te vier uur in de aula
van de Landbouwhogeschool te Wageningen

Voor mijn ouders

Voor Margo

STELLINGEN

I

In tegenstelling tot wat zij beweren, nemen de Feijter en Benjamins een voor elk geadsorbeerd molecuul gelijk oppervlak aan in plaats van een oppervlak evenredig met het molecuulgewicht.

J.A. de Feijter en J. Benjamins, J. Colloid Interface Sci. 81, 91 (1981).

II

Hesselink brengt in zijn polyelektrolietadsorptietheorie het effect van beeldladingen wel in rekening, al zegt hij van niet.

F.Th. Hesselink, J. Colloid Interface Sci. 60, 448 (1977).

III

Yaron et al. schrijven de toename van de optische draaiing van geladen oligo-L-lysine ten onrechte toe aan eindeffecten.

A. Yaron, E. Katchalski, A. Berger, G.D. Fasman en H.A. Sober, Biopolymers 10, 1107 (1971).

IV

Polymeeradsorptiegegevens tonen aan dat het met behulp van de dubbellaagcapaciteit bepaalde specifiek oppervlak van zilverjodide niet juist kan zijn.

Dit proefschrift, hoofdstuk 5.

V

Het is efficiënter de "efficiënte" vierstaps synthese van mono-geacyleerde diaminen volgens Kunesch te vervangen door de acylering van een enkelvoudig beschermd diamine en aansluitende verwijdering van de beschermgroep.

G. Kunesch, Tetrahydron Letters 24, 5211 (1983).

VI

De gaschromatografische bepalingsmethode van thiamine (vitamine B₁) volgens Echols et al. bepaalt ook ontleed thiamine mee.

R.E. Echols, R.H. Miller, W. Winzer, D.J. Carmen,
en Y.R. Ireland, J. Chromatography, 262,
257 (1983).

VII

Mosterd bevat van nature een hoger erucazuurgehalte dan is toegestaan op grond van artikel 3bis van het Algemeen Besluit (Warenwet).

VIII

Het wettelijk voorschrijven van analysemethoden aan de Keuringsdiensten van Waren belemmert deze bij het inspelen op de nieuwste ontwikkelingen in de analytische chemie.

IX

Het is in het belang van een efficiënte controle wanneer de Warenwet, de Landbouwkwaliteitswet en de Vleeskeuringswet tot één consumentenbeschermingswet worden samengevoegd.

X

Als bij veroordelingen op grond van overtredingen van de Warenwet de rechter als straf publikatie van het vonnis op zou leggen, zou de preventieve werking van de controle door de Keuringsdiensten van Waren worden versterkt.

XI

Het spreekwoord "hoe meer zielen, hoe meer vreugd" is niet van toepassing binnen het klaslokaal.

XII

Het is opmerkelijk dat juist tijdens het bewind van minister Deetman een nieuw museum voor onderwijs wordt gebouwd.

XIII

Het niet dragen van een rokkostuum bij de promotieplechtigheid doet afbreuk aan het toneelkarakter van de voorstelling.

XIV

Degenen die op het standpunt "liever dood dan rood" staan, kunnen hieraan geen argument voor de kernbewapening ontlenen. Zonodig kan hun op individuele oplossingen worden gewezen.

Proefschrift H.A. van der Schee

An Experimental and Theoretical Study of Oligo- and Polyelectrolyte Adsorption

Wageningen, 23 maart 1984.

VOORWOORD

Dit proefschrift staat niet op zichzelf maar is ontstaan in samenwerking en samenspraak met de mensen van de vakgroep Fysische en Kolloïdchemie Wageningen en ook van daarbuiten. De goede sfeer en de vele stimulerende discussies hebben veel tot het hier beschreven werk bijgedragen.

Enkele mensen wil ik graag persoonlijk noemen. Hans Lyklema, ik dank je voor de vrijheid waarmee ik dit onderzoek mocht doen, maar waarbij je de grote lijnen goed in het oog hield. De snelheid, nauwgezetheid en kritiek, waarmee je mij bij het schrijven bijstond, waren een grote steun.

De gastvrijheid van Frits Tesser aan de Katholieke Universiteit Nijmegen en zijn raad en daad, maakten de periode van de organische synthese tot een genoegen.

De inbreng van Jan Scheutjens is velerlei. Niet alleen vormden zijn computerprogramma's en wiskundige kennis een basis voor het theoretische werk, ook zijn scherp fysisch inzicht was een belangrijke steun.

Het vermogen van Dirk Stigter om moeilijke dingen gemakkelijk voor te stellen, hielp mij over de drempel om aan het theoretische werk te beginnen heen.

Arie de Keizer heeft mij de bijzonderheden van het zilveriodide en de titratie-opstelling bijgebracht.

Anton Korteweg wil ik graag bedanken voor de nauwkeurigheid, waarmee hij de adsorptiemetingen verricht heeft en Axel Themmen voor de electroforesemetingen. Ik dank Gert Buurman voor het tekenen van de figuren, Dory Neijenhuis van de afdeling Tekstverwerking voor het typen van het manuscript en Hennie van Beek, Ronald Wegh, Willem van Maanen en Ben Spee voor de technische assistentie.

Het onderzoek was mogelijk dankzij financiële steun van de Nederlandse organisatie voor Zuiver Wetenschappelijk Onderzoek (Z.W.O.) onder auspiciën van de stichting voor Scheikundig Onderzoek in Nederland (S.O.N.).

Margo, je hebt niet alleen veel geduld gehad, maar ook belangrijk bijgedragen door het corrigeren van het Engels en het voor de afdeling Tekstverwerking leesbaar maken van het manuscript.

Ik dank mijn ouders, die mij al vroeg een open oog leerden hebben voor verschijnselen in de natuur, en mij stimuleerden dit verder te ontwikkelen.

CONTENTS	page
1 INTRODUCTION	1
1.1 General Background	1
1.2 Purpose of this study	4
1.3 Outline of the investigations	4
1.4 References	5
2 THE APPLICABILITY OF EQUILIBRIUM THERMODYNAMICS TO POLYMER ADSORPTION	7
2.1 Introduction	7
2.2 The consistency of polymer adsorption theories with Gibbs' law for homodisperse polymers	10
2.3 The influence of heterodispersity on the formulation of Gibbs' law	15
2.3.1 Two-component systems	16
2.3.1.1. The adsorption isotherm of a two-component polymer mixture	17
2.3.1.2 The surface pressure curve of a two-component polymer mixture	20
2.3.2 Systems with a Flory-type chain length distribution	23
2.3.2.1 The preferential adsorption of long over short molecules	25
2.3.2.2 The adsorption isotherm of a Flory-type polymer	31
2.3.2.3 The surface pressure curve of a Flory-type polymer	32
2.3.2.4 Comparison between our theory and that of de Feijter and Benjamins	39
2.4 Concluding remarks	45
2.5 References	46
3 THE THEORY OF THE ADSORPTION OF FLEXIBLE POLYELECTROLYTES	47
3.1 Introduction	47
3.2 Description of the model	49
3.3 The potential distribution	51

	<u>page</u>
3.3.1 The potential distribution in the bulk of the solution	51
3.3.2 The potential distribution in the adsorbed layer	55
3.4 The electrical free energy	60
3.4.1 The electrical free energy of a flat double layer	60
3.4.1.1 Charging the surface in the absence of poly-electrolyte	61
3.4.1.1.1 Charging a surface in the presence of charged indifferent electrolyte	61
3.4.1.1.2 Simultaneous charging of a surface and indifferent electrolyte	62
3.4.1.2 Charging a surface in the presence of poly-electrolyte	64
3.4.1.2.1 Charging a surface in the presence of charged polyelectrolyte	65
3.4.1.2.2 Charging a surface with concomitant charging of the polyelectrolyte	65
3.4.2 The electrical free energy of a charged poly-electrolyte concentration profile	68
3.5 The electrical free energy of the bulk solution and consequences to phase separation	70
3.5.1 Phase separation with uncharged polymers	71
3.5.2 Phase separation with polyelectrolytes	74
3.5.2.1 The potential difference between the two phases	75
3.5.2.1.1 The Debye-Hückel approach	75
3.5.2.1.2 The Gouy-Chapman approach	76
3.5.2.2 The electrical free energy of mixing	77
3.5.2.2.1 The Debye-Hückel approach	78
3.5.2.2.2 The Gouy-Chapman approach	79
3.5.2.3 The electrical part of the chemical potential	79
3.5.2.3.1 The Debye-Hückel approach	79
3.5.2.3.2 The Gouy-Chapman approach	80
3.5.2.4 Phase equilibria	80
3.5.2.4.1 The Debye-Hückel approach	80
3.5.2.4.2 The Gouy-Chapman approach	82

	<u>page</u>
3.5.3 Results and discussion	84
3.5.3.1 The behaviour of polymer adsorption near the phase separation domain	84
3.5.3.2 Phase separation of polyelectrolytes	86
3.5.3.2.1 The spinodial	87
3.5.3.2.2 The binodial	91
3.6 Extension of polymer adsorption theories with electrostatic interactions	96
3.6.1 The Roe theory	96
3.6.2 The Scheutjens-Fleer theory	96
3.6.3 Results and discussion	97
3.6.3.1 Comparison with nonionic polymers	97
3.6.3.2 Influence of the Debye-Hückel linearization	105
3.6.3.3 Comparison with Hesselink's theory	106
3.6.4 Concluding remarks	108
3.7 References	109
Appendix 3A The potential distribution originating from space charges	111
 4 SYNTHETICALLY DEFINED OLIGOMERS OF L-LYSINE AS MODEL COMPOUNDS FOR ADSORPTION STUDIES	 117
4.1 Introduction	117
4.2 Experimental	118
4.3 Results and discussion	123
4.4 References	126
 5 ADSORPTION OF OLIGO- AND POLYPEPTIDES ON SILVER IODIDE, THEIR EFFECTS ON DOUBLE LAYER AND COLLOID STABILITY	 127
5.1 Introduction	127
5.2 Experimental	129
5.2.1 Materials	129
5.2.1.1 Silver iodide	129
5.2.1.2 Adsorbates	132
5.2.1.2.1 Synthesis of poly-DL-proline	132
5.2.2 Methods	133
5.2.2.1 Silver iodide charge-potential curves	133

	<u>page</u>
5.2.2.2 Electrophoretic mobilities	133
5.2.2.3 Critical coagulation concentrations	134
5.2.2.4 Adsorption measurements	134
5.3 Results and discussion	137
5.3.1 Poly-L-lysine	137
5.3.2 Poly-L-proline, poly-DL-proline and pyrrolidone derivatives	143
5.3.3 Poly-L-lysine and poly-DL-lysine	152
5.3.4 Oligo-L-lysine and poly-L-lysine	154
5.3.4.1 Influence of the electrolyte concentration	156
5.3.4.2 Influence of the surface charge	157
5.4 Concluding remarks	160
5.5 References	160
 6 COMPARISON BETWEEN EXPERIMENTAL WORK AND THEORETICAL RESULTS	 163
6.1 Comparison with literature data	163
6.2 Choice of the parameters	164
6.2.1 Coordination number of the lattice	164
6.2.2 The area of a lattice site a_0 and the distance between the lattice layers r_0	164
6.2.3 The degree of dissociation	165
6.2.4 The Flory-Huggings solvent quality parameter	165
6.2.5 The non-electrical free energy of adsorption parameter χ_s	167
6.3 Results and discussion	168
6.3.1 Adsorption isotherms	168
6.3.2 Dependence on electrolyte concentration	169
6.3.3 Influence of the surface charge	170
6.4 Concluding remarks and suggestions for further investigations	174
6.5 References	176
 LIST OF SYMBOLS	 179
SUMMARY	183
SAMENVATTING	185
CURRICULUM VITAE	189

1 INTRODUCTION

1.1 GENERAL BACKGROUND

This study deals with an important aspect of polymer adsorption.

Polymers usually consist of long chains of either identical or different entities, called the segments.

From aqueous solutions polymers adsorb on a variety of surfaces. This adsorption is usually of the high affinity type. The accumulation of the binding energy of many segments accounts for this high affinity, even if the affinity per segment is small. The segments of the adsorbed molecules need not all be attached to the surface. Part of them can reside in loops and tails protruding in the solution. Series of segments in contact with the surface are called trains. Trains, loops and tails together form the adsorbed layer. Such an adsorbed layer strongly influences the interfacial properties¹.

If two surfaces are covered with thick layers of polymer, they cannot approach each other closely. This enables the preparation of stable dispersions of solids in fluids or of emulsions. Such dispersions need a stabilizing mechanism, because the surface excess free energy tends to lower the surface area. Lumping of solids and aggregation of fluid drops lowers the surface area. In the case of fluid interfaces the surface free energy may be identified with the interfacial tension.

Stabilization against aggregation can be achieved by electrostatically charging the particles or droplets or by adsorption of enough polymer to obtain thick sheaths². The latter stabilizing effect is of great practical importance. Typical examples are milk, in which fat globules are stabilized by the adsorbed protein casein, latex dyes, which consist of dye-stuffs dispersed in a fluid using a stabilizing polymer layer, and many pharmaceutical formulas.

On the other hand, when only little polymer is present, it has

a destabilizing action. Long chains can adsorb on one particle with part of the molecule and on another with another part. Thus a bridge is formed that binds the particles together, inducing them to flocculate². This mechanism plays an important role in water purification processes, where finely dispersed matter is to be removed.

A special class of polymers is formed by the polyelectrolytes, which bear electrical charges along their chains.

Proteins are important representatives of this category. They consist of chains composed of about twenty different amino acids as the segments. Depending on pH and their nature some of these segments can bear a charge. The specific order of the segments is determined genetically. This order usually results in a stable three dimensional structure. If proteins adsorb, their structure can be changed, but the train-loop-tail model is hardly ever appropriate.

Simpler are the common polyelectrolytes, which have flexible chains. They usually consist of chains, built up from only one or a few different types of segments. The three-dimensional structure is governed by statistics. These types of polyelectrolytes also play a role in biological systems, e.g. the highly charged polysaccharide heparine prevents blood cells from sticking to the inner lining of veins and arteries. Polyelectrolytes are also used in technology, e.g. they are employed to separate oppositely charged mineral particles³.

The polyelectrolyte poly-L-lysine used in this study is related to both types of polyelectrolytes, proteins and flexible chains. It consists of only one type of amino acid, L-lysine. At low pH nearly all segments are charged and the molecules form expanded statistical coils. At high pH the charge is neutralized and helical structures are formed like those occurring in proteins⁴. In this study we used poly-L-lysine only in its highly charged form. Under those conditions it can be regarded as a model polyelectrolyte rather than as a model protein.

To predict properties of adsorbed polymer layers, e.g. their impact on colloid stability, a lot of attention has been paid to the theoretical description of polymer adsorption. Because of the nature of the problem statistical thermodynamical methods are in-

licated. Most modern theories employ lattice models. Flory used such a model advantageously before to describe the behaviour of polymers in solution⁵. The sites of his lattice are occupied either by a segment of a polymer chain or by a solvent molecule. The most comprehensive polymer adsorption theories are those of Roe⁶ and of Scheutjens and Fleer⁷, whereby the latter is even more refined. Electrostatic interactions are not taken into account in these theories. Hence, they cannot be applied to polyelectrolytes. A preliminary theory for polyelectrolyte adsorption was developed by Hesselink³. Although this theory is based on a number of oversimplifying assumptions, it nevertheless enables us to interpret some experimental observations: e.g. the formation of high adsorbed amounts is prevented by the mutual repulsion of charges of equal sign along the chain. In contrast to Hesselink's model, the lattice models of Roe and of Scheutjens provide the possibility of calculating the polymer concentration distribution perpendicular to the surface. As this polymer concentration profile is of crucial importance for the description of particle interaction, we decided to extend the aforementioned lattice theories with electrostatic interactions.

The polymer adsorption theories used are based on equilibrium thermodynamics. There are arguments that the premisses to apply equilibrium thermodynamics to polymer adsorption are not fulfilled. For example, adsorption must be reversible, but irreversibility upon dilution of the solution has often been observed. Before applying equilibrium statistical thermodynamics to polymer adsorption we will contribute to the clarification of this point.

In the experimental part of our study we adsorbed poly-L-lysines to silver iodide. Silver iodide is one of the classical model systems of colloid science⁸. Although uncertainties will always remain, the surface properties of dispersed silver iodide belong to the best known. A variety of experiments has been conducted to study this material. For instance, colloidal dispersions can be obtained readily. These are very suitable to investigate the influence of adsorbates on colloidal stability. Silver iodide particles are usually charged. The surface charge consists of an excess of iodide or silver ions and depends on the concentrations of these ions in solution. Changes in the surface charge can be measured by monitoring

the concentrations of the silver and iodide ions. A very advantageous aspect of our model system chosen is, that the charge of poly-L-lys depends on the pH, but not on the silver ion concentration, whereas the charge on silver iodide depends on the silver ion concentration but not on the pH. Hence, with our system the charges of adsorbent and adsorbate can be varied independently.

1.2 PURPOSE OF THIS STUDY

The aim of the present study is to give a description of the behaviour of a model polyelectrolyte at a model interface.

We will study both the theoretical and the experimental side of such a system. Adsorption theories for uncharged polymers have been elaborated to a high level of sophistication. We will modify the theories of Roe⁶ and of Scheutjens and Fleer⁷ in such a way, that they are also applicable to polyelectrolyte adsorption.

The experimental work is directed to the testing of our polyelectrolyte adsorption theory. As the theoretical work covers the whole chain length domain from monomer up to long chains, it is important to study not only polymers but also oligomers. To synthesize oligomers of a defined length, we devised a route via repeated coupling of entities of equal length. Peptides are a suitable class of compounds for this purpose, because methods of peptide synthesis have been standardized to a high level.

1.3 OUTLINE OF THE INVESTIGATIONS

The present study consist of three parts: a theoretical one, (chapters 2 and 3) an experimental one (chapters 4 and 5) and a comparison between experiment and theory (chapter 6).

Chapter 2 tackles the problem whether or not equilibrium thermodynamics may be applied to polymer adsorption. We focus our attention to the applicability of Gibbs' law. The influence of heterodispersity on surface pressure curves is analyzed.

Chapter 3 gives the extension of the Roe and the Scheutjens-Fleer theory for non-ionic polymers with electrostatic interac-

tions. We will present expressions for the electrical free energy of polyelectrolytes in the adsorbed and non-adsorbed state. Implications for phase separation equilibria are also discussed.

Chapter 4 reports the synthesis of the oligo-L-lysines. Oligomers up to the 32-mer have been obtained by repeated selective coupling of components of the same length.

Chapter 5 describes the experimental results obtained for the poly-L-lysine/silver iodide system. Various colloid chemical techniques have been employed, like the measurement of adsorption isotherms, of coagulation rates, of electrophoretic mobilities and of charge-potential curves for silver iodide covered with poly-lysines. The data are interpreted in terms of a physical picture of the adsorption behaviour of oligo- and poly-L-lysines.

In chapter 6 these data are compared with the theoretical picture as developed in chapter 3. Using model assumptions, most of the parameters used in the polyelectrolyte adsorption theory can be assessed. Only the value of the parameter χ_s for the non-electrostatic free energy of adsorption remains to be fitted to the experiments. Except for this adjustment, quantitative agreement between theory and experiment is achieved.

1.4 REFERENCES

- 1 See e.g. a. G.J. Fleer and J. Lyklema, in "Adsorption from Solution at the Solid/Liquid Interface" (G.D. Parfitt and C.H. Rochester, Eds.), Academic Press, London, 1983, p. 153.
b. B. Vincent and S. Whittington in "Surface and Colloid Science" (E. Matijević, Ed.) Vol XII, Plenum, New York, 1982.
- 2 See e.g. Th.F. Tadros in "The Effect of Polymers on Dispersion Properties" (Th.F. Tadros, Ed.), Academic Press, London, 1982.
- 3 F.Th. Hesselink, J. Colloid Interface Sci. 60, 448 (1977).
- 4 J. Applequist and P. Doty in "Polyaminoacids, Polypeptides and Proteins" (M.A. Stahmann, Ed.), Univ. Wisconsin Press, Madison, 1962, p. 162.
- 5 P.J. Flory, "Principles of Polymer Chemistry", Ch. XII, Cornell University Press, Ithaca, New York, 1953.
- 6 R.-J. Roe, J. Chem. Phys. 60, 4192 (1974).

- 7 J.M.H.M. Scheutjens and G.J. Fleer, a. J. Phys. Chem. 83, 1619 (1979); b. *ibidem*, 84, 178 (1980).
- 8 See e.g. B.H. Bijsterbosch and J. Lyklema, Advan. Colloid Interface Sci. 9, 147 (1978).

2 THE APPLICABILITY OF EQUILIBRIUM THERMODYNAMICS TO POLYMER ADSORPTION

2.1 INTRODUCTION

All highly developed theories for polymer adsorption, like those of Hoeve¹, Silberberg² and more recently, those of Roe³ and of Scheutjens and Fleer⁴--which also extend to oligomers--are based on equilibrium thermodynamics. However, several experimental observations raised questions about this premiss. In particular, there is some doubt about the reversibility (in the thermodynamic sense) of polymer adsorption. For example, by diluting the solution adsorbed polymers cannot be removed from the surface in many cases. However, this phenomenon is not at variance with equilibrium thermodynamics. The theoretically calculated affinity to the surface is so high that an extremely strong dilution is necessary to achieve desorption⁵. For polymers of about a hundred segments typical values of one molecule per cubic kilometer are obtained. Another example is that the shape of adsorption isotherms measured with decreasing concentrations is usually not equal to that measured with increasing concentrations (figure 2.1). Often the shape is also dependent on the adsorbent concentration. Cohen Stuart et al.⁶ showed that the last two phenomena can be attributed to the heterodispersity of the polymers used. From experiment^{6,7,8,9} as well as from theory^{5,10} it is known that at least at not too high volume fractions long chains adsorb preferentially over short ones and attain higher plateau values in the adsorption isotherm. Cohen Stuart et al.⁶ analyzed the simplified model of such a strong preference of longer chains over shorter ones that all polymer longer than a critical chain length is adsorbed, while the remainder stays in solution (figure 2.2). They also assumed that the conformation of none of the adsorbed components was influenced by any other component present in the adsorbed layer, and that this conformation was not sensitive to the volume fraction of polymer in the solution. Hence

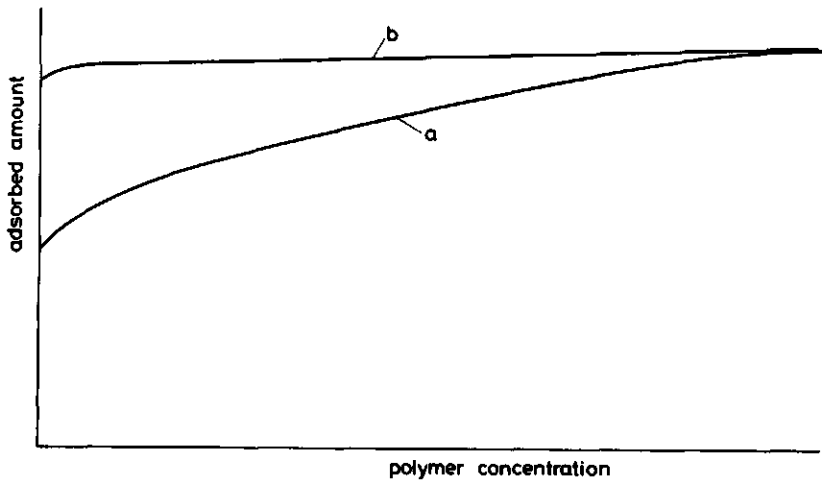


Figure 2.1. Often observed shapes of polymer adsorption isotherms. a, measured using increasing polymer concentration. b, measured by dilution.

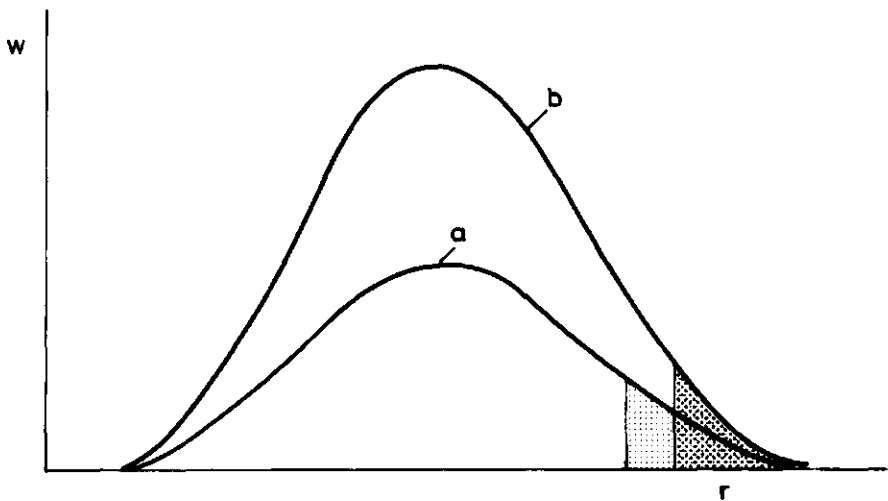


Figure 2.2. Distribution of amount of polymer W as a function of chain length r . a: low polymer concentration. b: high polymer concentration. The adsorbed fractions are shaded (after Cohen Stuart et al.⁶).

in this picture the total adsorption is a linear combination of the plateau values with the adsorbed amounts of the individual components of the mixture as the coefficients. At higher polymer concentrations progressively more long chains are present in the adsorbed layer when the isotherm is measured with increasing polymer concentration. Since these longer chains have higher plateau values, the adsorbed amount increases and a rounded shape of the isotherm is obtained, although the theory gives a distinct plateau value for the individual components. Because of the high affinity of the adsorbed long-chain molecules hardly any of the adsorbed polymer desorbs upon dilution. Then a very distinct plateau value is obtained (see figure 2.1).

The conversion of surface pressure values into adsorbed amounts using Gibbs' law has also raised doubt about the applicability of equilibrium thermodynamics to polymer adsorption. Here we want to contribute to this discussion. Special attention will be paid to the effect of heterodispersity. Gibbs' law has often been used in its simplest form

$$\frac{d\pi}{d \ln \phi_*} = RT\Gamma \quad (2.1)$$

where π denotes the surface pressure (N/m), ϕ_* the bulk volume fraction and Γ the molar adsorbed amount (moles/m²). R and T have their usual meaning. Equation 2.1 has been shown to be valid for a dilute solution of one monomeric component. When applied to heterodisperse polymers, adsorbed amounts obtained from surface pressure measurements greatly exceed realistic values, as can be seen from calculations based on experiments by Lankveld¹¹ on poly(vinyl alcohol), by Katchalski¹² on poly(methacrylic acid) and by Glass¹³ on several polymers. This disagreement has been put forward as an argument supporting the idea that polymer adsorption was irreversible so that Gibbs' law could not be applied at all. Thus using equilibrium thermodynamics to polymer adsorption becomes doubtful.

We will now verify that the polymer adsorption theory of Scheutjens and Fleer⁴, based on equilibrium thermodynamics, is consistent with Gibbs' law. Further we will examine in what way the heterodispersity of the polymer influences the way in which Gibbs' law should be applied. Obviously the simple form (eq. 2.1) is not suit-

able to describe such a complex system. We will use the adsorption theory of Roe³ and that of Roefs and Scheutjens¹⁴ to describe the adsorption of heterodisperse polymer. These theories contain no *a priori* assumptions about preferential adsorption of longer over shorter chains. Our analysis will be compared with that of de Feyte and Benjamins¹⁵, who recently analyzed surface pressure curves in terms of heterodispersity, using a simple Langmuir-type model with preset choice of preference.

2.2 THE CONSISTENCY OF POLYMER ADSORPTION THEORIES WITH GIBBS' LAW FOR HOMODISPERSE POLYMERS *)

One of the conspicuous features of surface pressure measurements with polymer solutions is the phenomenon that the slope of π -log ϕ_* curves is not very sensitive to the molecular weight of the polymer. This is contrary to expectation: as at given ϕ_* the adsorbed amount expressed in equivalent monolayers θ , is not very dependent on the molecular weight, the surface excess expressed in moles per unit area Γ , is about inversely proportional to the chain length. Because of equation 2.1 the same can be expected for the slope of the surface pressure curves. To solve this discrepancy we used the Scheutjens-Fleer polymer adsorption theory⁴ to calculate a set of π -log ϕ_* curves for several chain lengths.

The Scheutjens-Fleer theory is a lattice theory. Each site of the lattice is occupied by either a polymer segment or a solvent molecule. The entropical part of the partition function is found by counting the number of conformations that give a certain polymer volume fraction profile. Here the assumption is made that backfolding of the polymer chain is allowed. The error made by this approximation is partly compensated by the fact that the same assumption is made for the bulk solution and that all adsorbate properties are counted with respect to the bulk. The energy of mixing is obtained by using a formulation analogous to that of Flory¹⁶. Each contact between a solvent molecule and a polymer segment contrib-

*) These studies were presented at the annual scientific meeting of the section for interfaces and fluids of S.O.N. (Z.W.O.), Lunteren (1979).

utes an amount $kT\chi$ to the energy of mixing. In the derivation of the energy of mixing the approximation is made, that segments may be smeared out in each layer parallel to the surface. Thus the composition of each layer of the lattice is fully characterized by its volume fraction. It is assumed that this smearing out has no influence on the entropy of the system. This is the so-called Bragg-Williams approximation. The equilibrium polymer concentration profile perpendicular to the surface is found by using an iteration procedure, in which the partition function is maximized with respect to the volume fractions of the polymer in each of the layers.

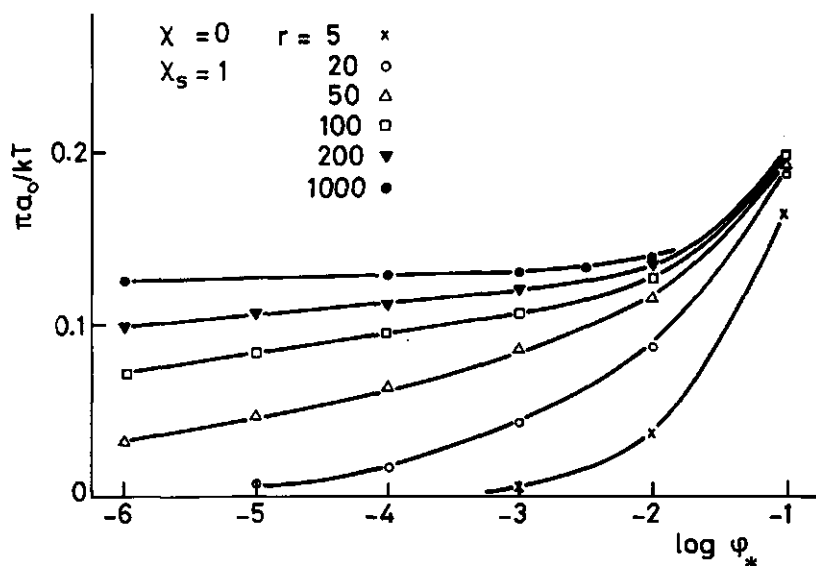


Figure 2.3. Surface pressure curves calculated with the Scheutjens-Fleer theory for homodisperse polymers. The number of segments per chain r is given. The surface pressure is expressed in kT units per area a_0 of a segment.

Figure 2.3 shows a number of surface pressure curves for several chain lengths computed from this theory. Contrary to practical experience, but in accordance with the expectation based on equation 2.1 the slopes of the curves decrease with increasing chain length. When the adsorbed amounts obtained directly from theory are compared with the values obtained from the surface pressure using equation 2.1, very good agreement is achieved if bulk volume fractions are low and the chain length is not too long. Deviations

that do occur can be explained bearing in mind that equation 2.1 involves the approximation:

$$d\mu = RT d \ln \phi_* \quad (2.2)$$

where μ is the chemical potential. The lattice theory of Scheutjens and Fler uses a Flory-type of statistics¹⁶ and then the correct expression for $d\mu$ is given by

$$d\mu = RT d[\ln(\phi_*) + r\phi_* + r\chi(\phi_*^2 - 2\phi_*)] \quad (2.3)$$

where r denotes the number of segments in a polymer chain. Hence equation 2.1 can be transformed into the more correct expression

$$\frac{d\pi}{d \ln \phi_*} = r \frac{d\mu}{d \ln \phi_*} \quad (2.4)$$

Using eq. 2.3 this gives

$$\frac{d\pi}{d \ln \phi_*} = RTf[1 + r\phi_* + 2r\chi(\phi_*^2 - \phi_*)] \equiv RTf \quad (2.5)$$

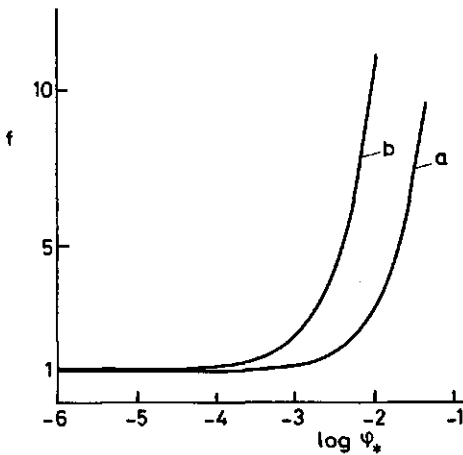


Figure 2.4. Correction factor f according to equation 2.5 to be applied to the simplified version of Gibbs' law as a function of the polymer volume fraction. $\chi=0$; $\chi_s=1$; a: $r=200$; b: $r=1000$.

The correction factor f of equation 2.5 with regard to 2.1, i.e. the term in square brackets is nearly unity at low ϕ_* and r , as observed above. However, this term can become considerable at high chain lengths and high volume fractions, especially in good solvents (figure 2.4). In a theta solvent --when χ is 0.5-- the two terms in equation 2.5 that are first order in ϕ_* cancel. Only the second order term remains, which is usually much smaller than the first one because ϕ_* is less than one. Figure 2.5 gives the $\phi_*(r)$ domains where deviations of more than 10% occur for a good and a

poor solvent. For poor solvents equation 2.1 is valid for nearly all conditions met in practice. For very good solvents--which are rather rare--deviations can become appreciable within the experimentally covered range. However, they are not large enough to explain the strong overestimation of Γ if equation 2.1 is used.

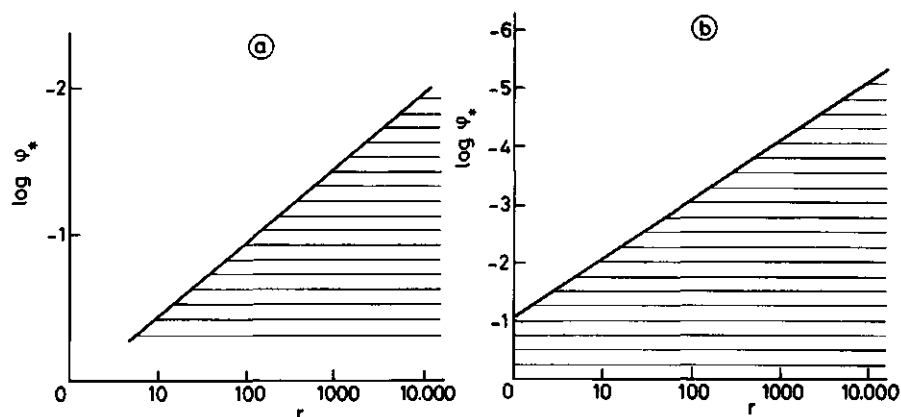


Figure 2.5. Domain of chain length r and volume fraction ϕ_* where the deviation of the simplified Gibbs' law exceeds 10% (shaded). a: $\chi = 0.5$; b: $\chi = 0$.

At bulk volume fractions exceeding 0.1, one should also be careful in the proper positioning of the Gibbs' dividing plane. Usually in experiments as well as in theory the excess adsorbed amount is defined with respect to the surface of the adsorbent. When adsorption of solute takes place, an equal amount of solvent is adsorbed negatively, whereas the adsorption of the adsorbent is zero by definition (figure 2.6a). For a flat surface the surface pressure is defined as the surface tension of the pure solvent minus the surface tension of the solution, so from surface pressure measurements the adsorption with respect to the solvent is obtained. As a consequence the Gibbs' dividing plane no longer coincides with the surface of the adsorbent, but is shifted toward the solution. In figure 2.6b area A represents a negatively adsorbed amount of solvent. Area B is an equal amount of positively adsorbed solvent, rendering the net adsorption zero. The solute is positively adsorbed to an amount of $B + C$ ($= A + C$), whereas a same amount of adsor-

bent is negatively adsorbed. The excess amount of solute adsorbed with respect to the adsorbent $\Gamma^{(s)}$ is easily converted into the amount with respect to the solvent $\Gamma^{(0)}$:

$$\Gamma^{(0)} = \frac{\Gamma^{(s)}}{1 - \phi_*} \quad (2.6)$$

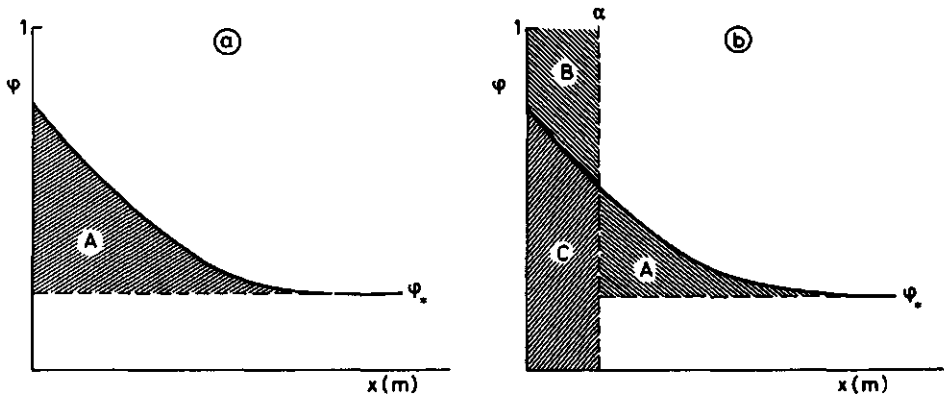


Figure 2.6. Volume fraction profile of solute as a function of distance x from surface.

a. With respect to the surface of the adsorbent the solute is adsorbed positively and the solvent negatively, both to an amount visualized by the area A.

b. With respect to the Gibbs' dividing plane α the net adsorption of the solvent is $B - A = 0$, the adsorption of the solute corresponds to area $A + C$ and the negative adsorption of the adsorbent to $B + C$.

Calculating the adsorption from surface pressure curves obtained from the Scheutjens-Fleer theory using equation 2.5 we arrive at $\Gamma^{(0)}$ values. From equation 2.6 we can easily see that only at high polymer volume fractions the two positions of the Gibbs' dividing plane lead to substantially different values. At $\phi_* = 0.1$ the two values, $\Gamma^{(0)}$ and $\Gamma^{(s)}$, differ by 10%. At pure polymer $\Gamma^{(0)}$ loses its sense and $\Gamma^{(s)} = 0$ by definition.

We can conclude that Gibbs' law can be applied to homodisperse polymers and elaborated with the Scheutjens-Fleer theory in a straightforward way. To close the gap between practice and theory

Lankveld¹¹ and Koopal¹⁷ suggest that equilibrium thermodynamics should be applied to adsorbed segments rather than to adsorbed molecules. Here we prove that the Scheutjens-Fleer theory is only consistent with Gibbs' law if applied to complete molecules and not to loose segments.

2.3 THE INFLUENCE OF HETERODISPERSITY ON THE FORMULATION OF GIBBS' LAW *)

We calculated curves of the surface pressure versus the adsorbed amount for various values of chain length, bulk volume fraction, solvent quality parameter and adsorption energy parameter. These curves nearly coincide, provided that the same value for the adsorption energy parameter is used. The calculated curves lie in a very narrow region around the drawn curves in figure 2.7.

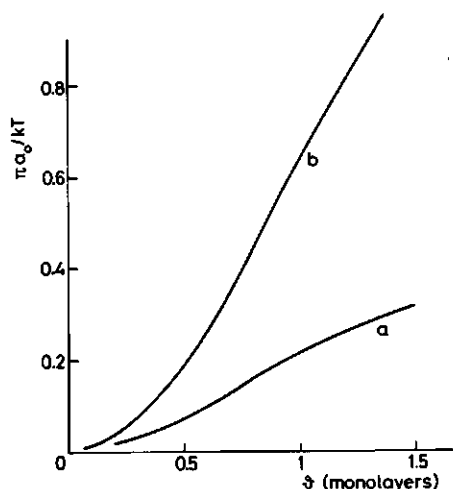


Figure 2.7. Relation between surface pressure and adsorbed amount, expressed in equivalent monolayers.

a: $\chi_s = 1$; b: $\chi_s = 2$.

The adsorption energy parameter χ_s is defined as the non-conformational free energy gain expressed in units of kT , when a solvent molecule at the surface is exchanged for a segment. The chain length, polymer concentration and solvent quality hardly influence the shapes of the curves. They only determine the position of a point on the curve. In the concentration range, where theory predicts distinct plateau values for adsorption isotherms of monodisperse poly-

*) Part of this section was presented at the Arbeitstagung "Adsorption aus Lösungen" der Kolloid Gesellschaft e.V., Bochum (1980).

mers, heterodisperse polymers give rounded shaped isotherms. So they have steeper slopes. When this observation is combined with the one to one relation between the surface pressure and adsorbed amount, it can be deduced that for a heterodisperse polymer the π -log ϕ_* relationship must also have a steeper slope than for a homodisperse species. Thus, this experimentally observed trend can be explained qualitatively.

2.3.1 TWO-COMPONENT SYSTEMS

To obtain a more quantitative insight we calculated a surface pressure curve and an adsorption isotherm for a system containing two polymeric components and solvent. For this purpose we used the polymer adsorption theory of Roe³. The model used in this theory is very similar to that of Scheutjens and Fleer⁴, except for one more approximation: when the number of ways to arrange the molecules of solvent ad polymer is evaluated, it is assumed that with the same probability each of the r segments of a polymer chain can be found in a layer i parallel to the surface. As segments near the end of a chain tend to accumulate in layers farther away from the surface⁴, this is generally not true. Roe defined his model as an open system, *i.e.* the bulk volume fractions are independent variables rather than the total amount of matter of each of the components. In experimental work using heterodisperse polymer the total amounts of each component are fixed and the bulk volume fractions adjust themselves to the equilibrium state. Numerically we did the same and adjusted the bulk volume fractions using an iteration procedure in such a way, that the ratio of the total amounts of the constituents satisfied a given value. Of course, these concentrations depend on the size of the system, as described by the volume/surface ratio. This ratio is expressed as the number of monolayers M that make up the liquid phase of the system. For the calculation of the surface pressure curve and the adsorption isotherm we chose a system containing equal amounts by weight of polymer with a chain length of 50 and of 200 segments respectively.

2.3.1.1 THE ADSORPTION ISOTHERM OF A TWO-COMPONENT POLYMER MIXTURE

Figure 2.8 shows the adsorption isotherm of the mixture, compared with the individual isotherms for homodisperse polymers of 50 and 200 segments respectively. The contribution of the two constituents of the mixture to the total adsorbed amount is also given. At low bulk volume fraction nearly all polymer is adsorbed. Hence the adsorbed amounts of the two components are nearly equal. When more polymer is added the longer chains adsorb preferentially, thereby driving the shorter ones out of the adsorbed layer into the solution. The bulk concentration of the longer component remains very low until the displacement in the adsorbate is nearly complete. In the present case this occurs at about 400 ppm total bulk volume fraction. This analysis illustrates the much higher affinity of the longer components for the surface. This strong preference was one of the assumptions of Cohen Stuart et al.⁶ used in their de-

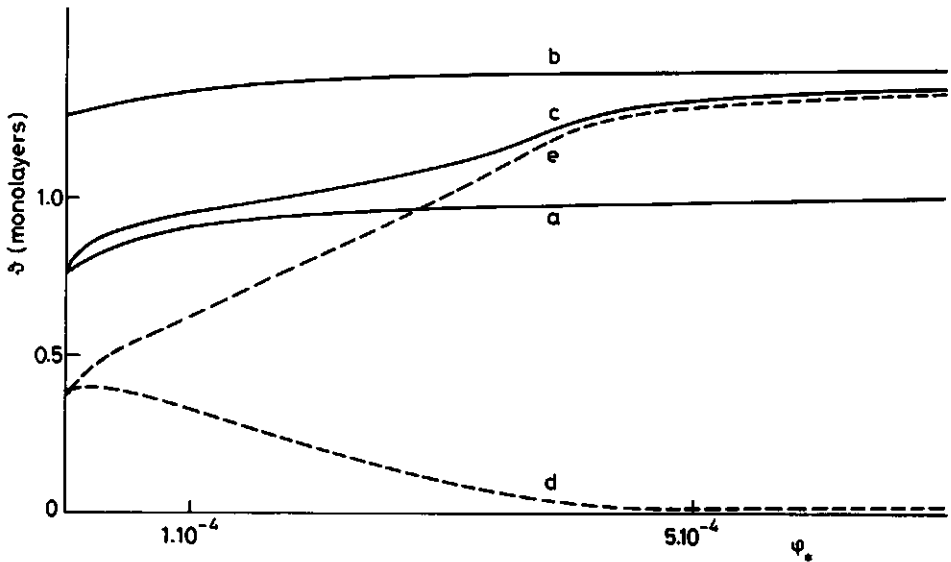


Figure 2.8. Adsorption isotherms of monodisperse polymer of $r = 50$ (a) and $r = 200$ (b) and of a mixture of equal amounts of $r = 50$ and $r = 200$ (c). d: contribution to the adsorption of the mixture of the 50-mer; e: contribution of the 200-mer. $\chi = 0.5$; $\chi_s = 1$; volume to surface ratio M is 3000 lattice layers.

scription of the adsorption isotherm of heterodisperse polymers. Consequently, in this respect their simple model works quite well. They also assumed that polymers adsorbed in a mixture have the same conformation as the pure components would have had at the same bulk volume fraction. This assumption is not supported, as in that case the adsorption isotherm of the mixture would have been sure to have left the axis in figure 2.8 just between the isotherms of the pure polymer. It would also have coincided with the curve for the longer polymer at a volume fraction of about 400 ppm. Both the adsorbed amount and the surface pressure (figure 2.9) are very close to those of the pure shorter component in the region where displacement is absent or only partly accomplished. In our case this region covers the domain of $\phi_* \lesssim 400$ ppm. Apparently the con-

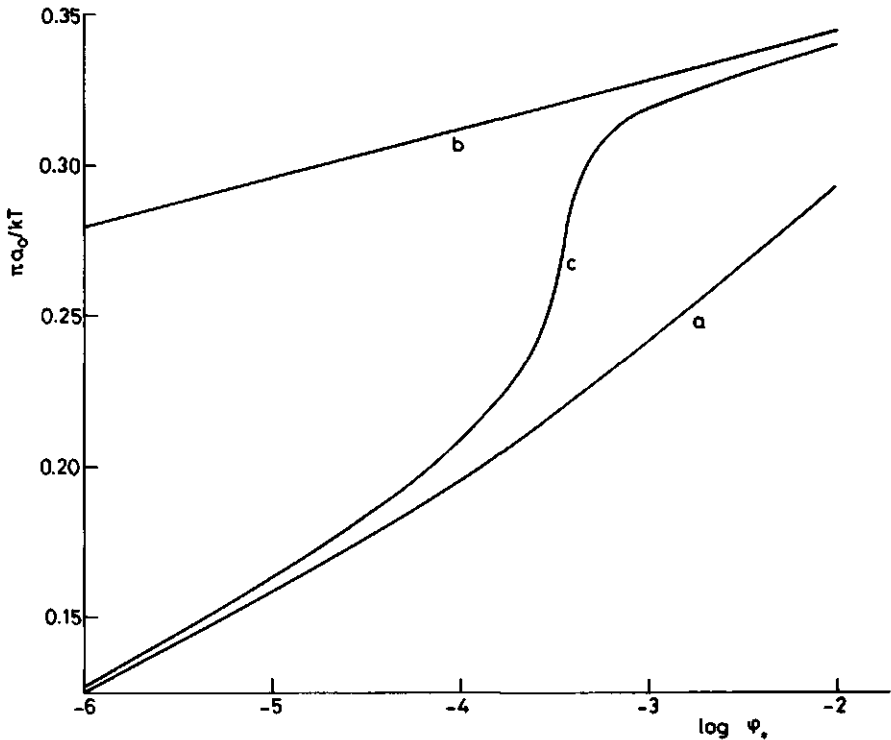


Figure 2.9. Surface pressure curves of monodisperse polymer of $r = 50$ (a) and $r = 200$ (b) and of the same two-component system as used in figure 2.8 (c).

formation of the adsorbed layer, including of that of the longer component therein, is governed by the major component present in the bulk. Under the prevailing conditions this is the shorter one, because the longer chains predominate in the adsorbed layer.

This feature is also reflected in the fraction p of segments directly attached to the surface. Although this is not a very sensitive parameter, it gives some information about the conformation of the adsorbed layer. High values point to flat adsorbed layers, whereas low values indicate that a large portion of the segments is present in loops and tails. Even at a bulk volume fraction of 2.4×10^{-4} , when 84% of the adsorbed matter consists of the longer component, the overall p -value (0.587) does not differ much yet from that for the pure shorter component at the same polymer concentration (0.612). The pure longer component has a distinctly lower value of p (0.486), because most of the amount adsorbed in excess of the amount in the mixture is accommodated in loops and tails. This effect is confirmed by the extension of the Scheutjens-Fleer theory by Roefs and Scheutjens¹⁴ for heterodisperse polymers. Under similar conditions the p -values are 0.578 for the mixture, 0.609 for the pure shorter polymer and 0.450 for the pure longer polymer. The p -values for the mixture and the pure short polymer hardly differ from the Roe-values. The value for the pure longer polymer is considerably lower than the Roe-value, because of Roe's underestimating the tails. Hence the Scheutjens-Fleer theory confirms our results based on Roe's theory. The Scheutjens-Fleer theory and thus the Roefs-Scheutjens extension evaluates the contribution of loops and tails to the total polymer concentration profile. It appears that both the loop and the tail contribution to the adsorbed layer are strongly suppressed in the mixed adsorbed layer. It is interesting to note that in the mixture the longer component even has a higher p -value (0.591) than that of the shorter one (0.569). These values are from Roe's theory. A qualitative explanation for the flatly adsorbed 200-mer is given by the fact that there is no need to form thick layers, because the surface is not full yet: it still contains easily displaceable short polymers. Under these conditions it is favourable to form thin layers, because then a high gain of adsorption energy is obtained.

When displacement of the shorter polymer by the longer one is

nearly complete, the longer component also appears in the solution. Then the structure of the adsorbed layer resembles progressively that of the pure long component. Under those conditions the adsorbed amount (figure 2.8) and the surface pressure (figure 2.9) approach the corresponding quantities for the pure 200-mer. This tendency is also reflected in the p -values, which is 0.486 for the mixture and 0.471 for the pure polymer at a total volume fraction of $\phi_* = 10^{-3}$.

Cohen Stuart *et al.*⁶ also used Roe's theory to support their model of independent conformations. They elaborated on a system containing two polymeric components, but chose equal volume fractions of the two polymers instead of our equal total amounts present in the system. They mainly examined the longer component, the conformation of which is indeed not altered by the shorter one present under those circumstances. They also examined the conformation of an 80-mer in the presence of a 100-mer. The p -value for the 80-mer (0.545) does not differ much from the value for the pure polymer (0.563), but even stronger resembles that of the 100-mer present (0.542) and that of the pure 100-mer (0.543). Hence these data support the view that the conformation of the adsorbed layer is determined by the longer component, if both components are present in the solution.

2.3.1.2 THE SURFACE PRESSURE CURVE OF A TWO-COMPONENT POLYMER MIXTURE

When adsorbed amounts are calculated from the surface pressure curve (figure 2.9) with equation 2.1 using the weight averaged chain length to convert the number of adsorbed molecules into the adsorbed amount in equivalent monolayers, irrational isotherms are found (figure 2.10). At the point of the maximum slope of the surface pressure curve the value of θ differs by a factor of 15 from that obtained directly from theory. This is due to the fact that it is not allowed to use equation 2.1 for a two component system. The correct description of the surface pressure curve is given by

$$d\pi = \Gamma_{r_1} d\mu_{r_1} + \Gamma_{r_2} d\mu_{r_2} \quad (2.7)$$

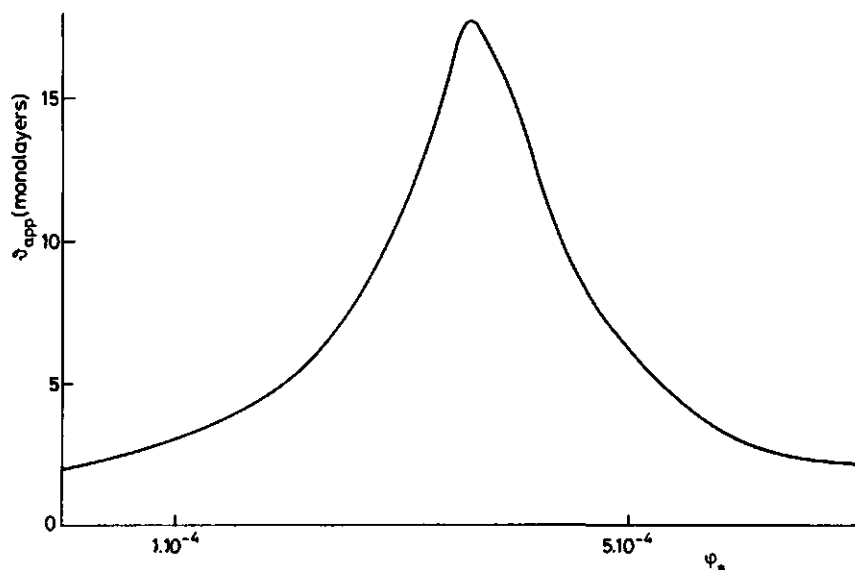


Figure 2.10. Apparent adsorption ϑ_{app} as calculated from surface pressure curve c in figure 2.9 using equation 2.1.

The change in the surface pressure $d\pi$ is obtained as a sum of the contributions of both components having chain lengths r_1 and r_2 . At low volume fraction and good solvent quality $d\mu$ can be approximated according to equation 2.2. Equation 2.7 does describe the slope of the surface pressure curve adequately. From the adsorption isotherms of the two individual components (figure 2.8) and the change of the composition of the bulk with the total volume fraction (figure 2.11) we obtain insight into the contribution of each component to the slope of the surface pressure curve. An illustration is represented in table 2-1.

Table 2-1 Contribution (%) of longer component to the slope of the surface pressure curve of a mixture containing equal amounts of polymers with $r = 50$ and 200 .

	ϕ_*	contribution (%)
1	$\times 10^{-6}$	50
1	$\times 10^{-5}$	55
4	$\times 10^{-5}$	60.2
1.5	$\times 10^{-4}$	82.7
3	$\times 10^{-4}$	99.8
1	$\times 10^{-3}$	98

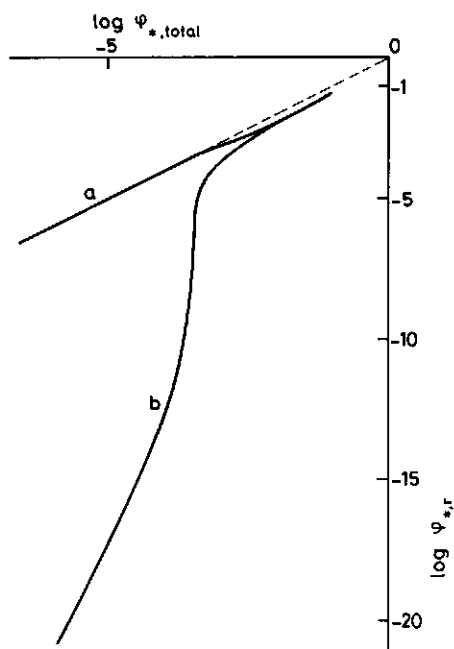


Figure 2.11. Volume fractions in solution of the individual components of the two-component system of figure 2.8 and 2.9.

a: $r = 50$; b: $r = 200$.

It can be seen, that at very low ϕ_* , when nearly all polymer is adsorbed, both components equally contribute to the slope of the surface pressure curve. As under these conditions the adsorption isotherm and the surface pressure curve of the mixture nearly coincide with the corresponding curves for the pure 50-mer, the contribution to the slope of the surface pressure curve of the shorter polymer is just half of that of the pure 50-mer. This phenomenon can be understood by realizing that nearly equal amounts of both polymers are adsorbed and that virtually only the shorter polymer is present in solution. On the basis of Γ_r , δ_r/r and equation 2.2 it can also be deduced from equation 2. that at very low concentrations

the slope of the curve of $\ln \phi_{*,200}$ versus $\ln \phi_{*,total}$ (figure 2.11) is four times as steep as that of the curve for $r = 50$, reflecting the ratio of molecular weights. At higher concentrations both Γ_{200} and the slope of the curve of $\ln \phi_{*,200}$ versus $\ln \phi_{*,total}$ rise with respect to the shorter chain. Just when nearly all shorter polymer has been displaced especially the $d\mu_{200}$ term in equation 2. which is correlated with $\ln \phi_{*,200}$, shows a very steep rise at about $\phi_{*,total} = 3 \times 10^{-4}$. The longer component then also starts to become an important constituent of the bulk of the solution. Hence the sharp peak in the apparent adsorption (figure 2.10) is fully caused by the very strong variation of $\phi_{*,200}$ with $\phi_{*,total}$, i.e. by the longer component. At very high polymer concentration the major part of the polymer is present in solution, so the bulk volume fractions of the shorter and the longer component are nearly

equal. The adsorbed layer mostly consists of the 200-mer, hence the change in surface pressure is mainly governed by this component.

Summarizing we can say that heterodispersity effects can strongly influence the shapes of adsorption isotherms and surface pressure curves. For a two-component system irrationally high adsorbed amounts are calculated when Gibbs' law is used in its simple form. The shapes of surface pressure and adsorption isotherms seem to be determined by the longer fraction of those molecules that have finite concentrations in solution.

2.3.2 SYSTEMS WITH A FLORY-TYPE CHAIN LENGTH DISTRIBUTION

In practice polymer systems usually do not consist of two components but of a wide distribution of chain lengths. Under ideal conditions some common polymerization mechanisms lead to the so-called Flory-distribution, in which the number of molecules with a certain chain length is an exponential function of the chain length. To obtain more quantitative information about the influence of polydispersity on adsorption isotherms and surface pressure curves we decided to analyse such a system with the Roe theory. The weight fraction $f(r)$ of each chain length for a Flory-distribution is given by

$$f(r) = r r_n^{-2} \exp (- r/r_n) \quad (2.8)$$

where r_n is the number averaged chain length. However, since the number of components to be analysed is limited by computational problems, we assumed the polymer to consist of eight homodisperse fractions subject to the following restrictions. We chose a system with a number averaged chain length of 50 segments. Using equation 2.8 it can be derived that the weight averaged chain length, r_w , is 100 segments. Each of the eight fractions has a width of 100 segments. The mid value was taken as the chain length of that fraction and the integral weight was used for the fraction weight (see table 2-2, system a). At a given volume/surface ratio of M monolayers the bulk volume fractions were iterated in such a way, that the total amounts of each fraction obeyed the required distribution.

Table 2-2. Eight-component systems mimicking Flory distributions. $r_n = 50$

System a				system b				system c			
chain	mimicking	weight	chain	mimicking	weight	chain	mimicking	weight	chain	mimicking	weight
length	chain	fraction	length	chain	fraction	length	chain	fraction	length	chain	fraction
used	region		used	region		used	region		used	region	
50	1 - 100	5.967×10^{-1}	25	1-50	2.687×10^{-1}	31	1-50	0.2679			
150	101 - 200	3.125×10^{-1}	75	51-100	3.298×10^{-1}	60	51-70	0.1437			
250	201 - 300	7.365×10^{-2}	125	101-150	2.063×10^{-1}	78	71-85	0.0982			
350	301 - 400	1.420×10^{-2}	175	151-200	1.071×10^{-1}	93	86-100	0.0868			
450	401 - 500	2.498×10^{-3}	225	201-250	5.091×10^{-2}	108	101-115	0.0748			
550	501 - 600	4.158×10^{-4}	275	251-300	2.296×10^{-2}	123	116-130	0.0631			
650	601 - 700	6.679×10^{-5}	325	301-350	1.000×10^{-2}	140	131-150	0.0678			
750	701 - 800	1.046×10^{-5}	375	351-400	4.250×10^{-3}	213	> 150	0.1977			

2.3.2.1 THE PREFERENTIAL ADSORPTION OF LONG OVER SHORT MOLECULES

Figures 2.12 and 2.13 visualize typical results in two different ways. Figure 2.12 gives the amount of polymer adsorbed, ϑ_r , compared with the total amount of polymer in the system, $\vartheta_{\text{sys},r}$, for each chain length. Figure 2.13 represents the amount of polymer adsorbed relative to the bulk volume fraction. From figure 2.12 we see that nearly all polymer with the long chain lengths is adsorbed and hardly any of the short polymer. There is a gradual transition from the adsorbed to the non-adsorbed domain. The linear relationship between $\log (\vartheta_r/\phi_{*,r})$ and r (see figure 2.13) can be derived from the Scheutjens-Fleer theory. In this theory it was found that (equation 11 in ref. 5)

$$\frac{\vartheta_{r_1}}{\phi_{*,r_1}} = \frac{\vartheta_{r_2}}{\phi_{*,r_2}} \left[\frac{\vartheta_{r_2}}{C_1 \phi_{*,r_2}} \right]^{\frac{r_1}{r_2} - 1} \quad (2.9)$$

C_1 is a numerical constant in the range 1-10. The quantity $\vartheta_r/\phi_{*,r}$ is a measure of the affinity to the surface of a component with chain length r . Curves of $\log (\vartheta_r/\phi_{*,r})$ versus r like those in figure 2.13 will be referred to as relative affinity curves. Equation 2.9 relates the affinity of a component with chain length r_1 to that of chain length r_2 . Of course equation 2.9 can be made symmetrical:

$$\left[\frac{\vartheta_{r_1}}{C_1 \phi_{*,r_1}} \right]^{1/r_1} = \left[\frac{\vartheta_{r_2}}{C_1 \phi_{*,r_2}} \right]^{1/r_2} \equiv C_2 \quad (2.10)$$

where C_2 is a constant independent of r . Taking logarithms we see that the relationship between $\log (\vartheta_r/\phi_{*,r})$ and r is linear:

$$\ln \left(\frac{\vartheta_r}{\phi_{*,r}} \right) = r \ln (C_2) + \ln (C_1) \quad (2.11)$$

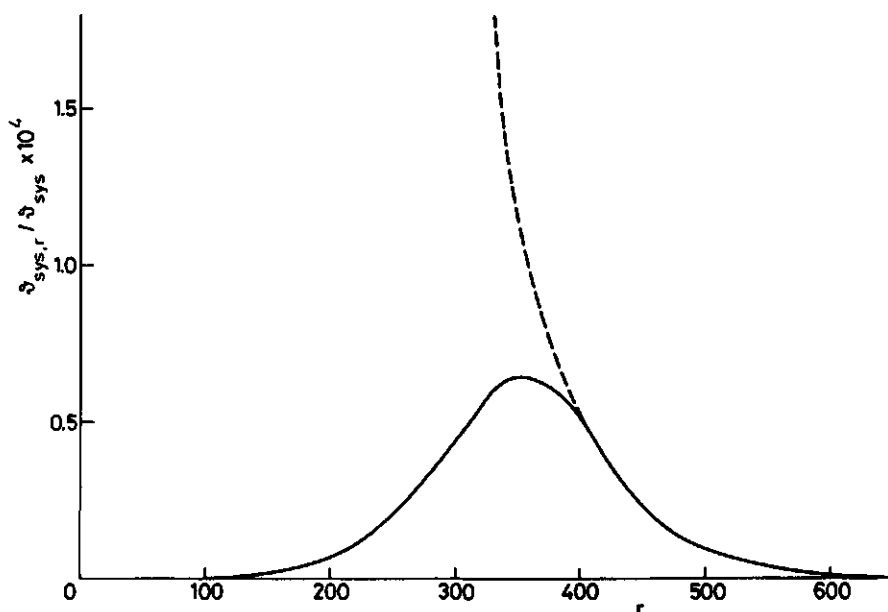


Figure 2.12. Comparison of the total amount of polymer $\delta_{\text{sys},r}$ (---) with the adsorbed fraction δ_r (—). The two amounts are normalized with respect to the total amount of polymer in the system δ_{sys} . $\chi = 0.5$; $\chi_s = 1$; $\phi_* = 10^{-4}$; $M = 10^6$.

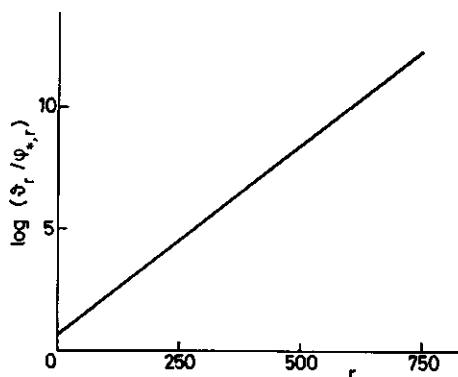


Figure 2.13. Relative affinity curve for the same system as used in figure 2.12.

The constant C_2 is a measure of the preference of longer chains over shorter ones and will be referred to as the preference parameter. Scheutjens and Fleer already showed the excellent agreement of this equation with the Roe theory for a two-component system. We have now found that it also works fairly well for a multicomponent system. It is expedient to define a specific value of r , r_{eq} , being that chain

length at which equal amounts of polymer are present in solution and in the adsorbed layer. Using equation 2.10 we can write the

relation

$$\left(\frac{M}{C_1}\right)^{1/r_{eq}} = C_2 \quad (2.12)$$

We can estimate r_{eq} --and from that we get insight into the extent of preference exhibited--by the simple model of Cohen Stuart *et al.*⁶, where above the certain chain length r_b all the longer polymer is taken to be adsorbed and none of the shorter polymer. Both r_{eq} and r_b are in the transition region between fully adsorbed and non-adsorbed polymer. r_b is directly correlated with the total adsorbed amount δ and the total amount of polymer present in the system, δ_{sys} , so this value can be used as an estimate of r_{eq} . The value of r_b follows from

$$\delta = \int_{r_b}^{\infty} \delta_{sys,r} dr = \delta_{sys} \left(\frac{r_b}{r_n} + 1\right) \exp(-r_b/r_n) \quad (2.13)$$

When the adsorbed amount δ and the total bulk volume fraction are given, then C_2 can be found by an iteration procedure from equation 2.10 and the material balance. From C_2 r_{eq} is obtained. Table 2-3 gives a comparison between r_{eq} and r_b .

Table 2-3 r_{eq} and r_b values for an adsorption isotherm of polymer having a Flory molecular weight distribution with $r_n = 50$. $M = 10^6$

ϕ_*	δ	r_b	r_{eq}
1.4×10^{-7}	0.53	42.4	39.0
5×10^{-7}	0.80	66.6	66.0
1×10^{-6}	0.90	88.2	88.9
1×10^{-5}	1.20	190.1	196.4
1×10^{-4}	1.35	315.4	337.5
1×10^{-3}	1.43	441.9	498.4

At low polymer concentration the accordance between r_{eq} and r_b is very good. At higher concentration, when there is a less pronounced transition between adsorbed and non-adsorbed polymer, some deviation occurs.

The order of magnitude of C_1 can be estimated along the lines of a suggestion put forward by Scheutjens in ref. 5, where the preference of long chains over monomers is shown. The adsorption of longer chains (length r_1) relative to shorter ones (length r_2) is governed by the difference in entropy of mixing and entropic losses incurred in conformational possibilities for segments attached to the surface. There are fewer possibilities to place a segment next to an adsorbed segment by a fraction $(1-\lambda_1)$, where λ_1 is the fraction of neighbouring lattice sites in two neighbouring lattice layers. If p_{r_1} and p_{r_2} represent the fractions of the segments of the adsorbed chains of length r_1 and r_2 bonded to the surface, we write in analogy to equation 9 in ref. 5 for the free energy Δf_{exch} to exchange $p_{r_1} r_1$ molecules of chain length r_2 against $p_{r_2} r_2$ molecules of length r_1 (keeping the first layer filled to the same extent):

$$\begin{aligned} \Delta f_{\text{exch}}/kT = & -(p_{r_1} r_1 - 1) \ln (1 - \lambda_1) + \\ & (p_{r_2} r_2 - 1) \ln (1 - \lambda_1) + \\ & p_{r_2} r_2 \ln \left[\frac{\phi_{1,r_1}}{\phi_{*,r_1}} \right] - p_{r_1} r_1 \ln \left[\frac{\phi_{1,r_2}}{\phi_{*,r_2}} \right] \end{aligned} \quad (2.14)$$

where $\phi_{1,r}$ and $\phi_{*,r}$ are the volume fractions in the first layer. In equilibrium $\Delta f_{\text{exch}} = 0$. Some rearrangements lead to

$$\begin{aligned} \frac{1}{p_{r_1} r_1} \ln \left[\frac{\theta_{r_1} p_{r_1} (1-\lambda_1)}{\phi_{*,r_1}} \right] = \\ \frac{1}{p_{r_2} r_2} \ln \left[\frac{\theta_{r_2} p_{r_2} (1-\lambda_1)}{\phi_{*,r_2}} \right] \end{aligned} \quad (2.15)$$

For a system containing two polymeric compounds we have seen that the p_r values are virtually independent of the chain length. The same holds for a Flory-type polymer distribution divided into eight homodisperse fractions as described above. A typical example is given in table 2-4. Here the p_r values of each of the fractions

are compared with those of the pure polymers. The values for the mixture are much more constant than those of the pure polymer. Only the value for the shortest fraction $p_{r=50}$ diverges. It must be noted that the polymer of this chain length is nearly fully expelled from the adsorbed layer. The p -value for the adsorbed layer as a whole is 0.492.

Table 2-4 p -values for a Flory-type distribution and for the pure polymers. $\chi = 0.5$, $\chi_s = 1$, $\phi_* = 10^{-4}$, $M = 10^6$

r	$p_{r,\text{mixture}}$	$p_{r,\text{pure}}$
50	0.531	0.630
150	0.479	0.517
250	0.487	0.481
350	0.493	0.462
450	0.495	0.449
550	0.497	0.440
650	0.498	0.433
750	0.499	0.427

Putting in 2.15 $p_{r_1} = p_{r_2} = p$, combination of equation 2.10 with 2.15 leads to:

$$C_1 = 1/[p(1-\lambda_1)] \quad (2.16)$$

Scheutjens and Flee⁵ found values for C_1 in the range 1-10 for a number of cases, which they calculated using the Roe theory. In the light of equation 2.16 this is quite reasonable in view of the usual range of p -values. However, their C_1 values do not match perfectly with eq. 2.16. In our case we find some discrepancy too. From the averaged p -value for the mixture used in table 2-4 we find for C_1 2.7, whereas a value of 4.3 is obtained from figure 2.13. The reason is not the difference between Roe's theory and the Scheutjens-Flee⁵ theory, which is the basis of equation 2.16. Preliminary results for the multicomponent version of the latter theory¹⁴ give about the same deviation. This deviation might

be attributed to an assumption underlying equation 2.14: the free energy exchange of one adsorbed segment is accounted for in the term $\ln(\phi_{1,r}/\phi_{*,r})$ --describing the free energy of mixing--and the free energy for the exchange of the other $p_{1,r} - 1$ adsorbed segments gives rise to a term $\ln(1 - \lambda_1)$. This is not a correct reasoning, since it cannot be defined which segments are adsorbed and which are not. For $\lambda_1 = 0$ we know that all segments of adsorbed molecules are attached to the surface--so $p = 1$ --since chains cannot leave a layer. In that case the uncertainty mentioned above is absent, and equation 2.15 is exact.

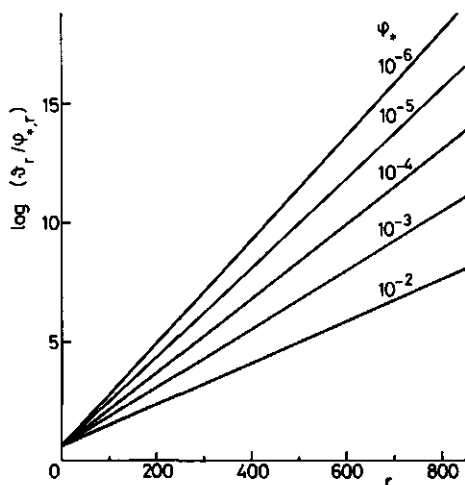


Figure 2.14. Relative affinity curves for different volume fractions ϕ_* as indicated in figure. Total amount of polymer in the system, $M\phi_*$, is constant (100). $\chi = 0.5$; $\chi = 10^6$.

Figure 2.14 gives the affinity-chain length curves of the Flory type polymer at different polymer concentrations. The total amount of polymer present in the system is kept constant by fixing $M\phi_*$. All curves have the same intercept i.e. C_1 is virtually constant. As the adsorption and the parameter C_1 are not very dependent on the polymer concentration, we infer from equation 2.10 that C_2 and hence the preferential adsorption of the higher r fractions increases when the concentration is lowered. This is also reflected in the slope of the curves in figure 2.14. Figure 2.15a shows that the influence of χ is negligible, provided that about the same percentage

of the polymer is adsorbed. The adsorption energy parameter χ_s also has only a minor influence (figure 2.15b). Since the conformations of long and short polymer are virtually the same, it is not to be expected that the energy part of the free energy of exchange, which contains the χ and χ_s terms, can have much influence. We conclude that entropical contributions govern the preference.

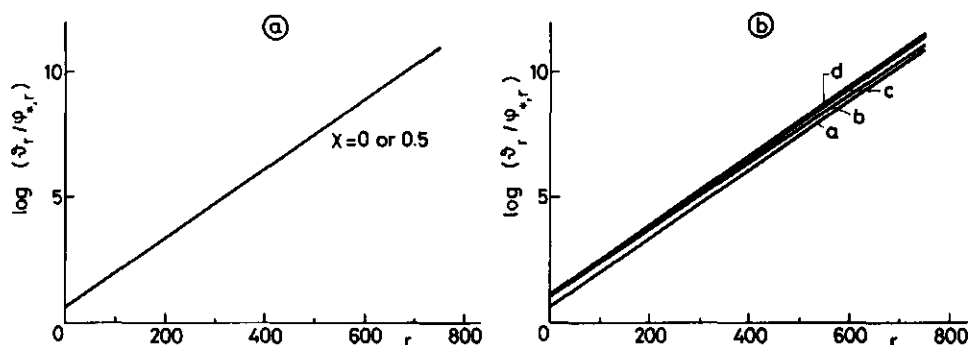


Figure 2.15.

a. Relative affinity curve for different solvent qualities, $\chi = 0$ and 0.5. The adsorption energy parameter is chosen in such a way that the adsorbed amounts are equal: $\chi_s = 4$ and $\chi_s = 1$, respectively. $\phi_* = 10^{-4}$; $M = 10^6$.

b. Relative affinity curves for different adsorption energies. a: $\chi_s = 1$; b: $\chi_s = 2$; c: $\chi_s = 3$; d: $\chi_s = 4$. $\chi = 0$; $\phi_* = 10^{-4}$; $M = 10^6$.

2.3.2.2 THE ADSORPTION ISOTHERM OF A FLORY-TYPE POLYMER

We calculated an adsorption isotherm mimicking the Flory-distribution by eight homodisperse polymer fractions as described in section 2.3.2. Figure 2.16 gives results for a fraction width of 100 and 50 segments (see table 2-2, system a and b respectively). In the curve for the first fraction width a distinct step is observed at $\phi_* \sim 10^{-6}$ and a less clearly visible one at 10^{-5} . The curve for the system with a fraction width of 50 segments shows a less pronounced step. This phenomenon is an artefact that must be attributed to the fact that the polymer is divided into distinct fractions. The narrower the fraction width the smoother the curves. The adsorption isotherm obtained using the Scheutjens-Fleer theory, modified for a polydisperse system¹⁴ gives no steps at all for the current Flory-type polymer. Proceeding upward along the isotherm steps appear whenever a fraction i , which hitherto has nearly only been present in the adsorbed layer, starts to appear in the bulk as well. In the case of the system with fraction width 100, the step at $\phi_* \sim 10^{-6}$ arises from the appearance of the 150-mer in

the solution. In the system with a fraction width of 50, the 125-mer appears in the same ϕ_* -region.

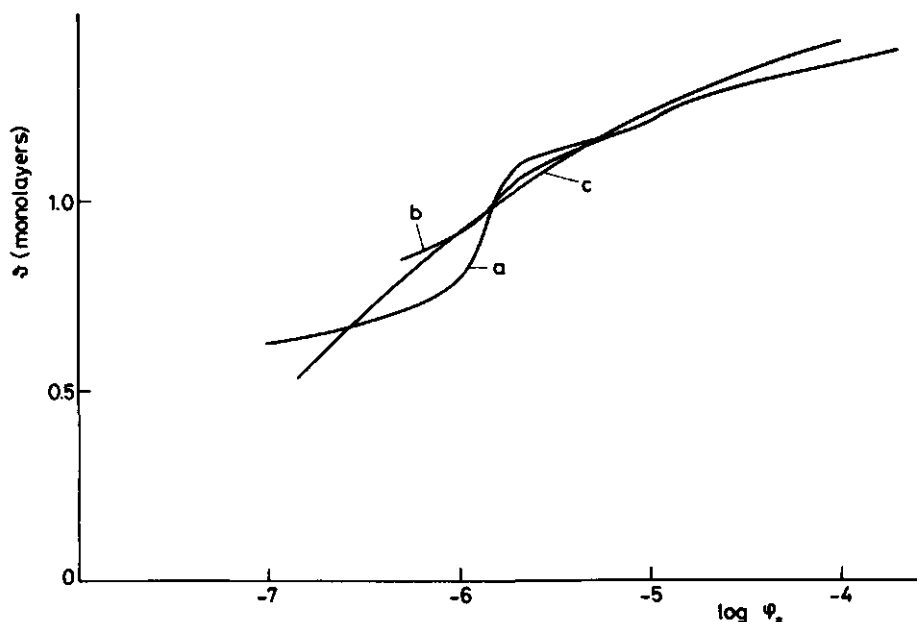


Figure 2.16. Adsorption isotherms for eight-component systems, mimicking a Flory-distribution, calculated with Roe's theory (a and b) and an adsorption isotherm for a continuous Flory-distribution calculated using the Scheutjens-Fleer theory (c). a: fraction width 100, b: fraction width 50 segments. $r_w = 100$; $\chi = 0.5$; $\chi_s = 1$; $M = 10^6$.

2.3.2.3 THE SURFACE PRESSURE CURVE OF A FLORY-TYPE POLYMER

Figure 2.17 gives surface pressure curves for a Flory-type polymer, again simulated by eight homodisperse fractions (see table 2-2). In section 2.3.1 we have already seen that the shape of the surface pressure curve is very similar to that of the adsorption isotherm for a system containing two polymeric compounds. The same holds when we analyze multicomponent systems instead of a two-component system. Again steps are visible upon the appearance of new components in the solution. For this system the Gibbs equation contains a sum over the eight fractions:

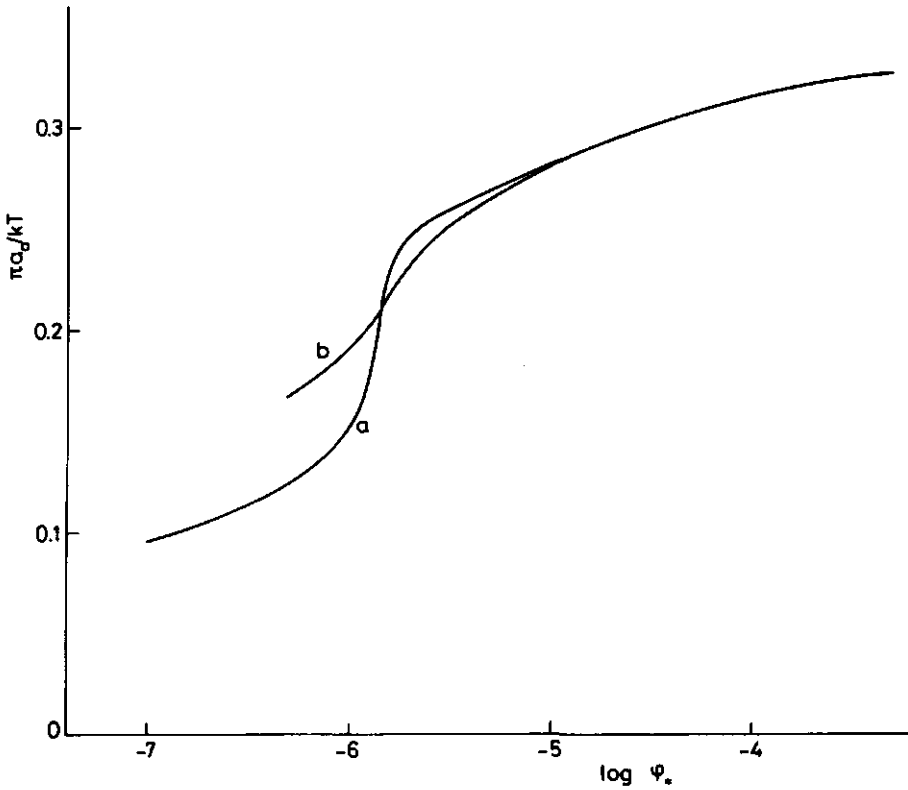


Figure 2.17. Surface pressure curves for the same eight-component systems as used for curves a and b of figure 2.16. a: fraction width 100; b: fraction width 50 segments.

$$d\pi = \sum_i \Gamma_i d\mu_i \quad (2.17)$$

or with the approximation of equation 2.2

$$d\pi = RT \sum_i \Gamma_i d \ln \phi_{*,i} \quad (2.18)$$

Steps occur when the $d \ln \phi_{*,i}$ terms in equation 2.18 assume high values for *all* adsorbed components, *i.e.* not only for component *j* just entering the solution, but also for the components $k \neq j$. This is illustrated in figure 2.18. For a true Flory-type distribution it seems allowed to draw a smooth curve through the steps in the surface pressure curve, analogous to the curve calculated with

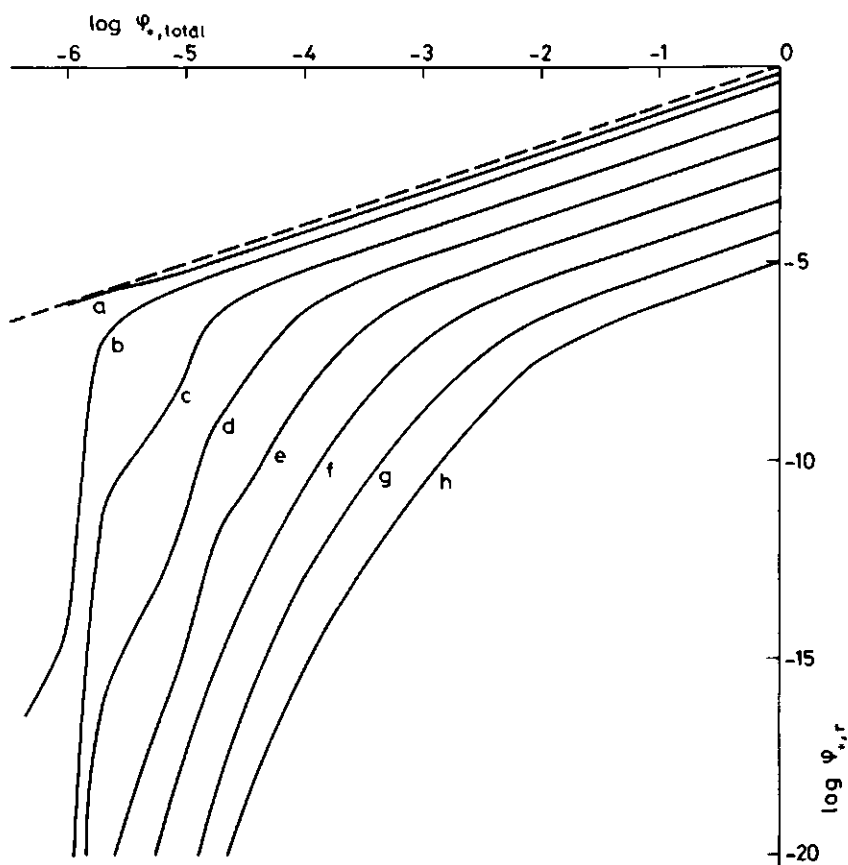


Figure 2.18. Volume fractions in solution of the individual components of the eight-component system of the curves a in figures 2.16 and 2.17. a: $r = 50$; b: $r = 150$; c: $r = 250$; d: $r = 350$; e: $r = 450$; f: $r = 550$; g: $r = 650$; h: $r = 750$.

the Scheutjens-Fleer theory (figure 2.16). In figure 2.19 the smoothed curve of the polydisperse system is compared with the corresponding surface pressure curves of homodisperse polymers. Although there are no steep steps--which are to be found for a mixture of discrete fractions--we find a much higher slope for the surface pressure curve of the heterodisperse polymer than those for the homodisperse species. However, at high polymer concentrations the surface pressure levels off. When adsorbed amounts are calculated from measured surface pressure curves using Gibbs' law in its simple form, a choice must be made for the molecular

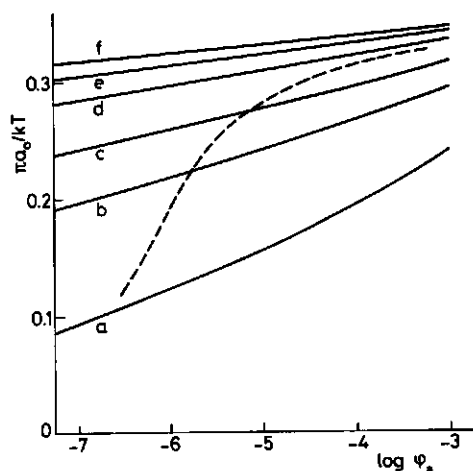


Figure 2.19. Interpolated surface pressure curve for a Flory-type heterodisperse polymer (----), and for homodisperse polymers of various lengths (—).

a: $r = 50$; b: $r = 100$;
c: $r = 150$; d: $r = 250$;
e: $r = 350$; f: $r = 450$.

disperse mixtures. At $\phi_* = 10^{-6}$, for instance, an adsorption of 7.6 equivalent monolayers is obtained. It must be recalled that at higher ϕ_* a considerable amount of polymer appears in solution, whereas at lower ϕ_* nearly all of it is adsorbed. When surface pressure curves are measured experimentally, only a small fraction of the polymer is usually adsorbed and the volume fraction is relatively high, so low slopes of the curves are predicted. Hence, these results obtained theoretically offer no explanation for the surface pressure curves obtained experimentally.

The behaviour of the surface pressure curves obtained theoretically can be understood on the basis of the behaviour of the various volume fractions of the constituents. Figure 2.20 shows the relative affinity curves for a number of cases, both for the eight-component system using Roe's theory and for the continuous distribution according to Roefs and Scheutjens¹⁴. For the latter

weight to convert the molar adsorption into an adsorbed amount in mg/m^2 . To that end the viscometric or weight averaged molecular weight is often used. For our system we did so, using the weight averaged chain length $r_w = 100$. For $\phi_* \gtrsim 10^{-4}$ the slope of the surface pressure curve of the heterodisperse polymer becomes lower than that of the curve of the pure 100-mer. Thus, using equation 2.1 for mixtures lower adsorbed amounts are calculated than for any of the constituting homodisperse fractions. This is contrary to the actual situation and direct experimental evidence. On the other hand, at low polymer concentrations very high adsorbed amounts are calculated in hetero-

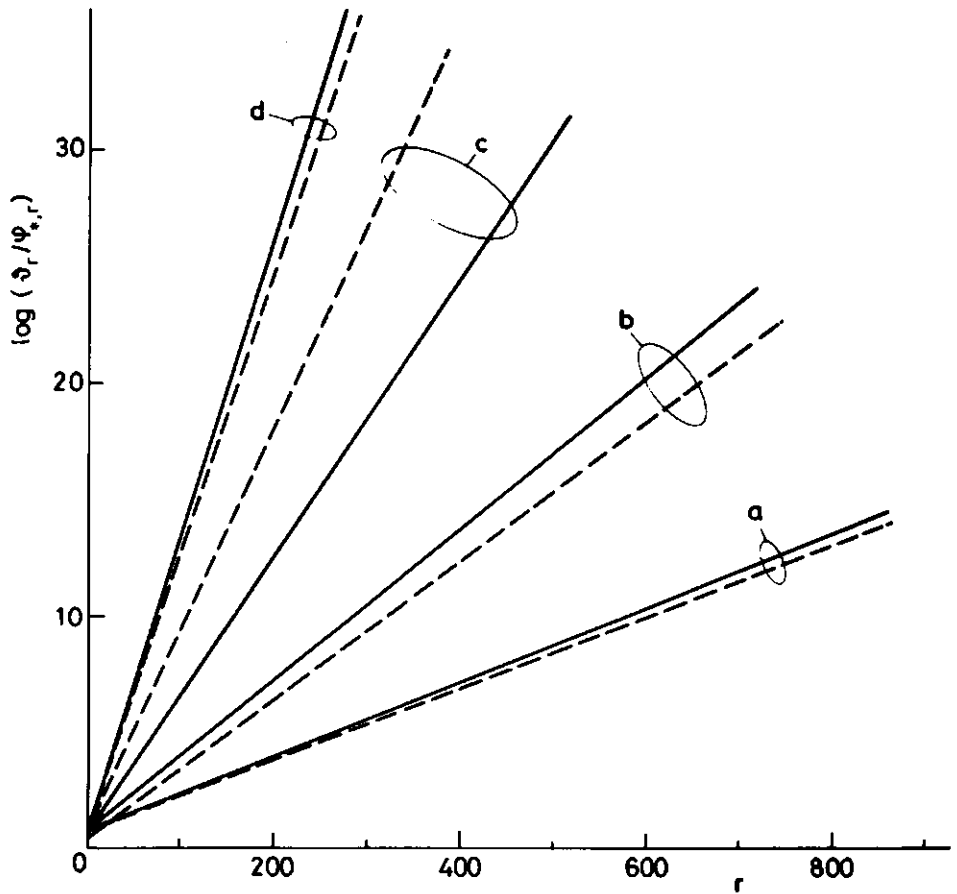


Figure 2.20. Relative affinity curves at various bulk volume fractions for an eight-component system (---) and a continuous model (—). a: $\phi_* = 10^{-4}$; b: $\phi_* = 10^{-5}$; c: $\phi_* = 10^{-6}$; d: $\phi_* = 10^{-7}$. $r_w = 100$; $\chi = 0.5$; $\chi_s = 1$; $M = 10^6$.

model we see a slope continuous increasing with r . This slope is a measure of the preference. For the other system we see a steep rise in preference between $\phi_* = 10^{-5}$ and 10^{-6} , whereas the slope of the curves hardly increases between 10^{-6} and 10^{-7} . We have just seen that the same holds for the surface pressure curves (figure 2.17).

On the basis of equations 2.9 and 2.18 the relation between ϕ_* , the preference parameter C_2 and the slope of the surface pressure curves can be further analyzed. Differentiating equation 2.18

with respect to $\ln \phi_*$ and substituting θ_r/r for Γ_i gives:

$$\frac{d\pi}{d \ln \phi_*} = RT \sum_r \frac{\theta_r}{r} \frac{d \ln \phi_{*,r}}{d \ln \phi_*} \quad (2.19)$$

Elimination of θ_r using 2.9 yields

$$\frac{d\pi}{d \ln \phi_*} = RT \sum_r \frac{C_1 C_2^r}{r} \frac{d\phi_{*,r}}{d \ln \phi_*} \quad (2.20)$$

From equation 2.9 and the mass balance:

$$\theta_r = \theta_{\text{sys},r} - M\phi_{*,r} \quad (2.21)$$

we get

$$\phi_{*,r} = \theta_{\text{sys},r} (C_1 C_2^r + M)^{-1} \quad (2.22)$$

$\theta_{\text{sys},r}$ is given by the total adsorbed amount θ , the total polymer bulk volume fraction ϕ_* , the number of monolayers of the system M and the Flory distribution $f(r)$:

$$\theta_{\text{sys},r} = (\theta + M\phi_*) f(r) \quad (2.23)$$

For given adsorption isotherms $\theta(\phi_*)$, whether they are obtained experimentally or theoretically, taking reasonable values for C_1 (e.g. $C_1 = 5$) and for the volume-surface ratio M , the values of $\phi_{*,r}$ are obtained by eliminating C_2 from equation 2.22 through a one dimensional iteration using the boundary condition $\sum \phi_{*,r} = \phi_*$. Then θ_r is obtained using eq. 2.11. Differentiating eq. 2.22 with respect to $\ln \phi_*$ gives

$$\frac{d\phi_{*,r}}{d \ln \phi_*} = \frac{\phi_* M f(r) (C_1 C_2^r + M) - \theta_{\text{sys},r} \phi_* r C_1 C_2^r \frac{d \ln C_2}{d \phi_*}}{(C_1 C_2^r + M)^2} \quad (2.24)$$

Substituting equation 2.24 in 2.20 gives the sought slope of the surface pressure curve, provided we obtain a value for the relative change of the preference parameter with the volume fraction as defined by $d \ln C_2 / d \phi_*$. The value of C_2 is closely related to

the transition region where the polymer changes from being nearly fully present in solution to fully adsorbed. Using equations 2.12 and 2.13 with the approximation $d \ln r_{eq} / d\phi_* = d \ln r_b / d\phi_*$ we arrive at

$$\frac{d \ln C_2}{d\phi_*} = - \frac{M(\frac{r_b}{r_n} + 1)}{\delta_{sys}} \frac{r_n^2}{r_b^2} \ln C_2 \quad (2.25)$$

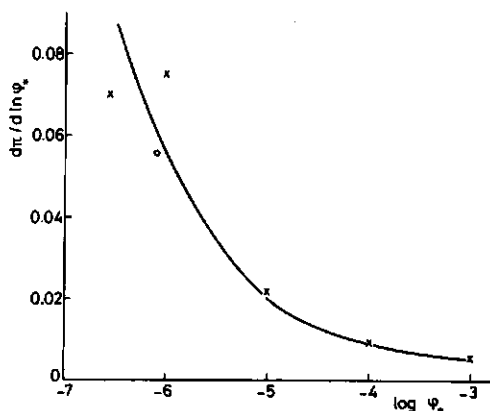


Figure 2.21. Slopes of surface pressure curves. — from equation 2.19 - 2.25. x, from figure 2.19. o, from the eight-component system c in table 2.2.

Figure 2.21 compares the slopes of the surface pressure curve based on equations 2.19 to 2.25 with some points obtained graphically from figure 2.19. Especially at high bulk volume fractions the accordance is striking. It must be emphasized that there is a great uncertainty in the graphically obtained points at low polymer concentrations, because in these cases the surface pressure curve was obtained by interpolation between several curves in figure 2.15.

In order to obtain more insight into the sensitivity of the computed surface pressures to the choice of the parameters defining the polymer mass distribution, we devised another eight-component system. Bearing in mind that the chain length transition region determines the slope of the surface pressure curve most of the fractions were chosen around the boundary chain length r_b . In our example we took $\phi_* = 10^{-6}$. Then $r_b \approx 88$. Again, we divided the polymer into eight homodisperse fractions and attributed the weight averaged chain length to each fraction. The composition of the system is presented in table 2-2, system c. The slope of the surface pressure curve--obtained from two ϕ_* values close to $\phi_* = 10^{-6}$ --much more closely corresponds with the value from the equa-

tion 2.19 to 2.25 than the graphically obtained one (see figure 2.21). The surface pressure is also very close to the interpolated curve in figure 2.19.

We can conclude that the equations 2.19 to 2.25 describe the behaviour of the surface pressure adequately.

2.3.2.4 COMPARISON BETWEEN OUR THEORY AND THAT OF DE FEIJTER AND BENJAMINS¹⁵

De Feijter and Benjamins¹⁵ analyzed surface pressure curves of polydisperse, *i.e.* Flory-type polymers theoretically and compared these results with their experimental work. We shall compare their theory with ours. We shall also reanalyze their experiments along the lines described in section 2.3.2.3.

In their model adsorbed polymer molecules have the same concentration profile irrespective of their chain length and occupy a surface area proportional to their molecular weight. An affinity parameter a_r is defined, which is assumed to depend exponentially on the chain length:

$$a_r = s \exp (qr) \quad (2.26)$$

where s and q are positive constants, depending on the nature of the polymer. A kinetic derivation of the adsorption isotherm is given, leading to a polycomponent Langmuir-type isotherm. The higher the value of q the stronger the preference of longer over shorter chains. When q approaches infinity, the model reduces to the simple model of Cohen Stuart *et al.*⁶, where all the polymer with a chain length exceeding r_b is adsorbed and none of the shorter polymer. This chain length r_b is also used by de Feijter and Benjamins to define the fraction of the polymer that is adsorbed. An equivalent monolayer is defined as the amount of polymer that is adsorbed when the surface is fully occupied. M is the volume to surface ratio expressed as the number of monolayers. The adsorbed amount expressed in equivalent monolayers is given by a Langmuir-type equation:

$$\theta = P / (1 + P) \quad (2.27)$$

with

$$P = \int_0^{\infty} a_r \phi_{*,r}^M dr \quad (2.28)$$

$\phi_{*,r}$ is not *a priori* known, since the state of the system is defined by ϑ and r_b . P is approximated assuming that q approaches infinity, i.e. if r is greater than r_b , $\phi_{*,r}$ is zero, whereas if r is less than r_b , $\phi_{*,r}$ is $\vartheta_{\text{sys},r}/M$. Hence we get

$$P = \int_0^{r_b} a_r \vartheta_{\text{sys},r} dr \quad (2.29)$$

From equations 2.8 and 2.13 $\vartheta_{\text{sys},r}$ is obtained from ϑ and r_b . The dependence of the relative affinity $\vartheta_r/\phi_{*,r}$ on r is given by

$$\frac{\vartheta_r}{\phi_{*,r}} = \frac{\vartheta a_r}{P} \quad (2.30)$$

To obtain more insight into the premisses of this theory, we analyzed to some extent a model corresponding with that of de Feijter and Benjamins¹⁵, but we used a thermodynamic derivation instead of a kinetic one. We attribute the same area to all components, whereas they define an area per molecule proportional to the chain length. In analogy to the affinity parameter a_r of de Feijter and Benjamins we define an adsorption energy parameter $\chi_{s,c}$ for each component c :

$$\chi_{s,c} = \ln a_c = \ln(s) + qc \quad (2.31)$$

and a weight distribution analogous to equation 2.8:

$$f_c = c r_n^{-2} \exp(-c/r_n) \quad (2.32)$$

The adsorption isotherm of each of the components can be found along the lines of the Roefs and Scheutjens¹⁴ theory for multi-component adsorption, which has a firm thermodynamic base. Under these conditions, where no solvent-solute interactions are involved the Scheutjens-Fleer model reduces to the Langmuir model. The unnormalized probability p_c to find a molecule in the adsorbed layer is defined as

$$p_c = (1 - \vartheta) \exp(\chi_{s,c}) \quad (2.33)$$

The probability p_* to find a molecule in a solution layer is

$$p_* = \phi_*^o \quad (2.34)$$

where ϕ_*^o is the volume fraction of solvent in the bulk. In order to obtain a normalization factor, the chain probability P_c can be defined as a sum over all layers.

$$P_c = p_c + (M - 1)p_* \quad (2.35)$$

So the total amount of each component present $\vartheta_{\text{sys},c}$ is given by

$$\vartheta_{\text{sys},c} = \phi_{*,c} P_c p_*^{-1} \quad (2.36)$$

After some rearrangement, bearing in mind that $\phi_* = \sum_c \phi_{*,c}$ and $\vartheta_{\text{sys}} = \sum_c \vartheta_{\text{sys},c}$ we arrive at

$$\phi_{*,c} = \frac{f_c P_c^{-1}}{\sum_c f_c P_c^{-1}} \phi_* \quad (2.37)$$

and the adsorbed amount ϑ_c

$$\vartheta_c = \phi_{*,c} P_c p_*^{-1} \quad (2.38)$$

De Feijter and Benjamins¹⁵ give the ratio of the adsorbed to the nonadsorbed amount $\vartheta_r / M\phi_{*,r}$, for each r as a measure of the preference. Except for a constant factor our model gives the same ratio. Unlike de Feijter and Benjamins we have the volume fractions $\phi_{*,c}$ at our disposal. Thus we can check the quality of the approximation that had to be made to obtain equation 2.29 from 2.28. Equation 2.28 yields a value of P exceeding by several factors that calculated from equation 2.29. Within a few percent the ratio

between these P-values is equal to the ratio between $\delta_r/M\phi_{*,r}$ from the work of de Feijter and Benjamins and that from our model. The small difference that remains might be caused by the fact that they integrate their equations, whereas we use summations. The equivalence of the outcomes of the two models shows that they are not fundamentally different. Hence, we may conclude that also in the work of de Feijter and Benjamins all molecular areas are taken equal implicitly. The alternative possibility, that the area per molecule is not important, can easily be rejected using the Roe theory. To this end we envisage two systems, both having equal bulk volume fractions of two components. The first consists of a mixture of molecules with $r = 1$, having $\chi_s = 7$ and also of molecules with $r = 1$ and $\chi_s = 14$. This system corresponds with the model of equal areas for all molecules and a χ_s -parameter proportional to the "chain length". The second system consists of molecules with $r = 1$ and molecules of $r = 2$, both having $\chi_s = 7$ per segment. Flat adsorption is imposed by choosing $\lambda_1 = 0$. This second mixture corresponds with a system in which the area of the molecule is proportional to the chain length of the adsorbed molecule. The total free energy of adsorption is also proportional to the chain length, since all molecules adsorb flat. The results are presented in table 2-7.

Table 2-7. Comparison of adsorptions for the model using equal areas per molecule and areas proportional to chain length.

$\chi = 0$, $\phi_* = 10^{-4}$, $\lambda_1 = 0$.

equal areas			areas proportional to chain length	
r	1	1	1	2
χ_s	7	14	7	7
δ_r	8.035×10^{-4}	0.9908	9.407×10^{-3}	0.9037

The models show a strong difference in preference. The model using equal areas for all molecules exhibits a much stronger preference than the other model. Hence we conclude that the equations of de Feijter and Benjamins are not in accordance with their model. Their stated assumption of an area proportional to the chain length is

nowhere used explicitly in their paper, but tacitly discarded. Of course, the assumption of proportionality is much more reasonable than that of constant area, which has been used implicitly, since molecules of different volume cannot have the same thickness and area.

In spite of the doubtful model used, de Feijter and Benjamins deduce quite constant q values from their experimental surface pressure curves for polymers of different length. However, in order to bring their theoretical results in agreement with their experimental work, de Feijter and Benjamins had to assume a very strong preference of molecules of higher r over those of lower r , much stronger than Roe's theory predicts. In figure 2.22 relative affinity

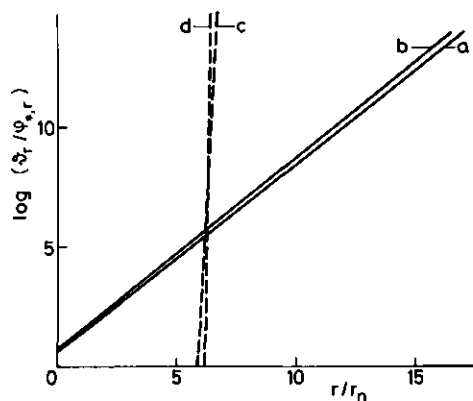


Figure 2.22. Relative affinity curves according to Roe's theory (—) and the theory of de Feijter and Benjamins (---). Parameters for the Roe theory: $\chi = 0.5$; $\chi_s = 1$; $\phi_* = 10^{-4}$; $M = 10^6$; $r_w = 100$ (a) and $r_w = 1000$ (b). Parameters for the de Feijter and Benjamins theory: $q/r_n = 41$ (c) and $q/r_n = 139$ (d).

curves are shown for typical examples. The much higher slopes of the curves according to de Feijter and Benjamins is conspicuous. Another important difference is the dependence of the extent of preference on the chain length. Since q is a property of the polymer and must therefore be a constant, the important quantity q/r_n varies strongly with r_n and so does the preference. In figure 2.22 the lines from the Roe theory are nearly parallel, showing the near independence of the relative affinity of the quantity r/r_n . Cohen Stuart et al.⁶ also found the same relative affinity for the same ratio of chain lengths, using Roe's theory for a two-component system. The chain length interval, where adsorption changes from almost complete to

nearly nothing, embraces about a factor of two both in Cohen Stuart's work and our analysis.

We also compared the experimental data of de Feijter and Benjamins¹⁵ with our formulas. Adsorption and surface pressure data were read from their figures 1 and 3, and transformed to dimensionless quantities (table 2-8) using the following data: molecular weight of one segment 44, segmental area a_0 0.2 nm^2 , monolayer thickness 0.4 nm ¹⁷. The weight averaged molecular weight was chosen equal to the viscometric molecular weight to estimate the weight averaged number of segments per chain r_w . All adsorptions were plateau values. The slopes of the surface pressure curves did not vary in the concentration range of $10^{-5} < \phi_* < 10^{-2}$. The theoretical results are given in table 2-9.

Table 2-8. Parameters from the experimental work of de Feijter and Benjamins¹⁵

PVA-type	205	217	224
M_v (g/mole)	42000	143000	200000
r_w (segments)	1000	3200	4400
Adsorption (mg/m^2)	3.0	3.5	3.7
Adsorption (eq. monolayers)	8.2	9.6	10.1
$d\pi/d \ln \phi_*$ (N / m)	0.006	0.006	0.006
$da_0/kT d \ln \phi_*$ (-)	0.29	0.29	0.29
Volume-surface ratio (m)	0.02	0.02	0.02
Volume-surface ratio M (eq. monolayers)	5×10^7	5×10^7	5×10^7

Table 2-9 Theoretical $da_0/kT d \ln \phi_*$ values for the system of de Feijter and Benjamins

r_w	1000	3200
10^{-3}	2.3×10^{-3}	8.7×10^{-4}
10^{-4}	3.7×10^{-3}	1.4×10^{-3}
10^{-5}	7.7×10^{-3}	3.0×10^{-3}

The theoretical slopes of the surface pressure curves are in strong contrast with those derived from the experiments. They are of the wrong order of magnitude and are concentration and chain length dependent, which is at variance with the experimental results. On the other hand, the theoretical data are in line with the results for the model system, studied with the Roe and Scheutjens-Fleer theories. We must conclude that the high slopes of the experimental surface pressure curves at high polymer concentrations cannot be explained in a straightforward way by the heterodispersity of the polymer. It must be noted that theoretically very high slopes are obtained for the situation that a sizable fraction of the total polymer is adsorbed. Until now we have not been able to show this situation to be identical with the experimental situation at high bulk volume fraction. On the other hand, we do not want to conclude that thus the premiss of the applicability of equilibrium thermodynamics does not apply to polymer adsorption, because for that the experimental work is not unanimous enough. For instance, de Feijter and Benjamins¹⁵ do not find a molecular weight dependence of the slope of the surface pressure curve, whereas Glass¹³ and Katchalski¹² do find such an effect. Both de Feijter and Benjamins and Katchalski used copolymers. This might well affect the slopes of the curves, although it cannot be indicated clearly yet in what direction. Glass' system was certainly not in equilibrium, since he used a stalagmometer with too short a drop-time. Siow and Patterson¹⁸ support the use of equilibrium thermodynamics by showing a good fit of experimental work with the adsorption theory of Prigogine and Maréchal¹⁹. These experiments concerned the adsorption of short homodisperse polymers from organic solvents. Although the Prigogine-Maréchal theory is a rather primitive one, it can work rather well because errors that occur in the adsorbed layer as well as in solution compensate.

2.4 CONCLUDING REMARKS

Although all problems with respect to the applicability of equilibrium thermodynamics to polymer adsorption have not been solved yet, we consider them not too serious to deter us from pursuing

the further development of the theory of polymer adsorption, based on equilibrium thermodynamics. Therefore we shall use equilibrium thermodynamics in extending polymer adsorption theories with electrostatic interactions to be described in the next chapter.

2.5 REFERENCES

- 1 C.A.J. Hoeve, a. J. Polymer Sci. C 30, 361 (1970); b. *ibidem* 34, 1 (1971); c. J. Chem. Phys. 44, 1505 (1966).
- 2 A. Silberberg, J. Chem. Phys. 48, 2835 (1968).
- 3 R.-J. Roe, J. Chem. Phys. 60, 4192 (1974).
- 4 J.M.H.M. Scheutjens and G.J. Fleer, a. J. Phys. Chem. 83, 1619 (1979); b. *ibidem* 84, 178 (1980).
- 5 J.M.H.M. Scheutjens and G.J. Fleer, in "The Effects of Polymers on Dispersion Properties" (T.F. Tadros, Ed.), Academic Press, London, 1982.
- 6 M.A. Cohen Stuart, J.M.H.M. Scheutjens and G.J. Fleer, J. Polymer Sci., Polymer Phys. Ed. 18, 559 (1980).
- 7 R.E. Felter and L.N. Ray, J. Colloid Interface Sci. 32, 349 (1970).
- 8 G.J. Howard and S.J. Woods, J. Polymer Sci. A2, 10, 1023 (1972).
- 9 C. van der Linden and R. van Leemput, J. Colloid Interface Sci. 67, 63 (1978).
- 10 R.-J. Roe. Polymer Sci. Tech. 12B, B, 629 (1980).
- 11 J.M.G. Lankveld, Thesis, Agricultural University, Wageningen (1970).
- 12 A. Katchalski and I. Miller, J. Phys. Chem. 55, 1182 (1950).
- 13 J.E. Glass, J. Phys. Chem. 72, 4450 (1968).
- 14 B. Roefs and J.M.H.M. Scheutjens, to be published.
- 15 J.A. de Feijter and J. Benjamins, J. Colloid Interface Sci. 81, 91 (1981).
- 16 P.J. Flory, "Principles of Polymer Chemistry", Ch. XII, Cornell University Press, Ithaca, New York, 1953.
- 17 L.K. Koopal, Thesis, Agricultural University, Wageningen (1978).
- 18 K.S. Siow and D. Patterson, J. Phys. Chem. 77, 356 (1973).
- 19 I. Prigogine and J. Maréchal, J. Colloid Sci. 7, 122 (1952).

3 THE THEORY OF THE ADSORPTION OF FLEXIBLE POLYELECTROLYTES*

3.1 INTRODUCTION

Polyelectrolytes used in adsorption studies can be divided in two classes. One comprises compounds like proteins, having an internal structure which dominates their behaviour in solution as well as that at interfaces. On the other hand, there are flexible polyelectrolytes. Some of these are of biological origin, like the highly charged polysaccharide heparine, while others are obtained synthetically. In this way a wide variety of compounds has become available.

The adsorption of flexible polyelectrolytes plays a role in several fields of practical interest. Such polyelectrolytes are often used as flocculants for particles charged oppositely to the polymer, e.g. in water purification, in mineral separation processes and in the paper industry. Blood clotting is prevented by the adsorption of heparin on the inner lining of arteries and veins.

In spite of the great importance for practice of the adsorption of flexible polyelectrolytes little work has been done¹ on the theoretical side.

As a starting point for the description of dissolved flexible polyelectrolytes theories on nonionic polymers are usually taken, in which electrostatic interactions are incorporated. To describe the electrical expansion of a macromolecular coil in solution due to charging, Odijk and Houwaart² show that it is expedient to consider the polymer as a Kuhn-type statistical chain. The electrostatic repulsion between adjacent segments gives rise to an electrical

* A preliminary account of this theory has been given in J. Marra, H.A. van der Schee, G.J. Fleer, J. Lyklema, "Polyelectrolyte adsorption from saline solutions", in "Adsorption from Solution" (R.H. Ottewill, C.H. Rochester and A.L. Smith, Eds.), Academic Press, London, 1983, p. 254.

contribution to the free energy of bending in addition to the ubiquitous steric restraints. This effect leads to an increased chain stiffness. Segments from different parts of the polymer cannot approach each other too closely because of the electrostatic repulsion, resulting in an additional excluded volume of the entire molecule.

Hesselink^{3,4} incorporated electrostatic interactions in Hoeve's theory for the adsorption of nonionic polymers. In Hoeve's picture^{5,6,7} a fraction of the adsorbed amount is directly bound to the surface, the remainder forming loops protruding into the solution. For the segment density profile in this loop layer Hesselink assumes a step function. The segment concentration in the loop layer is obtained from the theory of Hermans and Overbeek⁸ for a polyelectrolyte in solution. They describe the polyelectrolyte molecule as a chain obeying Kuhn's statistics, where the distribution of end-to-end distances is modified due to an electrostatic term. Since the concentration of the polyelectrolyte in the loop layer has a preset value, Hesselink's adsorption theory gives no information about the influence of electrostatic interactions on the shape of the concentration profile.

Silberberg⁹ modified his own adsorption theory for nonionic polymers with an electrical term. His model does not differ much from that by Hesselink. Silberberg also chooses the concentration of segments in the surface phase corresponding to that in an isolated chain in solution.

Below, we present a more *ab initio* approach, which is an extension of the adsorption theories for uncharged polymers of Roe¹⁰ and of Scheutjens and Fleer¹¹. In these theories the polymer concentration profile in the adsorbate layer is not chosen *a priori*. First we will calculate the electrical free energy of the adsorbed layer at any concentration profile, after which the equilibrium profile, corresponding with the state of minimum free energy, is obtained via an iteration procedure. The Scheutjens-Fleer theory accounts better for the effects of tails protruding into the solution than Roe's theory and gives the possibility to separate the distribution of trains, loops and tails. On the other hand, Roe's theory gives fewer computational problems.

After the description of the model we will evaluate the potential

distribution in solution and in the adsorbate. From the potential distribution the electrical free energy is derived. Using the electrical free energy of the bulk solution some implications of polyelectrolyte charge for phase separation phenomena will be described. Having obtained the electrical free energy of the adsorbed layer, the adsorption theories of Roe and Scheutjens-Fleer can be extended. Theoretical results for polyelectrolytes are compared with those for uncharged polymers. The consequences of the Debye-Hückel linearization will be shown. We will compare our results with those of Hesselink and in chapter 6 a comparison with experimental data will be presented.

3.2 DESCRIPTION OF THE MODEL

As has been described in the second chapter, the adsorption theories of Roe¹⁰ and Scheutjens-Fleer¹¹ are lattice theories. Each site of the lattice is occupied either by a polymer segment or by a solvent molecule. To each polymer segment a charge of magnitude $z\alpha e$ is attributed, where z denotes the valency, sign included, α the degree of dissociation and e the elementary charge. The restriction is made that α is independent of the potential and identical to the bulk value. This approximation is, of course, only important when weak polyelectrolytes are concerned. In principle it is possible to incorporate the dependence of the degree of dissociation in our numerical procedures. It can be anticipated that the results will tend more in the direction of uncharged polymers. In the evaluation of the electrical free energy these charges are taken as if they are smeared out in a plane through the centres of all unit cells equidistant to the surface. This is one of the most serious approximations. Even if low plane charge densities, originating from low volume fractions, are present, high local charge densities can occur, since the charges are connected with each other along the chains. New segments to be placed in a layer will tend to settle between those highly charged spots and will feel a lower potential than the smeared-out averaged potential. Thus our model will overestimate the electrostatic effects. In chapter 6 we will pay some more attention to this approximation,

when we will choose the parameters to compare theory and experiment. Hence, we define a plane charge σ_i in layer i parallel to the surface

$$\sigma_i = z\alpha e\phi_i/a_0 \quad (3.1)$$

where a_0 is the area of the unit cell and ϕ_i the volume fraction of polymer in layer i . Plane charges in bulk, σ_* , also obey eq. 3.1 with ϕ_* instead of ϕ_i .

Description of the charges as located on planes is not restrictive. An alternative model would have employed space charges, uniform within each layer. These two models would have given very similar results. The plane charge model has the advantage that it gives simpler equations if the Debye-Hückel linearization is used. In appendix 3A we will derive expressions for the potential distribution for space charges. For the description of the bulk solution the space charge model is to be preferred, since it is not elegant to use an anisotropic model to describe an isotropic situation.

The bulk solution is electroneutral. Hence, an equivalent amount of counterions compensates σ_* .

We have also indifferent electrolyte present in our system. Since multivalent ions often display specific effects, we will restrict ourselves to a symmetrical univalent electrolyte.

The small ions will be considered as point charges. The volume excluded by the polymer was neglected, which has only a minor influence on the potential distribution¹². These two approximations can be avoided by defining the small ions as charged monomeric components in the system. This is possible since the Roe and the Scheutjens-Fleer theories are also suitable for multicomponent systems. Preliminary results for such a treatment are in accordance with the present work¹³.

For the system, defined in this way, we have to evaluate the electrical free energy and, prior to that, the potential distribution.

3.3 THE POTENTIAL DISTRIBUTION

Potentials are obtained by solving the Poisson-Boltzmann equation. This can be done analytically, if this equation may be linearized, or numerically in the unlinearized form. From now on we will refer to the linearized form as the Debye-Hückel approach and to the full Poisson-Boltzmann equation as the Gouy-Chapman approach.

3.3.1 THE POTENTIAL DISTRIBUTION IN THE BULK OF THE SOLUTION

In the bulk of the solution we have an infinite sequence of identical plane charges which divide the space into infinite cells with a thickness equal to the distance between the lattice planes. The solution for one cell suffices to describe the whole bulk. Katchalski¹⁴ and Möller, van Os and Overbeek¹⁵ also developed a cell model for polyelectrolyte solutions. They considered cylindrical and spherical cells respectively. Katchalski could obtain an analytical solution for the case of no added salt only.

Following Möller et al. we define the stoichiometric concentrations expressed as numbers per unit volume of the positive ions \bar{n}_+ and of the negative ions \bar{n}_- . These concentration \bar{n}_+ and \bar{n}_- are related to the salt concentration and the amount of polymer present via the electroneutrality condition:

$$\bar{n}_+ - \bar{n}_- + z\alpha\phi_*/a_0r_0 = 0 \quad (3.2)$$

with r_0 being the distance between layers. By choosing a_0 unequal to r_0^2 it is possible to define an anisotropic lattice. If z is 1, \bar{n}_+ is equal to the number of salt molecules per unit volume. If z is -1, the same holds for \bar{n}_- . Between the layers the small ions distribute themselves according to the Boltzmann equation. The actual concentrations of the positive ($n_+(x)$) and the negative ($n_-(x)$) ions at each place x are related with respect to their stoichiometric concentrations \bar{n}_+ and \bar{n}_- through

$$n_+(x) = \bar{n}_+ \exp[-e(\psi(x) - \bar{\psi}_+)/kT] \quad (3.3)$$

and

$$n_-(x) = \bar{n}_- \exp[e(\psi(x) - \bar{\psi}_+)/kT] \quad (3.4)$$

The potentials $\bar{\psi}_+$ and $\bar{\psi}_-$ are the values at those places where the small ion concentrations equal \bar{n}_+ and \bar{n}_- respectively. T denotes the absolute temperature and k Boltzmann's constant. The Poisson equation between two plane charges reads

$$\frac{d^2\psi(x)}{dx^2} = -\frac{e}{\epsilon} \left[\bar{n}_+ \exp[-e(\psi(x) - \bar{\psi}_+)/kT] - \bar{n}_- \exp[e(\psi(x) - \bar{\psi}_-)/kT] \right] \quad (3.5)$$

where ϵ is the dielectric permittivity of the solvent. The charge of the polymer does not occur in this equation, because it is concentrated in volumeless plane charges. These plane charges give rise to a discontinuity in the field strength. Following Möller *et al.*¹⁵, we define the reciprocal shielding length κ :

$$\kappa^2 = (\bar{n}_+ + \bar{n}_-)e^2/\epsilon kT \quad (3.6)$$

Applying the Debye-Hückel approximation and inserting equations 3.2 and 3.6 into eq. 3.5 gives:

$$\frac{d^2\psi(x)}{dx^2} = \kappa^2 \left[\psi(x) + \frac{z\alpha\phi_*kT/a_o r_o e - \bar{n}_+\bar{\psi}_+ - \bar{n}_-\bar{\psi}_-}{\bar{n}_+ + \bar{n}_-} \right] \equiv \kappa^2 (\psi(x) + b) \quad (3.7)$$

Levine and Neale¹⁶ point out that for two layers this approach is restricted to lower potentials than when there is only one single plane charge in an infinite salt solution, *i.e.* the case where \bar{n}_+ and \bar{n}_- are equal. In the latter case second order terms in the expanded Poisson-Boltzmann equation cancel, which does not happen in our system. However, at high salt concentrations these terms do not play an important role. They suggest not to use the arithmetic mean $(\bar{n}_+ + \bar{n}_-)/2$ in the definition of κ , but the geometric mean $(\bar{n}_+\bar{n}_-)^{1/2}$. However, their expression cannot be used in the absence of salt, so we follow the route of Möller *et al.* We are free to choose a reference potential for our system. It is advantageous to do this in such a way that b is zero, implying

$$\frac{\bar{n}_+}{\bar{n}_-} = \frac{1 - e^{\bar{\psi}_-/kT}}{1 + e^{\bar{\psi}_+/kT}}$$

The reference potentials $\bar{\psi}_+$ and $\bar{\psi}_-$ are determined by the ratio of the polyelectrolyte to the small electrolyte concentration. If equation 3.7 is solved for the space between the plane charge of layer i at x_i and the plane charge of layer $i + 1$ at x_{i+1} , the potential distribution in the bulk solution is fully described. The general solution of eq. 3.7 is

$$\psi(x) = C_1 \exp(-\kappa x) + C_2 \exp(\kappa x) \quad (3.8)$$

where x goes from x_i to x_{i+1} . The coefficients C_1 and C_2 are determined by the following boundary conditions:

- (i) Right in the middle of the planar cell the field strength $d\psi(x)/dx$ is zero.
- (ii) At the place x_i of the plane charge there is a discontinuity in the field strength because of the plane charge σ_* (Gauss' law):

$$\left(\frac{d\psi(x)}{dx} \right)_{x \rightarrow x_i} - \left(\frac{d\psi(x)}{dx} \right)_{x \leftarrow x_i} = - \frac{\sigma_*}{\epsilon} \quad (3.9)$$

Since the potential decay is symmetrical with respect to the plane charges, the slope of $\psi(x)$ is given by

$$\left(\frac{d\psi(x)}{dx} \right)_{x \rightarrow x_i} = - \frac{\sigma_*}{2\epsilon} \quad (3.10)$$

The solution of equation 3.7 in the domain $x_i < x < x_{i+1}$ is

$$\psi(x) = \frac{\sigma_*}{2 \epsilon \kappa} \frac{\exp(-\kappa x) + \exp(\kappa x - \kappa r_o)}{1 - \exp(-\kappa r_o)} \quad (3.11)$$

or

$$\psi(x) = \frac{\sigma_*}{4 \epsilon \kappa} \frac{\exp[\kappa(r_o/2 - x)] + \exp[\kappa(x - r_o/2)]}{\sinh(\kappa r_o/2)} \quad (3.11a)$$

Using equations 3.11, 3.3 and the material balance

$$\bar{n}_+ = \int_{x_i}^{x_{i+1}} \frac{n_+(x)}{r_0} dx \quad (3.12)$$

the potential $\bar{\psi}_+$ can be determined. From the definition of $b = 0$ it appears that $\bar{\psi}_-$ is equal to $\bar{\psi}_+$:

$$\bar{\psi}_- = \bar{\psi}_+ = \sigma_*/\epsilon\kappa^2 r_0 \quad (3.13)$$

The potentials ψ_* at the plane charges are obtained from equation 3.11:

$$\psi_* = \frac{\sigma_*}{2 \epsilon \kappa} \frac{1 + \exp(-\kappa r_0)}{1 - \exp(-\kappa r_0)} \quad (3.14)$$

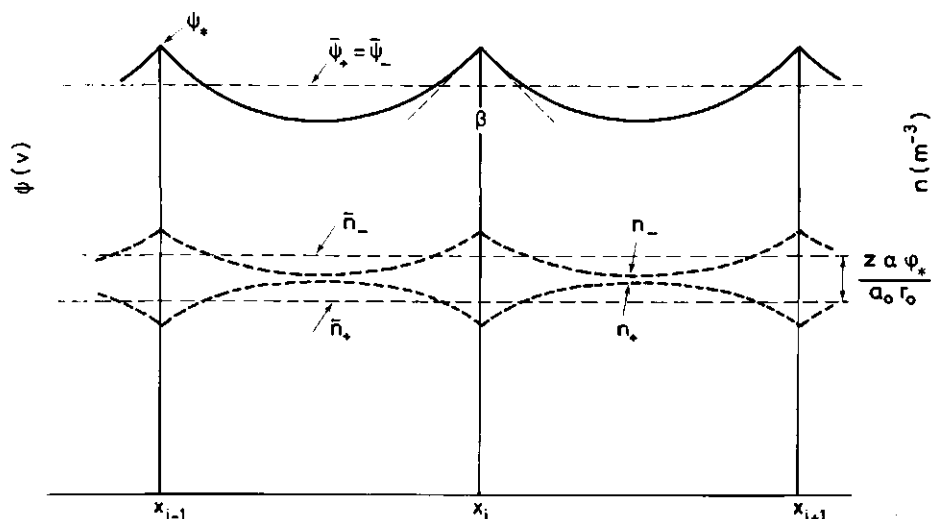


Figure 3.1. Potential and ion distribution in the bulk solution. $\tan \beta = -\sigma_*/\epsilon$. $z = +1$.

The distribution of potentials and ions is illustrated in figure 3. The negative small ions are attracted by the plane charges, the positive ones are repelled. These ions have their stoichiometric --i.e. averaged--concentration at those values of x where $\psi(x) = \bar{\psi}_+ = \bar{\psi}_-$.

It must be noted that as a consequence of our definition of the potentials nowhere in the system we have a zero potential. This has no consequences for the description of the adsorbed layer, since only potentials with respect to the bulk situation are involved. Physically our choice is equivalent to defining the Donnan-potential. For a polyelectrolyte in equilibrium with a dialysate this means that at a given moment the sequence of plane charges ends, whereby the potential drops to zero (the reference value in the dialysate) with a shielding length given by κ^{-1} . The indifferent electrolyte concentration in the dialysate is $2 \bar{n}_+ \bar{n}_- / (\bar{n}_+ + \bar{n}_-)$, as follows from equation 3.3 and 3.4, with $\psi(x) = 0$ and using the Debye-Hückel linearization.

3.3.2 THE POTENTIAL DISTRIBUTION IN THE ADSORBED LAYER

The adsorbed layer exists of M lattice layers, each with its own polymer volume fraction ϕ_i . Outside the M layers each layer has the polymer volume fraction ϕ_* . The potential in each layer contains a contribution originating from the M plane charges σ_i , from the infinite sequence of plane charges σ_* outside the M lattice layers and from the surface charge σ_0 of the adsorbent. First we will describe the potential distribution using the Debye-Hückel approximation, then we will show how the full Poisson-Boltzmann equation can be integrated numerically.

In the Debye-Hückel approximation potentials originating from different charges are independent and additive, hence only the solution has to be found of the Poisson-Boltzmann equation for one single plane charge σ_i . The total potential distribution is then obtained by a summation of all contributions.

To obtain a solution of the Poisson-Boltzmann equation in the Debye-Hückel approach (eq. 3.7) for a single plane charge we divide the space in two domains, $0 < x < x_i$ and $x > x_i$. The coefficients C_1 and C_2 in the general solution are found again from the boundary conditions. Since we consider for the moment only one plane charge σ_i , we have σ_0 and σ_* zero. Thus at the solution side of σ_i , $x > x_i$, we have the usual Debye-Hückel double layer with the boundary condition that $d\psi(x)/dx$ and $\psi(x)$ approach zero for infinite x .

The derivative of the potential at the position x_i of the plane charge at the solution side is

$$\left(\frac{d\psi(x)}{dx} \right)_{x \rightarrow x_i} = -\kappa \psi_i \quad (3.15)$$

where ψ_i is the potential at the location of the plane charge σ_i . Because of the charge localized at x_i the derivative at the surface side is

$$\left(\frac{d\psi(x)}{dx} \right)_{x \rightarrow x_i} = \frac{\sigma_i}{\epsilon} - \kappa \psi_i \quad (3.16)$$

Since we discuss now only a plane charge at x_i and no surface charge, we have at the surface of the adsorbent

$$\left(\frac{d\psi(x)}{dx} \right)_{x=0} = 0 \quad (3.17)$$

The solutions of the Poisson-Boltzmann equation for the two domains can be generalized by

$$\psi(x) = \frac{\sigma_i}{2\epsilon\kappa} \left[\exp(-\kappa|x - x_i|) + \exp(-\kappa(x + x_i)) \right] \quad (3.18)$$

This potential can be interpreted as a sum of two contributions, the first originating from the plane charge itself and the second from the image charge, both decaying exponentially with the Debye-Hückel shielding length κ^{-1} . Figure 3.2 illustrates the potential distribution. As in figure 3.1, there is a discontinuity in the field strength at x_i amounting to σ_i/ϵ . Because we consider only a plane charge in solution without any surface charge present, the slope of the potential curve is zero at the surface. As there is no space charge within the adsorbent the potential is constant there, at a level different from the potential at infinite distance

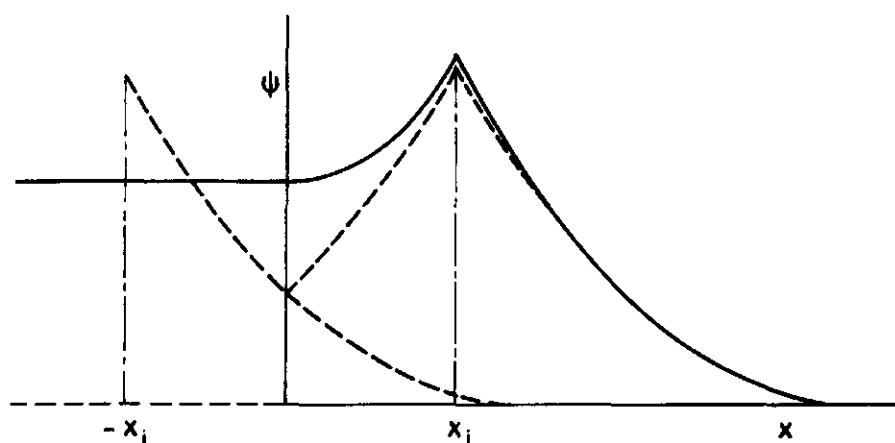


Figure 3.2. Debye-Hückel potential distribution due to a single plane charge at x_i . Charge and image charge give contributions to the potentials of $\sigma_i/2\epsilon\kappa$ (----) at x_i and $-x_i$ respectively, which decay with shielding length κ^{-1} (-----). For $x > 0$ the potential (—) is the sum of the two contributions. Within the adsorbent the potential is constant.

from the surface.

Equation 3.18 is in accordance with the formulation of Stillinger¹⁷. He gives the potential due to a fixed point charge in a solution in the neighbourhood of a dielectric. He analyzes the point charge in terms of a Fourier decomposition in a series of two-dimensional vectors. The zeroth order term of this series (which gives no contribution in the case of a point charge) correspond to a plane charge. In this zeroth order case the solution of the Poisson-Boltzmann equation shows to be invariant to the dielectric constant of the substrate behind the surface. This is the case as long as we smear out the charges in planes parallel to the surface. As soon as other types of symmetry come in, the difference in dielectric permittivity between solution and adsorbent has to be accounted for explicitly. The presence of a surface restricts the shielding power of the small ions. This reduction of the shielding is taken into account in the solution of the Poisson-Boltzmann equation by the choice of the boundary condition at the

surface. Thus this description of the potential distribution, as originating from charge and image charge, is equivalent to that obtained via the solution of the Poisson-Boltzmann equation for one planar charge at distance x_i with the appropriate boundary conditions. For his polyelectrolyte adsorption theory Hesselink⁴ also uses planarly smeared-out charges. So in his case image charges have been accounted for implicitly through the way in which the Poisson-Boltzmann equation is solved, notwithstanding Hesselink's statement that he does not take them into consideration.

From eq. 3.18 it can be seen, that when the plane charge coincides with the surface ($x_i = 0$), charge and image charge have the same x -coordinate. Then the potential distribution reduces to the usual Debye-Hückel solution for a surface charge:

$$\psi(x) = \frac{\sigma_{i=0}}{\epsilon \kappa} \exp(-\kappa x) \quad (3.19)$$

One of the potentials we are interested in is that at the centres of the layers i . These potentials originate from all plane charges j (i inclusive):

$$\psi_i = \sum_{j=1}^{\infty} \frac{\sigma_j}{2 \epsilon \kappa} \left[\exp(-\kappa r_0 |i - j|) + \exp(-\kappa r_0 (i + j)) \right] \quad (3.20)$$

The surface charge σ_0 also contributes to ψ_i . Since the plane charges are at the centres of the layers, the distance from the surface to the plane charge i is $r_0(i - \frac{1}{2})$.

Equation 3.20 provides an alternative derivation of the bulk plane potentials ψ_* (eq. 3.14). The bulk solution can be considered as an infinite row of equal plane charges σ_* . They all give a contribution decaying with κ^{-1} to the potential ψ_* :

$$\psi_* = \frac{\sigma_*}{2 \epsilon \kappa} \sum_{i=-\infty}^{\infty} \exp(-\kappa r_0 |i|) \quad (3.21)$$

The sum of this double geometric progression is identical to eq. 3

When the Debye-Hückel approximation may not be applied, the Poisson-Boltzmann equation 3.5 must be solved numerically. This can be done using a sixth order Runge-Kutte integration. In this procedure eq. 3.5 is solved from one plane charge to the next one. At the plane charges there is the discontinuity in the derivative of the potential analogous to eq. 3.10. The potential is continuous. At the surface we have a field strength

$$\left(\frac{d\psi(x)}{dx} \right)_{x=0} = - \frac{\sigma_0}{\epsilon} \quad (3.22)$$

This is one boundary condition. Beyond the M layers considered in the volume fraction iteration procedure, we assume the Debye-Hückel approximation to be valid. This leads to the other boundary condition. The potential at that layer M, ψ_M , contains a contribution ψ_M' and the field strength $(d\psi(x)/dx)_M$ contains a contribution $(d\psi'(x)/dx)_M$ of the layers beyond M, originating from the semi-infinite series of bulk plane charges σ_* . Bearing in mind that now we only have to take the sum for $i > 0$, we find from eq. 3.21:

$$\psi_M' = \frac{\sigma_*}{2 \epsilon \kappa} \frac{\exp(-\kappa r_0)}{1 - \exp(-\kappa r_0)} \quad (3.23)$$

The potential decays exponentially with decreasing x , with a shielding length κ^{-1} , so

$$\left(\frac{d\psi'(x)}{dx} \right)_{x=x_M} = \kappa \psi_M' \quad (3.24)$$

The surface charge σ_0 and the plane charges σ_i contribute to the field strength by an amount $(d\psi''(x)/dx)_{x \downarrow x_M}$ at the solution side of plane charge σ_M . Since there the Debye-Hückel approximation is assumed to be valid, we have

$$\left(\frac{d\psi''(x)}{dx} \right)_{x \rightarrow x_M} = -\kappa (\psi_M - \psi'_M) \quad (3.25)$$

Hence the total field strength at the solution side of plane charge σ_M is

$$\begin{aligned} \left(\frac{d\psi'(x)}{dx} \right)_{x \rightarrow x_M} &= \left(\frac{d\psi'(x)}{dx} \right)_{x=x_M} + \left(\frac{d\psi''(x)}{dx} \right)_{x \rightarrow x_M} = \\ &= -\kappa\psi_M + 2\kappa\psi'_M \end{aligned} \quad (3.26)$$

We have the two boundary conditions and the two unknowns, the surface potential ψ_0 and the potential ψ_M , at the two ends of the interval to be integrated. As they are not at one side, we need an iteration procedure to obtain a solution satisfying the boundary conditions. We used ψ_M as the iteration variable, so that ψ_0 is found as result.

3.4 THE ELECTRICAL FREE ENERGY

3.4.1 THE ELECTRICAL FREE ENERGY OF A FLAT DOUBLE LAYER

Our model for an adsorbed polyelectrolyte consists of a series of equidistant plane charges with low molecular weight ions in between. The derivation of an expression for the electrical free energy of such a system is closely related to that for a single double layer at a surface. Such a system has been studied in detail before¹⁸. The electrical free energy of a double layer with a surface charge σ_0 is the isothermal reversible work to bring the charge σ_0 from the reference state, the situation with $\sigma_0 = 0$, to the surface. Several routes have been developed to perform this process¹⁸. For instance, we can bring charge from infinity to its place on the surface while all other constituents of the system have their final charge. Alternatively, we can charge sur-

face and other constituents concomitantly. In our system we have, apart from the surface charge and indifferent electrolyte, polyelectrolyte in the solution. We will first envisage the electrical free energy of a surface charge in the absence of polyelectrolyte and then introduce polyelectrolyte as a homogeneous solution. The charging procedures we will discuss involve (i), the transfer of the polyelectrolyte to its place in the polymer profile while the small ions are already charged and (ii), the charging of a given polymer profile and the small ions originating therefrom, with the indifferent electrolyte charged.

3.4.1.1 CHARGING A SURFACE IN THE ABSENCE OF POLYELECTROLYTE

The two procedures to charge such a system, with already charged indifferent electrolyte or with concomitant charging of the latter, have been described before by Verwey and Overbeek¹⁸. Casimir proved the general equivalence of both procedures¹⁹. We will verify the equivalence of the two procedures under the simplifying conditions of the Debye-Hückel approximation in order to obtain a clear insight in the charging processes before elaborating the polyelectrolyte case.

3.4.1.1.1 CHARGING A SURFACE IN THE PRESENCE OF CHARGED INDIFFERENT ELECTROLYTE

The electrical free energy dF_{el} to bring a charge $d\sigma'$ to the surface is

$$dF_{el} = \psi_0(\sigma') d\sigma' \quad (3.27)$$

where $\psi_0(\sigma')$ is the surface potential at the value σ' of the surface charge. Alternatively, when we introduce a charging parameter λ , running from 0 to 1 we find

$$dF_{el} = \sigma_0 \psi_0(\lambda) d\lambda \quad (3.28)$$

where σ_o is the final charge of the surface and $\psi_o(\lambda)$ the surface potential at a fractional charge $\lambda\sigma_o$. The values of $\psi_o(\lambda)$ during the charging process are obtained from the Poisson-Boltzmann equation. For an indifferent electrolyte concentration of \bar{n}_o molecules per unit volume of bulk solution the linearized Poisson-Boltzmann equation reads:

$$\frac{d^2\psi(x,\lambda)}{dx^2} = \frac{2\bar{n}_oe^2}{\epsilon\kappa T} \psi(x,\lambda) \equiv \kappa^2\psi(x,\lambda) \quad (3.29)$$

where $\psi(x,\lambda)$ is the potential at place x at the moment of the charging process where the charging parameter assumes the value λ . As boundary conditions we have:

(i). $\psi(x,\lambda)$ and $d\psi(x,\lambda)/dx$ are zero when x approaches infinity.

$$(ii) \quad \frac{d\psi(x=0,\lambda)}{dx} = - \frac{\lambda\sigma_o}{\epsilon} \quad (3.30)$$

The solution for the surface potential is

$$\psi_o(\lambda) = \frac{\lambda\sigma_o}{\epsilon\kappa} \quad (3.31)$$

Substitution into eq. 3.28 and integration gives:

$$F_{el} = \int_0^1 \frac{\lambda\sigma_o^2}{\epsilon\kappa} d\lambda = \frac{\sigma_o^2}{2\epsilon\kappa} \quad (3.32)$$

3.4.1.1.2 SIMULTANEOUS CHARGING OF A SURFACE AND INDIFFERENT ELECTROLYTE

Using the charging parameter λ the electrical free energy of charging a surface and i types of electrolyte ions, having a valence z_i and a concentration $n_i(x,\lambda)$, is

$$dF_{el} = \sigma_o\psi_o(\lambda) d\lambda + \int_0^\infty \sum_i z_i en_i(x,\lambda) \psi(x,\lambda) dx d\lambda \quad (3.33)$$

The concentration $n_i(x, \lambda)$ at place x depends on λ , since the small ions rearrange during the charging process. The total small ion concentration remains constant. For a 1 - 1 electrolyte solution the Poisson-Boltzmann equation for partially charged ions reads

$$\frac{d^2\psi(x, \lambda)}{dx^2} = \frac{\bar{n}_0 \lambda e}{\epsilon} \left[\exp(\lambda e \psi(x, \lambda)/kT) - \exp(-\lambda e \psi(x, \lambda)/kT) \right] \quad (3.34)$$

Application of the Debye-Hückel approximation yields

$$\frac{d^2\psi(x, \lambda)}{dx^2} = \frac{2 \bar{n}_0 \lambda^2 e^2}{\epsilon kT} \psi(x, \lambda) = \lambda^2 \kappa^2 \psi(x, \lambda) \quad (3.34a)$$

We have the same boundary conditions as in the previous section. The solution for the surface potential is

$$\psi_0(\lambda) = \frac{\lambda \sigma_0}{\epsilon \lambda \kappa} = \frac{\sigma_0}{\epsilon \kappa} \quad (3.35)$$

So we see that this charging process is performed at constant surface potential, which is equal to the final potential ψ_0 . The potential in the double layer is

$$\psi(x, \lambda) = \psi_0 \exp(-\kappa \lambda x) \quad (3.36)$$

Comparison of the potential distribution in the previous and this section shows that in the former the surface potential rises with λ and that the shielding length is constant, whereas here the surface potential remains constant while the shielding length $(\lambda \kappa)^{-1}$ decreases. Substituting eq. 3.35, eq. 3.36 and the Boltzmann distribution of the indifferent electrolyte into eq. 3.33 gives

$$dF_{el} = \left[\frac{\sigma_0^2}{\epsilon \kappa} - \int_0^\infty \frac{\sigma_0^2}{\epsilon} \exp(-2 \kappa \lambda x) dx \right] d\lambda \quad (3.37)$$

The electrical free energy F_{el} is obtained by integration over x and λ :

$$F_{el} = \frac{\sigma_0^2}{2\epsilon\kappa} \quad (3.38)$$

This result was also obtained in the previous section (eq. 3.32), so that the equivalence has been proven.

3.4.1.2 CHARGING A SURFACE IN THE PRESENCE OF POLYELECTROLYTE

In a system containing a surface charge, a homogeneous polyelectrolyte solution and indifferent electrolyte, a variety of charging procedures can be developed. Since we are interested in charging plane charges and polyelectrolyte we consider the following alternatives:

- (i) Charging the surface, while the polyelectrolyte and the small ions are charged. This procedure mimicks the procedure to build up an adsorbed layer of polyelectrolyte by transferring segments from the reference potential at infinity to their place in the adsorbed layer. In this case an amount of segments corresponding to the bulk volume fraction need not to be transferred, i.e. charged.
- (ii) Charging the surface with concomitant charging of the polyelectrolyte while the indifferent electrolyte is charged. This procedure mimicks the charging of the uncharged polymer in a predetermined concentration profile, by which the adsorbed layer as well as the bulk polyelectrolyte are being charged.

We will now prove that both procedures lead to the same result. For the sake of simplicity we assume that the polymer has a homogeneous bulk concentration throughout the system. To arrive at simple expressions it is convenient to apply the Debye-Hückel approximation and a smeared out space charge density ρ_* here, rather than the plane charges σ_* . In doing so we avoid a toothed potential profile (figure 3.1). Instead, a potential decaying exponentially to a constant bulk value is obtained.

3.4.1.2.1 CHARGING A SURFACE IN THE PRESENCE OF CHARGED POLYELECTROLYTE

In this case the derivation of the electrical free energy is analogous to that in section 3.4.1.1.1. There is a slight difference: the Poisson-Boltzmann equation has to be modified to account for the space charge of the polyelectrolyte and its counterions. Instead of a plane charge σ_* we introduce the space charge ρ_* :

$$\rho_* = zae\phi_*/a_0r_0 \quad (3.39)$$

Combining eq. 3.39 with the Poisson-Boltzmann equation (3.7) yields

$$\frac{d^2\psi(x,\lambda)}{dx^2} = \kappa^2 \left[\psi(x,\lambda) - \frac{\bar{n}_+\bar{\psi}_+ + \bar{n}_-\bar{\psi}_-}{\bar{n}_+ + \bar{n}_-} \right] \quad (3.40)$$

with κ^2 defined as in eq. 3.6. Defining b zero in eq. 3.7 implies that here $\bar{\psi}_+$ and $\bar{\psi}_-$ are zero. Far away from the surface $\psi(x,\lambda)$ is zero and the small ions reach their stoichiometric concentrations \bar{n}_+ and \bar{n}_- . Following section 3.4.1.1.1 we obtain for F_{el} :

$$F_{el} = \frac{\sigma_0^2}{2\epsilon\kappa} \quad (3.41)$$

3.4.1.2.2 CHARGING A SURFACE WITH CONCOMITANT CHARGING OF THE POLYELECTROLYTE

In this case we must count the contribution to the electrical free energy due to the charging of the surface, as well as that of the polyelectrolyte and the small ions originating from this polyelectrolyte. In the bulk solution there are \bar{n}_p of such ions present per unit volume:

$$\bar{n}_p = \alpha\phi_*/a_0r_0 = \rho_*/ze \quad (3.42)$$

The electrical free energy to charge the polymer segments in an infinitesimal space shell with width dx by an amount $zed\lambda$ is, depending on the potential at the position of the unit volume:

$$dF_{el} = \rho_* \psi(x, \lambda) d\lambda dx \quad (3.43)$$

In such a volume the concentration of counterions, originating from the polymer and each bearing a charge λe , is

$$n_p = \bar{n}_p \exp(z\lambda e\psi(x, \lambda)/kT) \quad (3.44)$$

The electrical free energy of charging these ions in the space shell by $-zed\lambda$ is

$$dF_{el} = -zen_p \exp(z\lambda e\psi(x, \lambda)/kT) \psi(x, \lambda) d\lambda dx \quad (3.45)$$

or, applying the Debye-Hückel approximation

$$dF_{el} = -zen_p \psi(x, \lambda) (1 + z\lambda e\psi(x, \lambda)/kT) d\lambda dx \quad (3.46)$$

Combining eq. 3.43 and 3.46 with the electrical free energy of charging the surface (eq. 3.28) gives

$$dF_{el} = \left[\sigma_o \psi_o(x, \lambda) - \int_{-\infty}^0 \bar{n}_p \lambda e^2 \psi(x, \lambda) dx \right] d\lambda \quad (3.47)$$

Again the values of $\psi(x, \lambda)$ are obtained from the Poisson-Boltzmann equation. Herein the same components of charge are incorporated as in the presence of already charged polyelectrolyte (see section 3.4.1.2.1). However, now the charge of the polymer and the counterions originating from that polymer both depend on λ :

$$\frac{d^2 \psi(x, \lambda)}{dx^2} = (2 \bar{n}_o + \bar{n}_p \lambda^2) e^2 \psi(x, \lambda) / \epsilon kT \quad (3.48)$$

In this model the shielding length κ^{-1} depends on λ :

$$\kappa(\lambda)^2 = (2 \bar{n}_o + \bar{n}_p \lambda^2) e^2 / \epsilon k T \quad (3.49)$$

Introducing the usual boundary conditions, the solution for the surface potential is found to be

$$\psi_o(\lambda) = \frac{\lambda \sigma_o}{\epsilon \kappa(\lambda)} \quad (3.50)$$

From equation 3.49 and 3.50 it can be seen that, as long as (charged) indifferent electrolyte is present, neither $\psi_o(\lambda)$ nor $\kappa(\lambda)$ is constant during the charging process. In analogy to the charging of a double layer with simultaneous charging of surface and indifferent electrolyte (see section 3.4.1.1.2), $\psi_o(x, \lambda)$ is constant and $\kappa(\lambda)$ is proportional to λ , if no indifferent electrolyte is present. If the polyelectrolyte concentration is zero, the procedure described in this section converges with that of the charging of a flat surface with the indifferent electrolyte charged. Then $\psi_o(\lambda)$ is proportional to λ and κ is constant. The value of $\psi(x, \lambda)$ in the double layer is given by

$$\psi(x, \lambda) = \psi_o(\lambda) \exp(-\kappa(\lambda)x) \quad (3.51)$$

Substitution of eq. 3.50 and 3.51 into 3.47 and integration with respect to x gives:

$$dF_{el} = \frac{\sigma_o^2 (\epsilon k T)^{\frac{1}{2}}}{\epsilon e} \left[\frac{\lambda}{(2 \bar{n}_o + \lambda^2 \bar{n}_p)^{\frac{1}{2}}} - \frac{\lambda^3 \bar{n}_p}{2(2 \bar{n}_o + \lambda^2 \bar{n}_p)^{\frac{3}{2}}} \right] d\lambda \quad (3.52)$$

Partial integration of the second term of the right hand side gives

$$\int_0^1 \frac{\lambda^3 \bar{n}_p}{2(2\bar{n}_o + \lambda^2 \bar{n}_p)^{3/2}} d\lambda = \frac{\lambda^2}{2(2\bar{n}_o + \lambda^2 \bar{n}_p)^{1/2}} \bigg|_0^1 - \int_0^1 \frac{\lambda}{(2\bar{n}_o + \lambda^2 \bar{n}_p)^{1/2}} d\lambda \quad (3.53)$$

The second right hand term of eq. 3.53 just cancels against the first right hand term of equation 3.52, so we end up with

$$F_{el} = \frac{\sigma_o^2}{2 \epsilon \kappa (\lambda=1)} \quad (3.54)$$

This result was also obtained with pre-charged polyelectrolytes (section 3.4.1.2.1). At $\lambda = 1$ the definitions of the shielding length κ^{-1} converge, since $\bar{n}_+ + \bar{n}_- = 2\bar{n}_o + \bar{n}_p$.

We can conclude that in the case of a double layer of a planar surface charge with polyelectrolyte at the bulk concentration throughout the system, the same electrical free energy is obtained in the Debye-Hückel approach, when we bring charge to the surface while charged polyelectrolyte is present or when we charge surface and polyelectrolyte simultaneously.

3.4.2 THE ELECTRICAL FREE ENERGY OF A CHARGED POLYELECTROLYTE CONCENTRATION PROFILE

In section 3.4.1 we envisaged several charging procedures for a Debye-Hückel type double layer of a surface charge. These procedures can be generalized for a given series of plane charges near a surface. For such a system the equivalent of eq. 3.27 is

$$dF_{el} = \sum_i \psi_i d\sigma_i \quad (3.55)$$

In this case the integration over λ to obtain the electrical free

energy is not easily achieved analytically. However, if the Debye-Hückel approximation is applied, the results for a surface charge can easily be generalized for a series of plane charges, because the potentials originating from each charge are independent and additive. Using the charging parameter λ we can write

$$dF_{el} = \sum_i \psi_i(\lambda)(\sigma_i - \sigma_*) d\lambda \quad (3.56)$$

As $\psi_i(\lambda)$ is proportional to λ integration yields

$$F_{el} = \frac{1}{2} \sum_i \psi_i (\sigma_i - \sigma_*) \quad (3.57)$$

If the Debye-Hückel approximation may not be used, only a numerical evaluation of the electrical free energy is possible. We employed both procedures of charging planes described in section 3.4.1.2 for a predetermined exponential polymer concentration profile with the use of the full Poisson-Boltzmann equation. As could be anticipated, the same electrical free energy is obtained. However, the build-up during the charging process is different, as can be seen from figure 3.3. When adsorbed and bulk polyelectrolyte are charged simultaneously (case a), the shielding power of the counterions of the polymer is small at low λ because of their low charge. So the potentials ψ_i show an initial steep rise and so does F_{el} . At higher values of λ shielding increases and at a not too high indifferent electrolyte concentration the potentials even decrease. On the other hand, when the bulk polyelectrolyte is already charged and only the excess adsorbed polymer is to be charged, or for that matter, when the polymer is charged by transferring charge from infinity to its position in the double layer, the shielding power is constant and the potentials rise monotonically. The levelling off of $dF_{el}/d\lambda$ in curve b stems from the fact that at high potentials the potential rises less strongly than at low ones, if the Debye-Hückel approximation is not applied. The more gradual build-up of the electrical free energy using this method facilitates accurate numerical integration and hence our computations to be discussed below are mainly based on this second procedure.

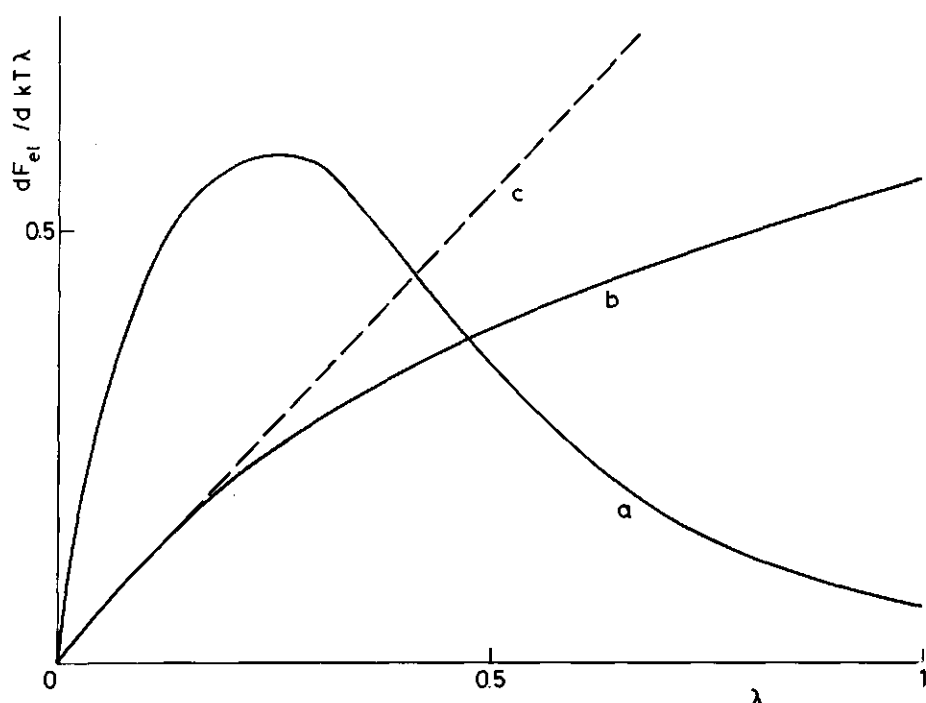


Figure 3.3. Change in electrical free energy during the charging procedure. a. Simultaneous charging of adsorbed polyelectrolyte, bulk polyelectrolyte and counterions originating from the polyelectrolyte. b. Charging of the excess adsorbed amount by transferring charge from infinity to the adsorbed layer. c. as b, but in the Debye-Hückel approximation. In all cases the indifferent electrolyte is already charged. Uncharged adsorbent, electrolyte 10^{-3} M, $\alpha = 1$, $a_0 = 1 \text{ nm}^2$, $r_0 = 1 \text{ nm}$, $\phi_* = 10^{-2}$, $\phi_i = 0.1 \exp(-0.4 i)$.

3.5 THE ELECTRICAL FREE ENERGY OF THE BULK SOLUTION AND CONSEQUENCES FOR PHASE SEPARATION

As the homogeneous bulk volume fraction is used as the reference state in the polyelectrolyte adsorption theory, it is worthwhile to pay some attention to the electrical free energy of the bulk solution and its consequences for phase separation.

Phase separation occurs in polymer solutions when the solvent is

poor, *i.e.* when the Flory solvent quality parameter χ is high. A high χ -value means that the polymer segments attract each other preferentially over the solvent. Then it is thermodynamically favourable for the solution to separate into a polymer-rich and a polymer-poor phase. It is anticipated that, as compared with uncharged macromolecules of the same molecular weight, polyelectrolytes will give stable solutions up to higher χ -values, since in concentrated phases high potentials develop that oppose the non-electrical attracting forces.

3.5.1 PHASE SEPARATION WITH UNCHARGED POLYMERS

Flory²⁰ derived an expression for the free energy of mixing a polymer and a solvent using a lattice model which was later used by Roe¹⁰ and Scheutjens and Fleer¹¹. Since he describes the situation in the bulk solution, no layers had to be specified and a homogeneous volume fraction was assumed. For the free energy of mixing ΔF_M for a system containing N_1 polymer molecules and N_0 solvent molecules Flory obtained

$$\Delta F_M = kT (N_1 \ln \phi_* + N_0 \ln (1-\phi_*) + \chi N_0 \phi_*) \quad (3.58)$$

with ϕ_* the polymer bulk volume fraction. Differentiation of ΔF_M with respect to N_1 and N_0 gives the thermodynamic potentials of the polymer, μ_1 , and that of the solvent, μ_0 , respectively. If two phases can coexist, the equilibrium criterion²¹ is

$$\begin{aligned} \mu_0 &= \mu_0^+ \\ \mu_1 &= \mu_1^+ \end{aligned} \quad (3.59)$$

where the plus indicates the--arbitrarily chosen--reference phase. When polymer and solvent are miscible in all proportions, μ_0 and μ_1 are monotonically decreasing and increasing functions of ϕ_* respectively. The values of μ_0 and of μ_1 at $\phi_* = 0$ and $\phi_* = 1$ do not depend on the solvent quality parameter χ . Consequently, if there are two polymer volume fractions with equal chemical poten-

tials, μ_0 and μ_1 must both have a maximum and a minimum as a function of ϕ_* . There is a certain value of χ and of ϕ_* , which is called the critical point. In this point neither a minimum nor a maximum is present, but just an inflection point. The following conditions are met here:

$$\begin{aligned}\frac{d\mu_0}{d\phi_*} &= 0 \\ \frac{d^2\mu_0}{d\phi_*^2} &= 0\end{aligned}\tag{3.60}$$

If eq. 3.60 is satisfied, the first and second derivative of μ_1 are also zero, since μ_1 is obtained from the same free energy of mixing. However, this gives no additional information, since μ_0

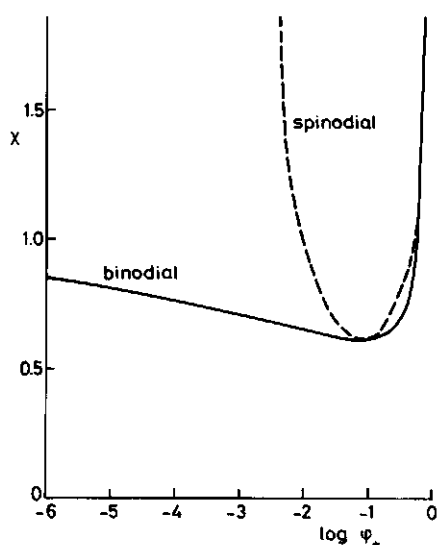


Figure 3.4. Phase diagram for uncharged polymer. $r = 100$.

and μ_1 are related through the Gibbs-Duhem equation. Figure 3.4 gives a phase diagram containing the so-called binodal as obtained from eq. 3.58 and 3.59. The minimum is the critical point determined by eq. 3.60. Below the corresponding χ -value the polymer-solvent system is completely miscible over the entire composition range. Figure 3.4 also presents the so-called spinodal. It appears that solutions can exist in a metastable state in the domain between the binodal and spinodal. If at some place in the solution the concentration rises to a value higher than the boundary of the spinodal area,

phase separation occurs, and two phases with concentrations corresponding to the binodal ensue. The background of the spinodal is illustrated by figure 3.5.

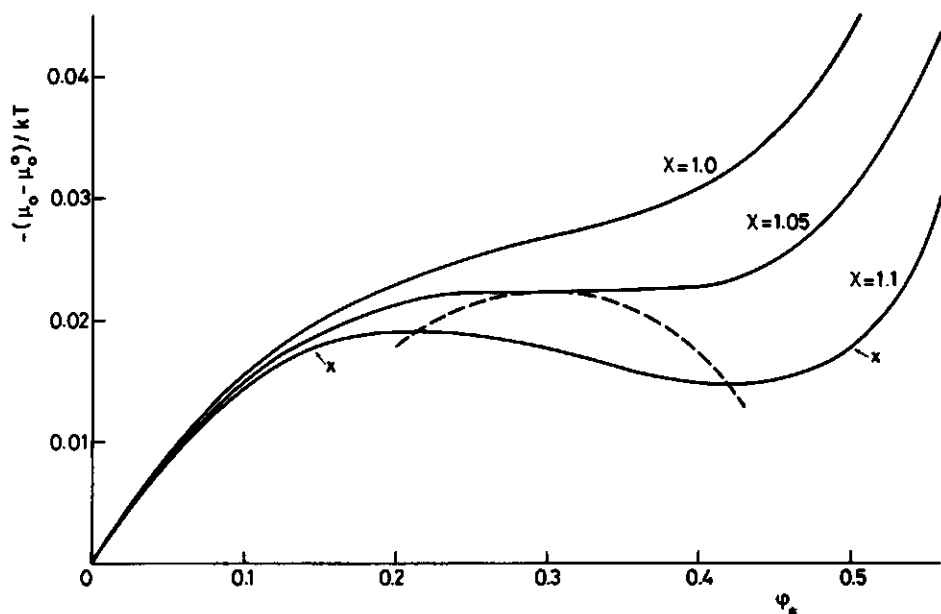


Figure 3.5. Thermodynamic potential of the solvent as a function of the polymer volume fraction (—). The critical χ -value is 1.05. Chain length $r = 5$. x : volume fractions from binodal at $\chi = 1.1$. The points forming the spinodal are indicated (----). μ_0^0 is the chemical potential of the pure solvent.

Figure 3.5 gives the chemical potential of the solvent as a function of the polymer fraction. At χ -values exceeding the critical one (here $\chi = 1.05$) a minimum and a maximum are observed. Only in the cases of the curves a and b there is full miscibility. In the case of curve c there is miscibility until the volume fraction of the corresponding binodal (x) is reached. However one can imagine that as long as the slope of the chemical potential curve is not very different from that of a curve for a stable solution, no discontinuity is observed in reality either, i.e. metastable solutions are possible. This situation persists until the maximum in $-(\mu_0 - \mu_0^0)$ is reached after increasing ϕ_* , or if the minimum is reached after decreasing ϕ_* . At volume fractions higher than those corresponding to the maximum or the minimum, phase separation must occur. So the spinodal range is bound by the two concentrations

where

$$\frac{d\mu_0}{d\phi_*} = 0 \quad (3.61)$$

3.5.2 PHASE SEPARATION WITH POLYELECTROLYTES

To describe phase separation of polyelectrolyte solutions we follow the Flory line²¹. The electrical free energy of mixing, $\Delta F_{M,el}$, is given and from this $\Delta F_{M,el}$ the electrical part of the chemical potential of the solvent, $\mu_{0,el}$, and of the polymer, $\mu_{1,el}$, is obtained. The electrical free energy of mixing $\Delta F_{M,el}$ is obtained from the potential difference between two polymer phases. We will derive the potential difference by solving the Poisson-Boltzmann equation in both phases. An equivalent derivation is possible, i.e. considering the distribution of the small ions and the potentials as a Donnan equilibrium. The description of Donnan equilibria usually refers to one colloid- or polymer-containing phase in equilibrium with a phase only comprising in different electrolyte. Here we deal with two macromolecular phases, but also then it is possible to follow the Donnan line. Of course, there exists always an electrolyte solution of such a composition as to be in equilibrium with both phases, the (equilibrium) dialysate.

As it is inconsistent to use a plane model for a homogeneous bulk solution, it is better to use smeared out polyelectrolyte charges. The use of smeared out polyelectrolyte charges has been criticized by Klaarenbeek²³ and Overbeek^{24,25}, since inhomogeneities occur, because the segments are bound to each other. At low polymer concentration the polyelectrolyte charge is restricted to the individual coils. As a consequence low activity coefficients are found for the counterions, which is reflected by a reduced osmotic pressure. As we only pay attention to the interaction between polymer segments and solvent molecules, the classical Donnan picture will work better in our case.

Our analysis can be done both for the Debye-Hückel and the Gouy-Chapman approach of the Poisson-Boltzmann equation. Since the potential difference between two phases can attain considerable

values, the Gouy-Chapman approach will usually lead to better results. However it is useful to elaborate the Debye-Hückel case as well, since then we arrive at equations that physically can be interpreted more easily.

3.5.2.1 THE POTENTIAL DIFFERENCE BETWEEN THE TWO PHASES

For a polyelectrolyte solution with volume fraction ϕ_* we define the space charge ρ_* originating from the polyelectrolyte

$$\rho_* = z\alpha e\phi_*/v_0 \quad (3.62)$$

where v_0 is the volume of a lattice cell. In analogy to eq. 3.5 we have the Poisson-Boltzmann equation:

$$\frac{d^2\psi(x)}{dx^2} = -\frac{e}{\epsilon} \left[\bar{n}_+ \exp[-e(\psi(x) - \bar{\psi}_+)/kT] - \bar{n}_- \exp[e(\psi(x) - \bar{\psi}_-)/kT] + \rho_*/e \right] \quad (3.63)$$

The potential is constant throughout such a polyelectrolyte solution and the electroneutrality condition must be satisfied, so $d^2\psi(x)/dx^2 = 0$. We shall now work out the potential difference between the two phases, first by using the Debye-Hückel approximation of eq. 3.63 and then for the Gouy-Chapman approach.

3.5.2.1.1 THE DEBYE-HÜCKEL APPROACH

Linearization of eq. 3.63 gives

$$\frac{d^2\psi(x)}{dx^2} = \kappa^2 \left[\psi(x) - \frac{(\bar{n}_+ - \bar{n}_-)kT/e + \bar{n}_+\bar{\psi}_+ + \bar{n}_-\bar{\psi}_- + \rho_*kT/e^2}{\bar{n}_+ + \bar{n}_-} \right] \quad (3.64)$$

An obvious solution is $\bar{\psi}_+ = \bar{\psi}_- = \psi(x) = 0$ with $\bar{n}_+ - \bar{n}_- + \rho_*/e = 0$. If we have two phases in equilibrium we can choose one of them as the reference phase where $\bar{\psi}_+ = \bar{\psi}_- = \psi(x)^+ = 0$ and calculate the potential of the other phase with respect to the reference potential. We will indicate the potential, the volume fraction and the polyelectrolyte space charge of the reference phase with a plus sign. Here we encounter one of the more serious imperfections of the Debye-Hückel approximation. The fact is that the solution of the linearized Poisson-Boltzmann equation is not invariant with respect to the choice of the reference potential. In other words, it matters which phase is chosen as the reference phase. Attributing a space charge ρ_*^+ to the reference phase and a space charge ρ_* to the other, eq. 3.64 can be transformed to the corresponding equation for the non-reference phase:

$$\frac{d^2\psi(x)}{dx^2} = \kappa^2 \left[\psi(x) + \frac{\rho_*^+}{\epsilon\kappa^2} - \frac{\rho_*}{\epsilon\kappa^2} \right] \quad (3.65)$$

Since this phase is also electroneutral, the potential with respect to the reference phase is

$$\psi(x) = (\rho_* - \rho_*^+)/\epsilon\kappa^2 \quad (3.66)$$

The asymmetry is in the definition of κ^2 . This κ^2 contains the total number of small ions in the reference phase, but this number is different for both phases.

3.5.2.1.2 THE GOUY-CHAPMAN APPROACH

Again we choose a reference phase with $\bar{\psi}_+ = \bar{\psi}_- = \psi(x)^+ = 0$ and also $\bar{n}_+ - \bar{n}_- + \rho_*^+/e = 0$. The Poisson-Boltzmann equation for another phase having a space charge density ρ_* reads then

$$\frac{d^2\psi(x)}{dx^2} = -\frac{e}{\epsilon} \left[\bar{n}_+ \exp(-e\psi(x)/kT) - \bar{n}_- \exp(e\psi(x)/kT) + \rho_*/e \right] = 0 \quad (3.67)$$

When we substitute y for $\exp(e\psi(x)/kT)$ we obtain a quadratic equation in y :

$$\bar{n}_- y^2 - \rho_+ y/e - \bar{n}_+ = 0 \quad (3.68)$$

The physically interesting solution is

$$\psi(x) = \frac{kT}{e} \ln \left(\frac{\rho_+/e + \sqrt{(\rho_+/e)^2 + 4\bar{n}_+\bar{n}_-}}{2\bar{n}_-} \right) \quad (3.69)^*$$

The concentration of the small ions in the non-reference phase, $\bar{n}_+'_+$, which corresponds to the indifferent electrolyte concentration is given by

$$\bar{n}_+'_+ = \bar{n}_+ \exp(-e\psi(x)/kT)$$

If the phase having a polymer space charge ρ_+ and a salt concentration equal to $\bar{n}_+'_+$ is chosen as the reference phase--(i.e. $\psi(x)' = \bar{\psi}_+ = \bar{\psi}_- = 0$)--the same potential difference with the phase with space charge ρ_+ and positive ion concentration \bar{n}_+ is found. So the calculated potential difference between the two phases does not depend on the choice of the reference potential. The salt concentration difference between the two phases is given by the Donnan membrane equilibrium condition. For example, for a polymer-free solution in equilibrium with a reference polyelectrolyte solution equations 3.67 and 3.69 give $\sqrt{\bar{n}_+\bar{n}_-}$ for the salt concentration. This is in agreement with the Donnan equilibrium^{24,25}.

3.5.2.2 THE ELECTRICAL FREE ENERGY OF MIXING

The electrical free energy of mixing $\Delta F_{M,el}$ of a system containing N_0 solvent and N_1 polymer molecules is found from the

* Obviously this equation cannot be used in the case of negative polyelectrolyte without added salt. In that case we can choose $y = \exp(-e\psi(x)/kT)$ and derive a complementary set of equations.

electrical free energy per lattice cell Δf_{el} and the size of the system. Flory derives the non-electrical free energy of mixing with respect to the pure components as the reference states²⁰. For our purpose these are not suitable reference states because of the above mentioned asymmetry due to the Debye-Hückel linearization and cumbersome definition of the salt concentration that would be needed in the Gouy-Chapman approach. Since we are only interested in differences in thermodynamic potentials we can in principle choose the reference state freely. To bear out the implications of this choice it is useful to choose one of the phases under investigation as the reference phase.

In analogy to eq. 3.27 we can write for the change in electrical free energy of a unit volume, df_{el} , upon raising the space charge density by an amount $d\rho_*$

$$df_{el} = \psi(x) d\rho_*' \quad (3.70)$$

To obtain Δf_{el} with respect to a reference phase we must integrate the space charge from ρ_*^+ to ρ_* . As before we will do this first for the Debye-Hückel and then for the Gouy-Chapman approach.

3.5.2.2.1 THE DEBYE-HÜCKEL APPROACH

Substitution of equation 3.66 into 3.70 and integration yields

$$\Delta f_{el} = \int_{\rho_*^+}^{\rho_*} \psi(x) d\rho_*' = \frac{(\rho_* - \rho_*^+)^2}{2 \varepsilon_K^2} \quad (3.71)$$

The total electrical free energy of mixing is

$$\Delta F_{M,el} = (N_0 + rN_1)v_0 \Delta f_{el} \quad (3.72)$$

or

$$\Delta F_{M,el} = (N_0 + rN_1) \frac{\alpha^2 e^2 (\phi_* - \phi_*^+)^2}{2 v_0 \varepsilon_K^2} \quad (3.73)$$

3.5.2.2.2 THE GOUY-CHAPMAN APPROACH

Substitution of equation 3.69 into 3.70 and integration yields

$$\Delta f_{el} = \int_{\rho_*^+}^{\rho_*} \psi(x) d\rho_*' = \rho_* \psi(x) - kT \left[\sqrt{(\rho_*/e)^2 + 4 \bar{n}_+ \bar{n}_-} - \sqrt{(\rho_*^+/e)^2 + 4 \bar{n}_+ \bar{n}_-} \right] \quad (3.74)$$

The total electrical free energy of mixing is again

$$\Delta F_{M,el} = (N_0 + rN_1) v_0 \Delta f_{el} \quad (3.72)$$

3.5.2.3 THE ELECTRICAL PART OF THE CHEMICAL POTENTIAL

Differentiation of $\Delta F_{M,el}$ with respect to N_0 and N_1 respectively gives the electrical part of the chemical potential of the solvent $\mu_{0,el}$ and of the polymer $\mu_{1,el}$. This differentiation can be applied both for the linearized and full Poisson-Boltzmann equation.

3.5.2.3.1 THE DEBYE-HÜCKEL APPROACH

Bearing in mind that the bulk volume fraction is

$$\phi_* = \frac{rN_1}{N_0 + rN_1} \quad (3.75)$$

we obtain from eq. 3.72 for the chemical potentials:

$$\mu_{0,el}/kT = - \xi [(\phi_*^2 - (\phi_*^+)^2)] \quad (3.76)$$

and

$$\mu_{1,el}/kT = - r\xi [(1 - \phi_*)^2 - (1 - \phi_*^+)^2] \quad (3.77)$$

with

$$\xi = \frac{e^2 \alpha^2}{2 v_o \epsilon \kappa^2 kT} = \frac{\alpha^2}{2 v_o (\bar{n}_+ + \bar{n}_-)} \quad (3.78)$$

3.5.2.3.2 THE GOUY-CHAPMAN APPROACH

From the equations 3.74 and 3.72 we obtain

$$\mu_{o,el}/kT = - v_o [\sqrt{(\rho_*/e)^2 + 4 \bar{n}_+ \bar{n}_-} - \sqrt{(\rho_*/e)^2 + 4 \bar{n}_+ \bar{n}_-}] \quad (3.79)$$

and

$$\mu_{1,el}/kT = - v_o r [\sqrt{(\rho_*/e)^2 + 4 \bar{n}_+ \bar{n}_-} - \sqrt{(\rho_*/e)^2 + 4 \bar{n}_+ \bar{n}_-}] + r \alpha e \psi(x)/kT \quad (3.80)$$

3.5.2.4 PHASE EQUILIBRIA

The electrical parts of the chemical potentials of solvent and polymer can be added to the non-electrical parts as given by Flory. Here we do not choose the pure bulk polymer as the reference state but a given volume fraction ϕ_*^+ .

3.5.2.4.1 THE DEBYE-HÜCKEL APPROACH

Combining the non-electrical part (ref. 20 equations 26 and 32) and the electrical part (equations 3.76 and 3.77) of the chemical potential gives

$$\mu_o/kT = \ln \frac{(1 - \phi_*)}{(1 - \phi_*^+)} + (1 - 1/r)(\phi_* - \phi_*^+) + (\chi - \xi)(\phi_*^2 - (\phi_*^+)^2) \quad (3.81)$$

and

$$\mu_1/kT = \ln \frac{\phi_*}{\phi_*^+} - (r-1)(\phi_*^+ - \phi_*) + r(\chi - \xi)[(1 - \phi_*)^2 - (1 - \phi_*^+)^2] \quad (3.82)$$

The result is that the expression for the chemical potential is similar for charged and uncharged polymers. The difference is, that the Flory polymer solvent parameter χ is replaced by an effective interaction parameter $\chi - \xi$.

The critical point,--(i.e. the highest χ -value, where solvent and polymer are miscible in all proportions)--is given by the criteria of eq. 3.60. They yield

$$\phi_{*,cr} = (1 + \sqrt{r})^{-1} \quad (3.83)$$

and

$$\chi_{cr} = \frac{1}{2(1 - \phi_{*,cr})^2} + \xi \quad (3.84)$$

where $\phi_{*,cr}$ and χ_{cr} are the volume fraction and χ -value at the critical point respectively. These expressions show that the critical volume fraction is not changed by the presence of charges. However, the critical χ -value is increased, as anticipated.

The spinodial--(i.e. the curve that forms the boundary between the region where metastable solutions can exist and the unstable region)--is given by the criterion of equation 3.61. Differentiating eq. 3.81 yields

$$\frac{d\mu_0/kT}{d\phi_*} = -\frac{1}{(1 - \phi_*)} + (1 - 1/r) + 2(\chi - \xi)\phi_* = 0 \quad (3.85)$$

Each combination of χ and ϕ_* satisfying eq. 3.85 can be found readily.

The binodial--(i.e. the curve giving the stable phase compositions)--is found by equating the thermodynamic potentials of the two coexisting phases (eq. 3.59). These two equations contain two unknowns, viz. the polymer concentrations in the two phases, ϕ_* and ϕ_* , which can be obtained numerically by using an iteration procedure.

3.5.2.4.2 THE GOUY-CHAPMAN APPROACH

In this case, the introduction of an electrical contribution into the thermodynamic potential cannot be formulated generally as a modification in one of the terms in the non-electrical part. The first and second derivatives of the electrical part of the thermodynamic potential can be evaluated and added to the non-electrical part. Proceeding this way we obtain two equations with two unknowns for the critical point and a relation for the spinodal. These equations can easily be solved numerically. The first and second derivatives of the electrical part of the chemical potential read as follows

$$\frac{d\mu_{o,el}/kT}{d\phi_*} = \frac{\alpha\rho_*}{e [(\rho_*/e)^2 + 4 \bar{n}_+ \bar{n}_-]^{1/2}} \quad (3.86)$$

and

$$\frac{d^2\mu_{o,el}/kT}{d\phi_*^2} = \frac{4 \alpha^2 \bar{n}_+ \bar{n}_-}{v_o [(\rho_*/e)^2 - 4 \bar{n}_+ \bar{n}_-]^{3/2}} \quad (3.87)$$

Only in the case of the absence of salt the expressions can be simplified. For the potential difference between the two phases we have then:

$$\psi(x) = \frac{kT}{e} \ln \frac{\phi_*}{\phi_*} \quad (3.88)$$

and for the electrical parts of the chemical potentials

$$\mu_{O,el}/kT = -\alpha (\phi_* - \phi_*^+) \quad (3.89)$$

and

$$\mu_{1,el}/kT = -r\alpha (\phi_* - \phi_*^+) + r\alpha \ln \frac{\phi_*}{\phi_*^+} \quad (3.90)$$

Combination with the non-electrical part gives for the thermodynamic potential of the solvent

$$\begin{aligned} \mu_O/kT = \ln \frac{(1 - \phi_*)}{(1 - \phi_*^+)} + (1 - 1/r - \alpha)(\phi_* - \phi_*^+) + \\ \chi[\phi_*^2 - (\phi_*^+)^2] \end{aligned} \quad (3.91)$$

and for the polymer, expressed per segment

$$\begin{aligned} \mu_1/rkT = (1/r + \alpha) \ln \frac{\phi_*}{\phi_*^+} - (1 - 1/r - \alpha)(\phi_*^+ - \phi_*) + \\ \chi[(1 - \phi_*)^2 - (1 - \phi_*^+)^2] \end{aligned} \quad (3.92)$$

Comparison with the equations 3.81 and 3.82 shows that we can interpret the influence of the electrostatic interactions as a reduction in the effective chain length r_{eff} :

$$r_{eff} = \frac{r}{1 + \alpha r} \quad (3.93)$$

As is the case with the Debye-Hückel approach, the phase composition is found by combining the electrical and non-electrical contributions to the chemical potentials and equating them for both phases.

3.5.3 RESULTS AND DISCUSSIONS

3.5.3.1 THE BEHAVIOUR OF POLYMER ADSORPTION THEORIES NEAR THE PHASE SEPARATION DOMAIN

The two polymer adsorption theories that we will employ, namely the Roe theory and the Scheutjens-Fleer theory, both assume a pre-determined polymer bulk volume fraction and thus a fixed chemical potential. So they assume an open system. The total amount of polymer in the concentration profile is a result of the computations. If the bulk volume fraction is outside the phase separation domain, the polymer concentration profile decays to the bulk volume fraction. If a chemical potential is chosen in the phase separation domain, the computer programme gives a profile that decays to a

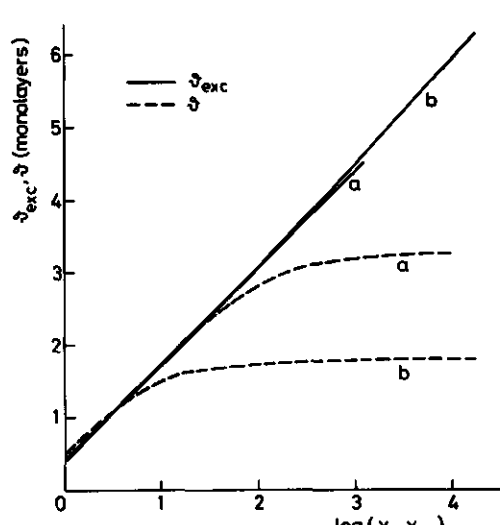


Figure 3.6. Adsorbed amount $\bar{\phi}$ (---) and excess adsorbed amount $\bar{\phi}_{exc}$ (—) as a function of $\log(\chi - \chi_{cr})$. a: $\chi_{cr} = 0.7$, $\chi_s = 1$, $\phi_* = 0.0015014430$, $r = 100$; b: $\chi_{cr} = 1$, $\chi_s = 1$, $\phi_* = 0.0427971$, $r = 10$.

volume fraction corresponding to the given chemical potential but in the stable domain. Because of iteration problems it is difficult to obtain results under the conditions with the Scheutjens-Fleer theory. If the chemical potential is in the metastable domain, a disturbance of the polymer concentration profile must ensue to bring the concentration within the spinodal. Such a disturbance can be caused by an adsorbing surface. As long as the macromolecules remain uncharged, the results of both adsorption theories appear to be very sensitive to super-critical conditions. However, for polyelectrolytes the results show a less sharp reaction to critical conditions. In this case, possibly due to long-range electrical

interaction forces, oscillating volume fraction profiles are calculated, which depend very much on the starting estimation of the profile.

With uncharged polymers very thick adsorbed layers develop, when at a given volume fraction the critical χ is approached. Only part of the adsorbed polymer molecules is directly attached to the surface. A considerable part is only present by virtue of the polymer-polymer attraction. Figure 3.6 gives the directly adsorbed amount, δ , and the excess amount adsorbed, δ_{exc} , as a function of the difference between χ and the critical χ , as calculated with the Scheutjens-Fleer theory. The near-linear relationship between δ_{exc} and $\log(\chi - \chi_{\text{cr}})$ is striking. At very small differences between

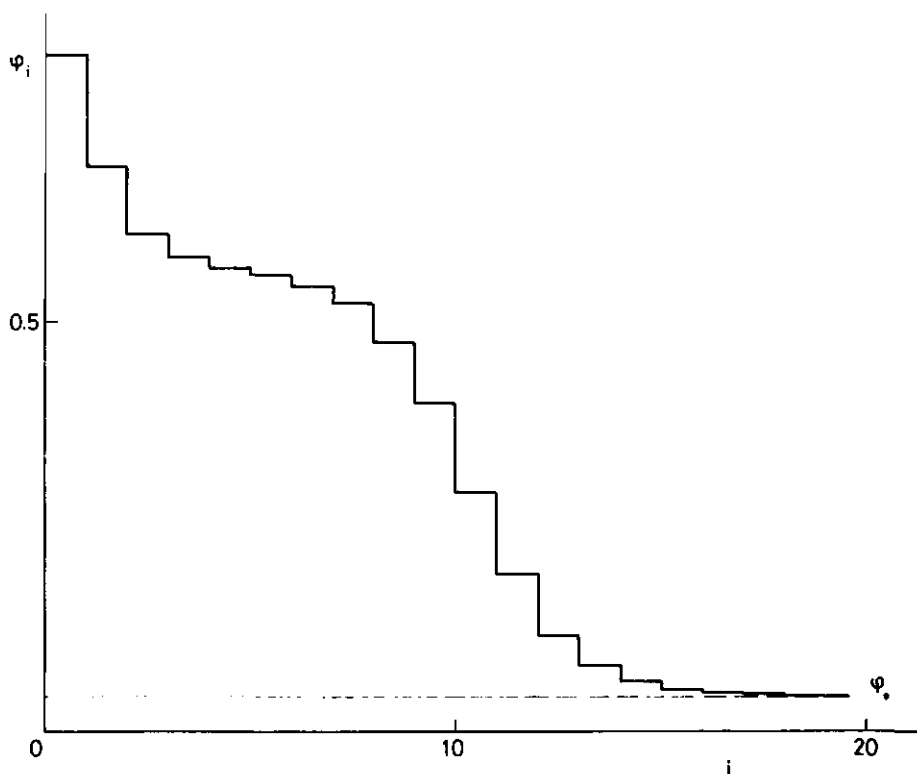


Figure 3.7. Polymer concentration profile near the critical χ calculated by using the Scheutjens-Fleer theory. $\chi = 0.9999$, $\chi_s = 1$, $\phi_* = 0.0427971$, $r = 10$.

χ and χ_{cr} considerable iteration problems are encountered. Therefore we cannot decide whether or not the relationship remains linear. At very high θ_{exc} a rather flat region in the volume fraction profile exists (figure 3.7). There the polymer concentration corresponds with the volume fraction of the concentrated phase, which is in equilibrium with the dilute critical phase. This suggests incipient phase separation with the adsorbate being the polymer-rich phase.

Silberberg²² concluded that the ratio between θ_{exc} and θ can never exceed two. Here we see that in the case of $r = 10$ even a ratio as high as 3.5 is attained. At $r = 100$ we did not come to such a high value, but here we could not approach the critical χ as near as in the case of the short chain. Possibly Silberberg's statement can be applied to infinitely long chains.

3.5.3.2 PHASE SEPARATION OF POLYELECTROLYTES

As has already been pointed out in sections 3.5.2.4.1 and 3.5.2.4.2, the phase separation domains can be obtained by using the electrical part of the chemical potential. It has been noted, that care must be taken in the choice of the reference polymer concentration. In the Gouy-Chapman approach the choice of the reference concentration influences the salt concentration in the two phases, since the salt concentration is also involved in the definition of the reference polymer concentration. Of course, the salt concentrations can readily be converted into another reference state, since the potential difference between the phases and the reference polymer concentration are known, but special attention must be paid to the conditions that are compared. The same problem crops up, when the Debye-Hückel approximation is applied, but then the situation is even more complicated, since the solution of the linearized Poisson-Boltzmann equation is not invariant with respect to the choice of the reference state.

We will consider three cases:

- (i) In the first case the reference state is either the phase, where the volume fraction is the lower one (for coexisting phases), or the homogeneous phase (for complete miscibility).

The same salt concentration is chosen in the reference state when different polymer volume fractions are considered.

- (ii) The second case resembles the first one, but the same total ionic strength--the small ions originating from the polyelectrolyte included--is chosen in the reference state, when different polymer fractions are considered.
- (iii) The third case has the volume fraction of the critical point for the Debye-Hückel approximation as the reference state and the salt concentration is defined at that volume fraction. This volume fraction, $\phi_{*,cr}^{(DH)}$, only depends on the chain length (see eq. 3.83).

The first case is interesting from a practical point of view. When we investigate binodial situations, we usually have an extensive dilute phase and a small amount of concentrated phase. For example, this is the case at cloud point determinations. For situations near the spinodial curve this homogeneous phase would also be a logical reference. The disadvantage is that with a given salt concentration each volume fraction has another ionic strength.

Electrostatic effects are strongly influenced by salt effects. When electrostatic and non-electrostatic effects must be separated, it is probably the best way to choose the same ionic strength in the reference state. This is done in cases (ii) and (iii). For the Debye-Hückel situation this means that systems with the same shielding length κ^{-1} are compared. So here the value of the reference volume fraction is not important, because we can choose any combination of polymer and electrolyte concentrations, provided that the same total small ion concentration is maintained. Thus, in the Debye-Hückel approach the cases of constant ionic strength (ii) and that of fixed reference polymer concentration (iii) coincide. Of course the concentration of small ions originating from the polymer may not exceed the total ion concentration as defined by κ .

3.5.3.2.1 THE SPINODIAL

The spinodial is the boundary between the unstable and the metastable domain. For this curve we consider only one homogeneous phase

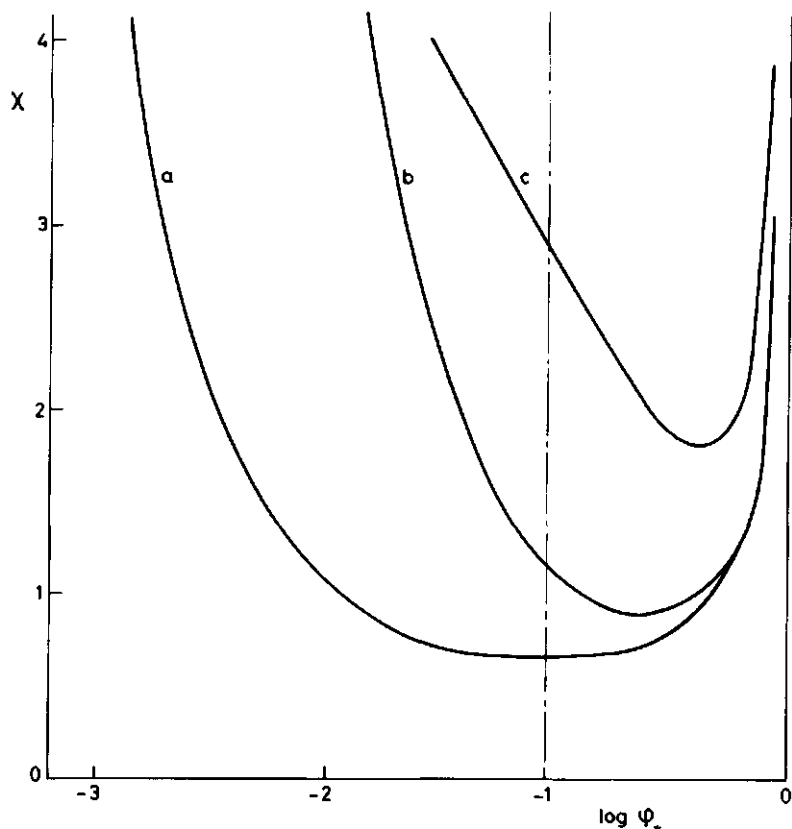


Figure 3.8. Spinodal curves. At each point the corresponding ϕ_* is chosen as the reference state. $r = 100$. $\cdots\cdots\phi_{*,cr}^{(DH)}$.
 a: electrolyte (c_s) 0.1 M, $\alpha = 0.1$; b: in the absence of electrolyte, $\alpha = 0.1$; c: $c_s = 0.1$ M, $\alpha = 1$.

and find out whether or not this phase can be stable.

Figure 3.8 presents spinodal curves in the case of this phase being chosen as the reference phase, with the same indifferent electrolyte concentration present at all polyelectrolyte volume fractions. Below the curves (meta)stable solutions are possible, above the curves phase separation always occurs. The Debye-Hückel and the Gouy-Chapman approach give the same curves, although the interpretation is different. In the Debye-Hückel case the minima of the curves do not correspond with the critical points. Instead, those points are on the dot and dash line at the critical concentration obtained from eq. 3.83. The curves are collections of spi-

nodial points, each having another reference state. In the case of the Gouy-Chapman approach the minima are veritable critical points, i.e. both the first and second derivatives of the chemical potential are zero. Again the curves are collections of spinodal points having different reference states.

The curves a, b and c in figure 3.9 are spinodials in the case of constant ionic strength at all volume fractions. The volume fractions themselves are chosen as references. Again the Debye-Hückel and the Gouy-Chapman approach give the same results. The curves

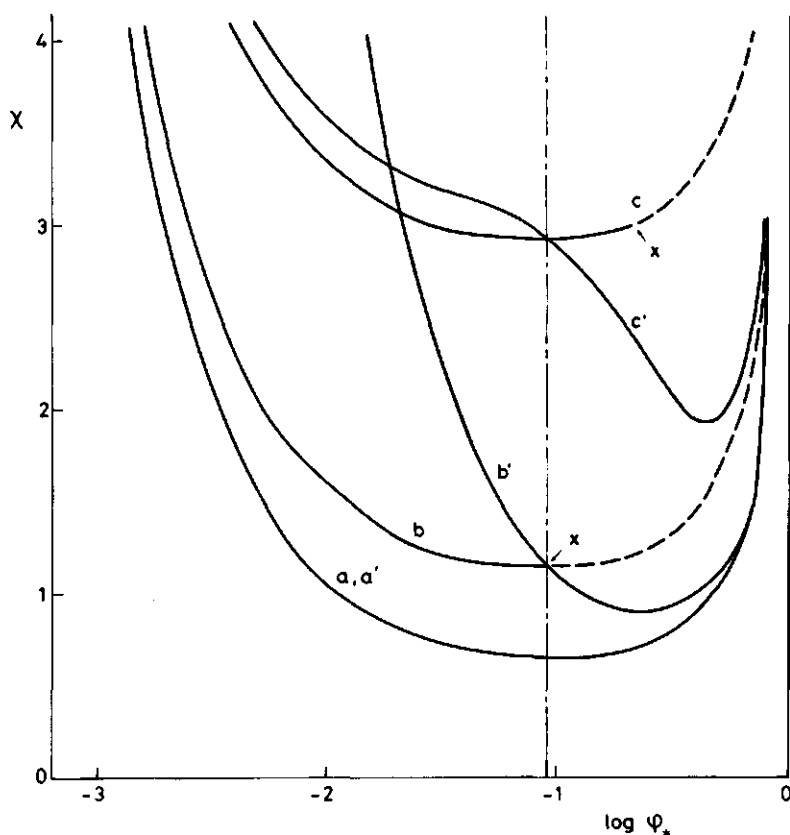


Figure 3.9. Spinodal curves, (i) at constant ionic strength (a, b, c) and (ii) with $\phi_{*,cr}(\text{DH})$ as the reference using the Debye-Hückel approach (also a, b, c) and the Gouy-Chapman approach (a', b', c'). a, a': $c_s = 0.1 \text{ M}$, $\alpha = 0.1$; b, b': in the absence of salt, $\alpha = 0.1$; c, c': $c_s = 0.1$, $\alpha = 1$. The values of c_s are defined at $\phi_{*,cr}(\text{DH})$. $r = 100$.

are only meaningful at volume fractions lower than those indicated with x . At those polymer concentrations all small ions originate from the polymer. As the points of one curve have the same value of ξ , the curves have the same shape and are only shifted along the x -axis with respect to each other.

If the volume fraction $\phi_{*,cr}^{(DH)}$ is chosen as the reference state, we also obtain the curves a, b and c using the Debye-Hückel approach. As we have again a fixed ionic strength in the reference state, κ and hence ξ are constant too. Along the curves the indifferent electrolyte concentration varies, governed by the theoretical potential difference with respect to the reference phase. As the linearization of $\exp(-x)$, i.e. $(1 - x)$, leads to erroneous results at high x , the dashed part of the curves have no physical meaning, because negative salt concentrations are involved.

With the choice of $\phi_{*,cr}^{(DH)}$ as the reference state, the Gouy-Chapman approach no longer gives the same result as the Debye-Hückel approach, because different potentials with respect to the reference phase are calculated. At a low value of α and 0.1 M electrolyte (curves a and a'), the differences remain within drawing accuracy. The Debye-Hückel approximation overestimates the potential difference, thus too much salt attraction is calculated at volume fractions lower than the critical one and too little at a higher one. So the curves cross over at $\phi_{*,cr}^{(DH)}$. The curves b of figure 3.8 and b' of figure 3.9 are identical since a different choice of the reference state only affects the indifferent electrolyte concentration, which is zero.

It is illustrative to pay some extra attention to the curves b' and b of figure 3.9 which refer to the case of the absence of salt with a fixed reference state. These are especially suited to demonstrate the consequence of the Debye-Hückel linearization. Curve b' the Gouy-Chapman curve is independent of the choice of the reference state, since there salt is absent. If the abscissae axis value of the volume fraction is chosen as the reference state, curve b' is obtained for the Debye-Hückel approximation too (i.e. figure 3.8, curve b). Curve b can be interpreted in two ways: (i) representing the case of constant ionic strength with the abscissae axis value of the volume fraction as the reference, both in the Gouy-Chapman and Debye-Hückel approach and (ii) representing the case of ab-

sence of salt in the Debye-Hückel approach with $\phi_{*,cr}(DH)$ as the reference. In the first interpretation there is also indifferent electrolyte present at any volume fraction except for that indicated with the x , which coincides with $\phi_{*,cr}(DH)$. Considering the second interpretation of b , we can conclude that the difference between the curves b and b' is a consequence of the improper accounting for the indifferent electrolyte concentration in the Debye-Hückel approximation.

3.5.3.2.2 THE BINODIAL

From a practical point of view, the binodial curves are more interesting than the spinodial curves, since they present the physically stable and unstable regions. The metastable regions between the spinodial and binodial are hardly ever important, since phase separation occurs readily, for example by concentration fluctuations induced by adsorption on a surface or particle anywhere in solution. Figure 3.10 collects results for systems with $\alpha = 0.1$ and electrolyte concentrations 0.1 or 0 M. Figure 3.11 presents the corresponding data for systems with $\alpha = 1$ and 0.1 M electrolyte.

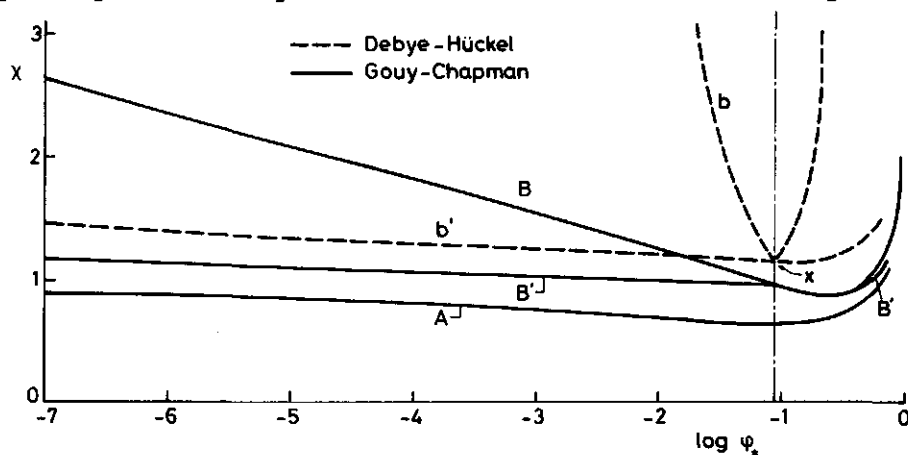


Figure 3.10. Binodial curves; $\alpha = 0.1$, $r = 100$. A: electrolyte 0.1 M. B, B', b: abscissae axis value is reference (B, b in the absence of electrolyte, B' constant ionic strength at reference). b' : $\phi_{*,cr}(DH)$ (----) is reference. b' can also be interpreted as if at constant ionic strength.

In the case of $\alpha = 0.1$ and 0.1 M salt the amount of counterions originating from the polyelectrolyte is vanishingly low compared with that from the salt, so that the choice of the reference state is immaterial. Because of the low charge and the high indifferent electrolyte concentration the potentials between the two phases remain low, so that the Debye-Hückel linearization does not greatly affect the results. Within drawing accuracy the same curve is obtained as with the Gouy-Chapman approach.

Curve B of figure 3.10 gives the phase diagram for the Gouy-Chapman approach in the case of absence of salt. The curve is independent of the choice of the reference state, just as it was the case with the spinodial. The χ -value of incipient phase separation rises rapidly when a lower concentration of the dilute phase is considered, because this dilute phase has a very low ion concentration. Then very high potential differences develop between the two phases, e.g. at $\chi = 2$ the value of $e\psi(x)/kT$ is 10.6. This value can also be obtained from the volume fraction ratio using Nernst's law.

Curve B' relates to the case of constant ionic strength in the dilute phase, which is also the reference phase. For this aim the ionic strength of the salt-free polymer solution at $\phi_{*,cr}(DH)$ was chosen. The low concentration branch only goes as far as this volume fraction $\phi_{*,cr}(DH)$. At higher volume fractions negative salt concentrations would be needed to maintain constant ionic strength. The χ -value of incipient phase separation rises less steeply with decreasing polymer volume fraction than in the case of the absence of indifferent electrolyte. The electrolyte added to maintain constant ionic strength destabilizes the polyelectrolyte solution. The high volume fraction branch is at higher volume fractions than that of curve B, because the electrolyte added reduces the potential difference between the two phases that opposes the concentration of the polyelectrolyte.

Curves b and b' of figure 3.10 represent Debye-Hückel results. For curve b the lower volume fraction of the coexisting phases is chosen as the reference state and no electrolyte is added. The χ -value of incipient phase separation rises even more steeply than that according to the Gouy-Chapman approach. The concentration in the concentrated phase is much lower than the one predicted by

means of the full Poisson-Boltzmann equation. The Debye-Hückel approximation overestimates the stability and restricts the volume fraction of the concentrated phase too much because it overestimates the potential in this phase that hinders polyelectrolyte accumulation. The minimum of the curve is at the critical point at volume fraction $\phi_{*,cr}^{(DH)}$. As each point has another reference state--the abscissae axis value of the volume fraction--, the slope of curve b is not zero at this point. So the minimum is a singularity. If a constant ionic strength in the reference phase is assumed, curve b' is obtained. Qualitatively the same trend is observed as is shown by the Gouy-Chapman approach. The low volume fraction branch has a much lower slope than curve b and the concentrations of the high volume fraction branch are higher.

Again curve b' can be interpreted in two ways: (i) the volume fraction $\phi_{*,cr}^{(DH)}$ in the absence of electrolyte is chosen as the reference state and (ii) the abscissae axis value of the volume fraction is chosen as the reference state and electrolyte is added to main constant ionic strength. Considering the first interpretation, curve b' must be compared with curve B, the Gouy-Chapman curve, to see the influence of the Debye-Hückel approximation. The only difference between b and b' is a different choice of reference state. This illustrates very clearly what erroneous results the Debye-Hückel approximation may lead to. Considering the second interpretation of curve b', this curve must be compared with the Gouy-Chapman curve B'. As electrolyte is present, potentials occur, which are less high than those of the case of curve b. Thus the Debye-Hückel results diverge less from those obtained by means of the full Poisson-Boltzmann equation in the case of constant ionic strength (curve B').

Figure 3.11 (curves for $\alpha = 1$ and 0.1 M electrolyte) shows again how the Debye-Hückel results do depend on the reference state chosen. These results are in line with the difference between the curves b and b' of figure 3.10. Curve b' of figure 3.11 refers to a curve at a constant ionic strength in the reference state. Since the curves a and b' in figure 3.10 and b' in figure 3.11 only differ with respect to the values of κ , and thus of ξ , they have the same shape, the only difference being that they are shifted along the χ -axis with respect to each other and the curve for uncharged polymer.

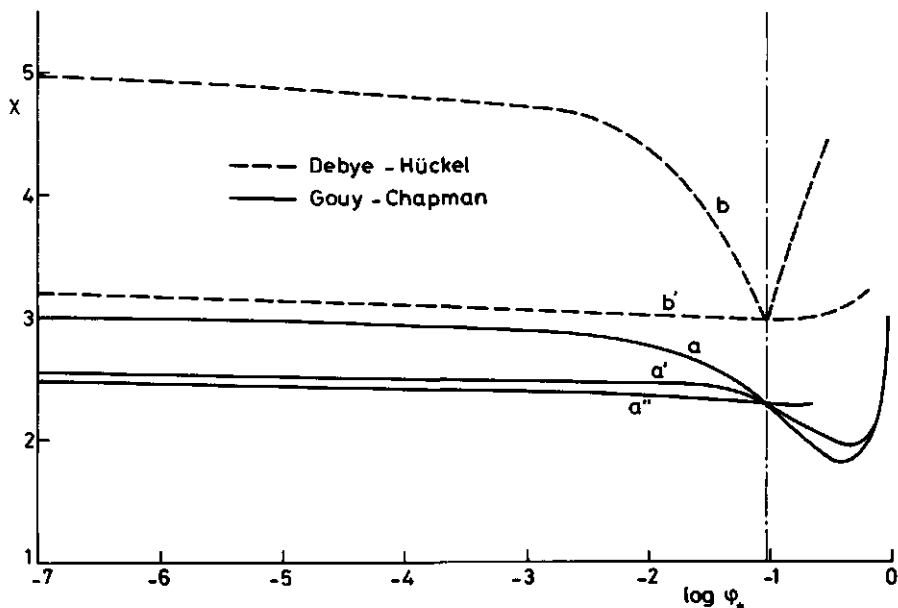


Figure 3.11. Binodial curves; $\alpha = 1$, $r = 100$. a , a'' , b : abscissae axis value is reference (a , b : electrolyte 0.1 M at reference, a'' : constant ionic strength at reference). a' , b' : $\phi_{*,cr}^{(DH)}$ is reference. b' can also be interpreted as if at constant ionic strength.

In the case of the full Poisson-Boltzmann equation different curves are also obtained when different reference states are chosen and salt is present. In curve a (figure 3.11) the lower concentration is chosen as the reference state, whereas for curve a' the critical concentration of the Debye-Hückel case $\phi_{*,cr}^{(DH)}$ was selected. The salt concentration is defined at the reference volume fraction, so along the lower volume fraction branch of curve a the salt concentration is constant, but along curve a' it varies depending on the potential difference between the dilute phase and the reference state. The ion concentrations distribute according to the Boltzmann-factor. With positive polyelectrolyte the potentials at low ϕ_* are more negative than the reference, so coions are attracted by the dilute phase. As the indifferent electrolyte concentration is equal to the concentration of coions, the dilute phase has a higher salt concentration than the reference phase, such in accordance with the Donnan equilibrium conditions. This

higher ionic strength lowers the χ -value of incipient phase separation of curve a' with respect to curve a at volume fractions lower than $\phi_{*,cr}(DH)$.

A curve at constant ionic strength is also given (figure 3.11a"). The remarkably flat path of this curve, as well as that of curve B in figure 3.10, indicates that the total ionic strength is an important factor in the description of polyelectrolyte solution stability. At a volume fraction of the dilute phase slightly exceeding 0.1 there is a minimum in curve a". At one value of χ two pairs of phase compositions can exist with the same total ionic strength in the dilute phase, one with a high polyelectrolyte and a low salt concentration and the other with these concentrations the other way round. The high concentration branch is not connected with the low concentration branch, since the given total ion concentration restricts the viable range of the dilute phase volume fractions. The highest possible polymer concentration is that obtainable in the absence of salt.

Summarizing we can conclude that the χ -value of incipient phase separation is largely determined by the total small ion concentration. For instance, the differences between the curves a, a' and a" in figure 3.11 originate from the different variation of the total ionic strength along the curves. As could be expected, the stability against phase separation is decreased by raising the salt concentration and increased by higher degrees of dissociation. The Debye-Hückel results are very sensitive to the choice of the reference state. Because of the overestimation of the potentials much too high χ -values of incipient phase separation are found. In spite of the elegant formulation of the charge effect on polymer stability by means of the Debye-Hückel approximation, this formulation should not be used to describe practical systems.

3.6 EXTENSION OF POLYMER ADSORPTION THEORIES WITH ELECTROSTATIC INTERACTIONS

3.6.1 THE ROE THEORY

The model used by Roe¹⁰ has already been described in section 2. Here it suffices that Roe derives an expression for the grand partition function Ξ . Then that polymer concentration profile is sought that corresponds to the maximum term of Ξ , or, what is equivalent, the characteristic function has to be minimized. For uncharged polymer the characteristic function is $-\pi a_0$:

$$-\pi a_0 = -kT \ln \Xi / \Xi_* \quad (3.94)$$

where the asterisk refers to the reference state. Since in a grand canonical ensemble the characteristic function equals the sum of all reversible work, we must add the electrical work, i.e. the electrical free energy to $-\pi a_0$ in order to extend the theory to charged polymers. Again the volume fractions ϕ_i of the layers i are iterated, so that the characteristic function is minimized.

3.6.2 THE SCHEUTJENS-FLEER THEORY

The model of Scheutjens and Fleer¹¹, as described in section 2.2 closely resembles Roe's model. For polyelectrolytes, the free energy term has to be incorporated in the energy term of the canonical partition function, eq. 15 of ref. 11. In fact this term is not an energy but a free energy term, containing all entropic contributions except those due to the conformation of the polymer. The equilibrium polymer concentration profile is given by the number of molecules in each possible conformation. A conformation is defined by the distribution of segments over the layers of the system. The distribution of conformations is governed by the conformational entropy and a weighting factor p_i , being the probability to find a segment in layer i if it were not constrained by the fact it is part of a chain. This factor contains

the excluded volume and the derivative of the energy term with respect to the number of segments of polymer in layer i . In our polyelectrolyte case we have to subtract the derivative of the electrical free energy, i.e. $\alpha e \psi_i / kT$, from $\ln p_i$.

3.6.3 RESULTS AND DISCUSSION

In this section we will compare the adsorption behaviour of polyelectrolytes with that of uncharged polymers. Numerical results for the full Poisson-Boltzmann equation are compared with Debye-Hückel data. Furthermore we will show the differences between Hesselink's theory and our work. Because Roe's theory gives less computational problems than the Scheutjens-Fleer theory without undue loss of detail, it is used as the nonionic basis unless stated otherwise.

3.6.3.1 COMPARISON WITH NONIONIC POLYMERS

When the non-electrostatic free energy of adsorption exceeds the critical value¹¹, adsorption takes place both with ionic and nonionic polymers. In the case of nonionic polymers part of the polymer is attached to the surface while the remainder is accommodated in loops and tails protruding into the solution. Hence the amount adsorbed can easily go beyond that of a monolayer. When a charged polymer adsorbs, a potential of the same sign as that of the polymer is generated near the surface. This potential expels polyelectrolyte segments from the adsorption layer, which in the segment density profile (figure 3.12) shows up as a minimum. Consequently, nearly all adsorbed polymer is present in the first layer, i.e. the adsorbed layers are very flat and the adsorbed amount corresponds to less than a monolayer. Only at low χ_s ($\chi_s < 1$), where only low potentials build up and a small amount of polymer is adsorbed and at high salt concentrations (> 0.1 M), a significant amount can be adsorbed in the second and following layer. Longer chains show a higher adsorption in the first layer. This gives rise to a higher potential near the surface and a deeper minimum

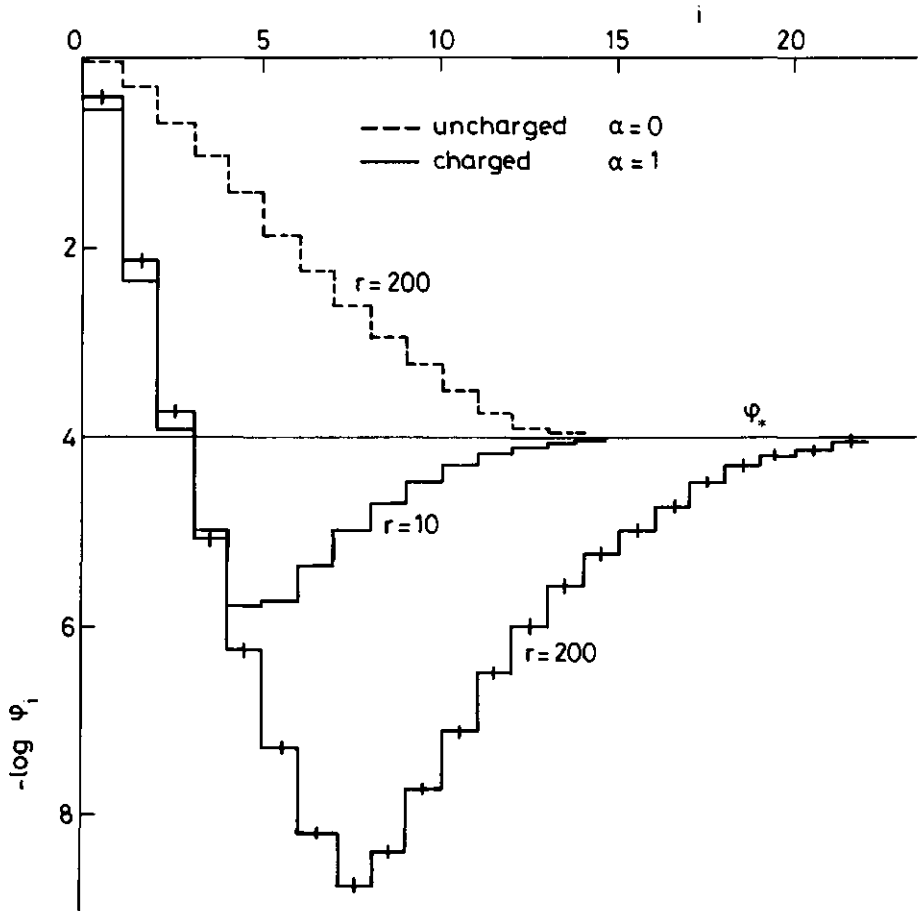


Figure 3.12. Polymer concentration profile for uncharged and charged polymers. $\chi = 0.5$, $\chi_s = 4$, monovalent electrolyte 0.01 M, $\sigma_0 = -0.1 \text{ e/a}_0$, $a_0 = 1 \text{ nm}^2$, $r_0 = 1 \text{ nm}$.

in the concentration profile. Although there is some chain length dependence of the adsorption, this dependence is much less pronounced than with uncharged polymers (figure 3.13). Above a certain chain length the adsorption becomes virtually independent of chain length, unlike the uncharged case. For long chains the adsorption isotherms are of the high affinity type, with a very distinct plateau (figure 3.14).

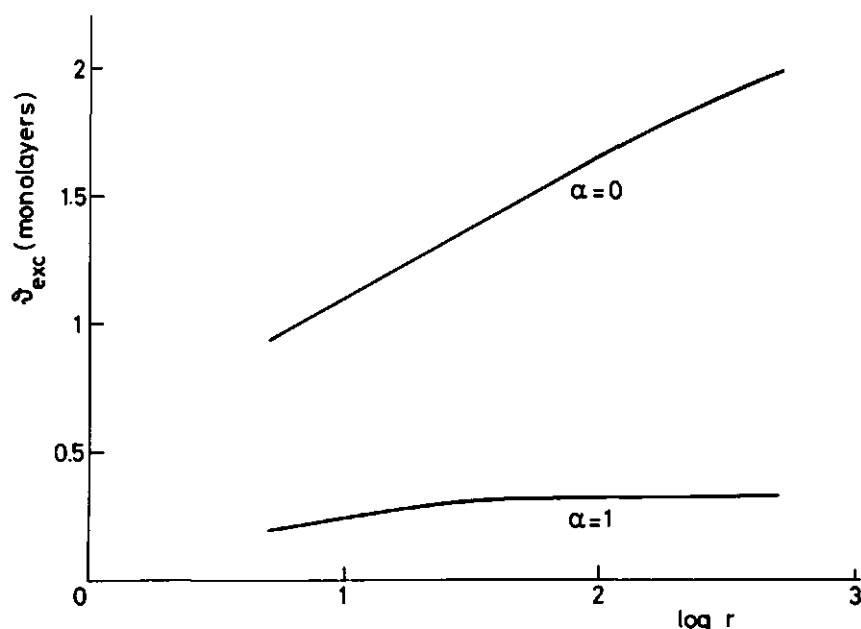


Figure 3.13. Chain length dependence of the adsorption for charged ($\alpha = 1$) and uncharged ($\alpha = 0$) polymer. $\chi = 0.5$, $\chi_s = 4$, electrolyte 0.01 M, $\sigma_0 = -0.1 \text{ e}/a_0$, $a_0 = 1 \text{ nm}^2$, $r_0 = 1 \text{ nm}$.

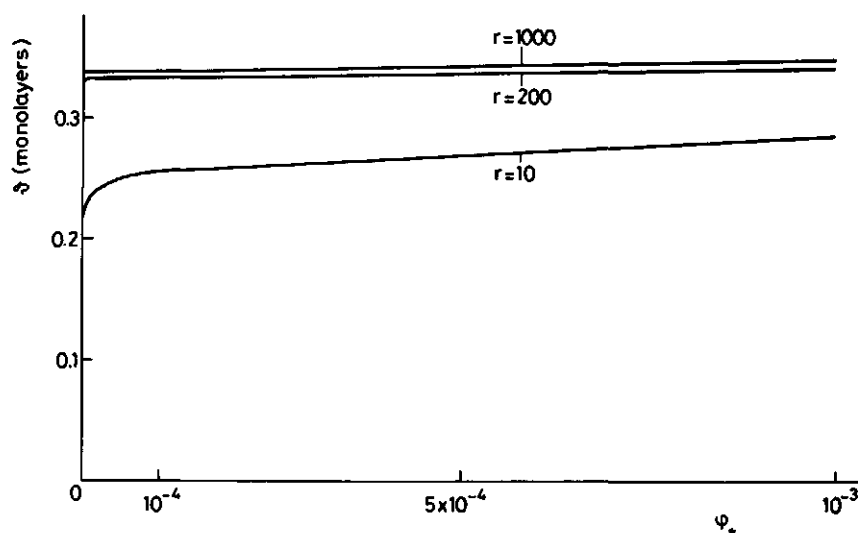


Figure 3.14. Adsorption isotherms of polyelectrolytes. $\chi = 0.5$, $\chi_s = 4$, $\alpha = 1$, electrolyte 0.01 M, $\sigma_0 = -0.1 \text{ e}/a_0$, $a_0 = 1 \text{ nm}^2$, $r_0 = 1 \text{ nm}$. The chain length, expressed as the number of segments r is indicated.

Nonionic polymers also show high affinity adsorption, but have much less pronounced plateaus. These features can be understood on the basis of the fact that in the polyelectrolyte case the occurrence of loops and tails is greatly suppressed. In the nonionic case the rise of the adsorption with molecular weight and bulk concentration is due to segments accommodated in loops and tails.

For nonionic polymers the adsorption in the first layer hardly depends on chain length and bulk volume fraction (see ref. 11, figures 5b and 9b). In this respect the adsorption of polyelectrolytes strongly resembles the behaviour of nonionic polymers. As in the case of uncharged polymers the plateau value of first layer coverage for ionic polymers is very sensitive to the nonionic adsorption energy, χ_s . However, for polyelectrolytes, much higher χ_s values are needed to obtain the same adsorption as for uncharged polymers. The segments in the first layer all undergo the attraction of the surface, expressed through χ_s , and the repulsion due to the potential in that layer, ψ_1 . Hence we can define an effective adsorption energy $\chi_{s,eff}$:

$$\chi_{s,eff} = \chi_s - \alpha e \psi_1 / kT \quad (3.95)$$

In those circumstances in which there is no significant adsorption in the second layer, the adsorption in the first layer only depends on $\chi_{s,eff}$, irrespective of σ_0 , salt concentration and, in the case of long chains, of chain length and bulk volume fraction (figure 3.15). The occupancy ϕ_1 of the first layer is always less than the corresponding value for nonionic polymers. This stems from the fact that the formation of loops and tails facilitates the adsorption in the first layer entropically. When, in nonionic polymer adsorption theory, we suppress the formation of loops and tails artificially by setting the volume fraction of polymer equal to that in the bulk in all but the first layer, the same curve of ϕ_1 versus χ_s is obtained as in the polyelectrolyte case at low indifferent electrolyte concentration. At low $\chi_{s,eff}$ there is only a low amount of polyelectrolyte adsorbed. Then the potential in the second layer will be low and some loop formation may occur. At high salt concentrations (>0.1 M) the potential drops very steeply with distance

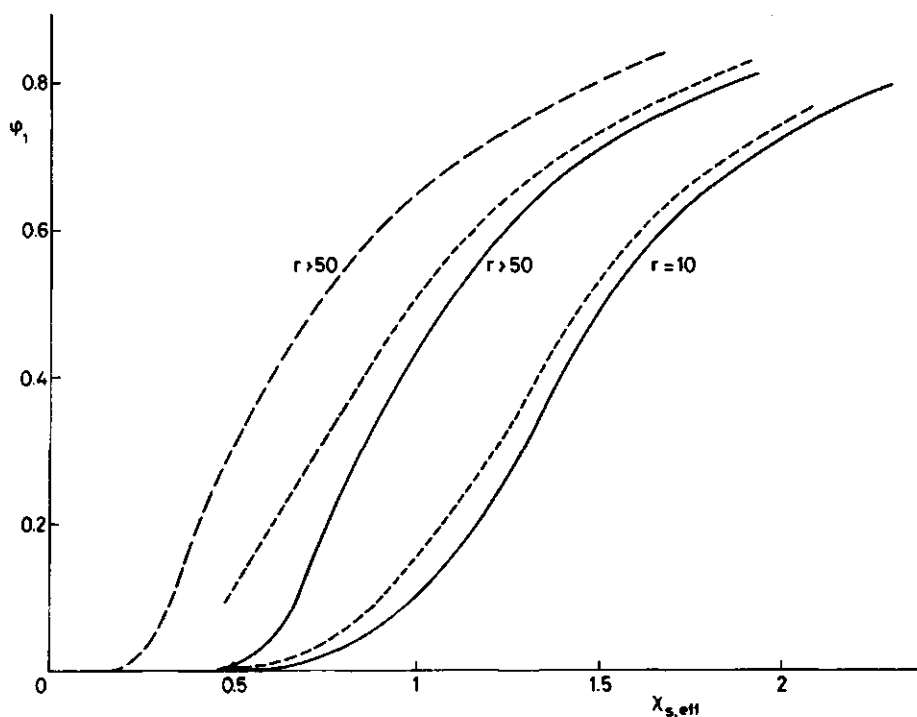


Figure 3.15. First layer volume fraction as a function of $\chi_{s,\text{eff}}$.
 — polyelectrolyte, $c_s = 0.05$ M; --- polyelectrolyte, $c_s = 0.1$ M;
 - - - nonionic polymer. $\chi = 0.5$, $\phi_* = 10^{-3}$, $\alpha = 1$. The chain length r is indicated.

and loop and tail formation is less effectively suppressed. In those cases the curve is more similar to the nonionic polymer curve.

In poor solvents nonionic polymers can give phase separation. For infinitely long chains the critical value of the Flory-Huggins parameter χ for phase separation is 0.5. When supercritical conditions are considered, the computer programmes can react in two ways: in some cases convergence of the polymer concentration profile iteration is not obtained; in other cases the calculated profile does not decay to the bulk value far away from the surface. However, in the case of polyelectrolytes profiles are obtained which do converge towards their bulk value (figure 3.16) at χ -values that would have given rise to phase separation in the case of absence of charge.

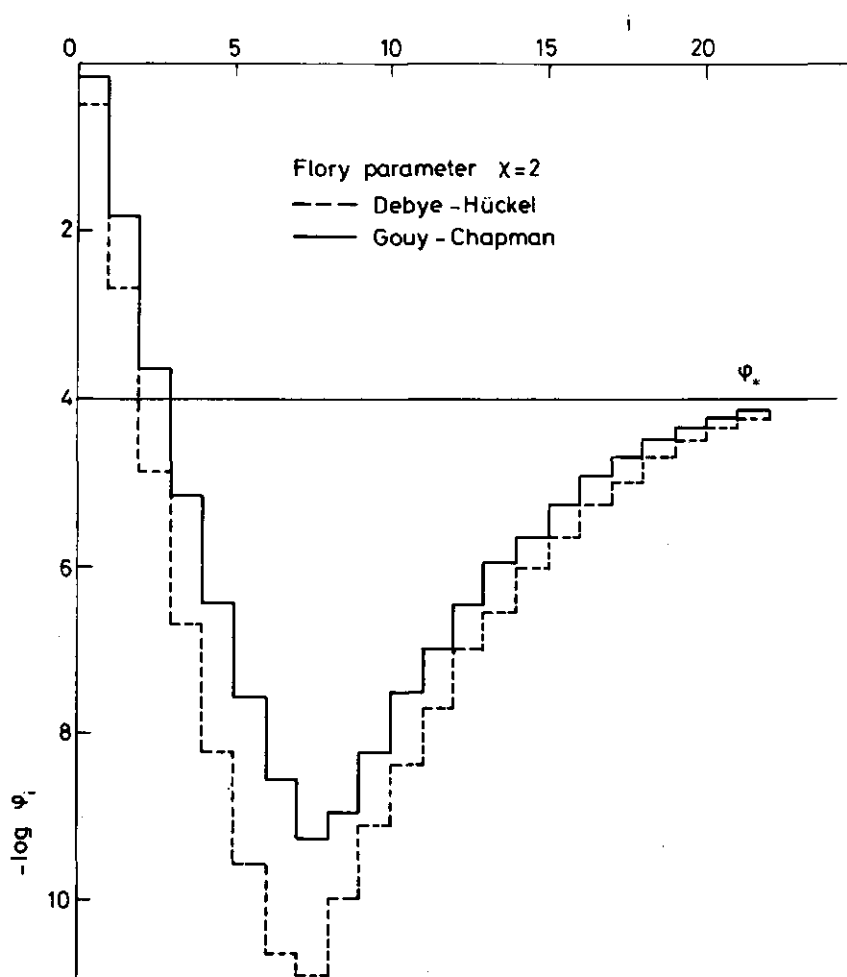


Figure 3.16. Polymer concentration profile for a poor solvent; influence of the Debye-Hückel approximation. $\chi_s = 5$, $r = 100$, $\alpha = 1$, electrolyte 0.01 M, $\sigma_0 = -0.1 \text{ e}/a_0$, $a_0 = 1 \text{ nm}^2$, $r_0 = 1 \text{ nm}$.

As for nonionic polymers, considerable discrepancies exist between the results of the theory of Roe on the one hand and those of Scheutjens and Fleer on the other hand. This can be explained in the light of Roe's approximation that all segments of a chain have the same density distribution, an approximation which does not hold for the long tails. Tail segments tend to be in layers

farther away from the surface than segments from the central part of the chain. In our polyelectrolyte case the influence of the tails is greatly suppressed, so that the two theories yield very similar results (figure 3.17). Note that, if the logarithmic volume fraction axis is replaced by a linear one, the difference in the region of the minimum will become invisible.

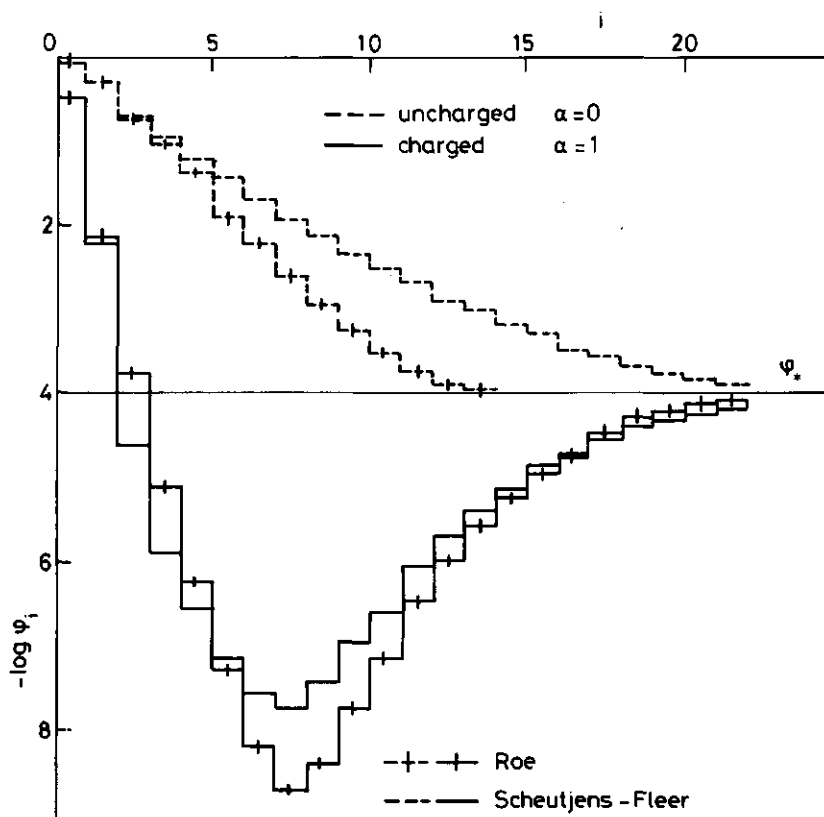


Figure 3.17. Comparison of the polymer concentration profile for charged and uncharged polymers for the theories of Roe and of Scheutjens and Fleer. $\chi = 0.5$, $\chi_s = 4$, $r = 200$, $c_s = 0.01$ M, $\sigma_o = -0.1 e/a_o$, $a_o = 1$ nm², $r_o = 1$ nm.

The theory of Scheutjens and Fleer enables us to calculate the contributions of loops and tails to the segment density. It is a typical feature of nonionic polymers that the volume fraction of

loop segments decays exponentially with the distance from the surface, as Hoeve^{5,6,7} predicted for infinitely long chains. This feature can be ascribed to a Gaussian distribution of loop lengths. In the case of polyelectrolytes there is a much steeper density decay over the first layers (figure 3.18). The distribution of loop lengths is not Gaussian but very short loops dominate. Far away from the surface, where the potentials are low, the density decay becomes less steep. The volume fraction of loops is very low then. Quantitatively, they do not play a role of any consequence.

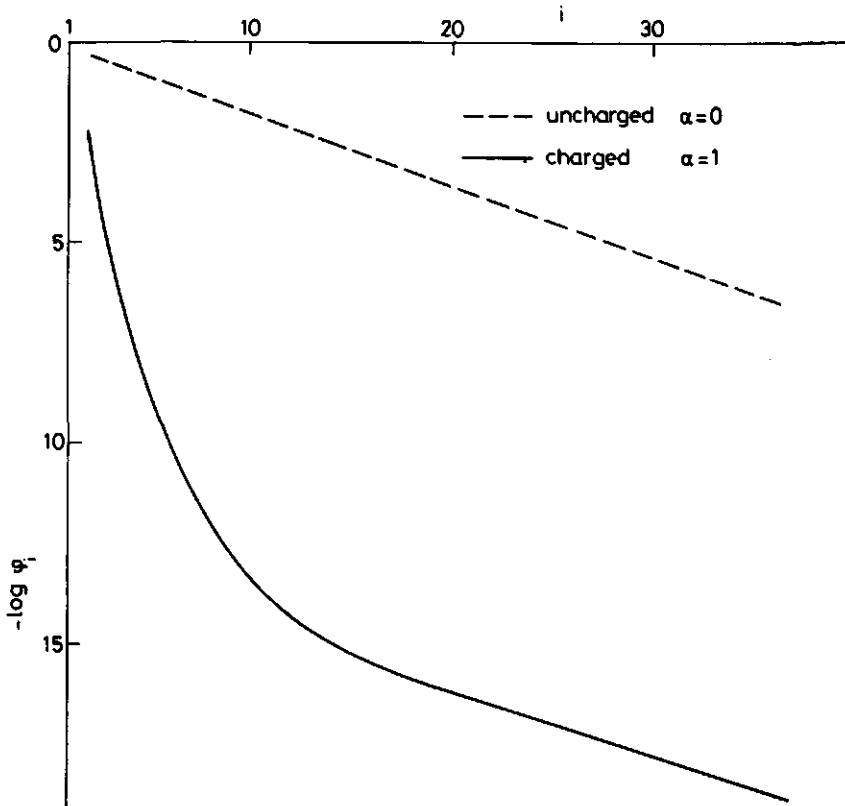


Figure 3.18. Volume fraction of loops for charged and uncharged polymers. $\chi = 0.5$, $\chi_s = 4$, $\phi_* = 10^{-4}$, $r = 1000$, electrolyte 0.01 M, $\sigma_0 = -0.1 \text{ e/a}_0$, $a_0 = 1 \text{ nm}^2$, $r_0 = 1 \text{ nm}$.

At high polymer concentration we meet with an interesting phenomenon: the volume fraction of tails shows a maximum after a minimum near the surface (figure 3.19). The high potential in the first layers expels tail segments from the surface. Farther away from the surface the potential is low and the tails can curl up. Just like the loops the tails constitute a very small part of the total volume fraction and as far as the physical properties of the adsorbed layer are concerned they can be neglected. There is only one tail at about ten chains and they comprise only a very small fraction ($\pm 0.3\%$) of the segments.

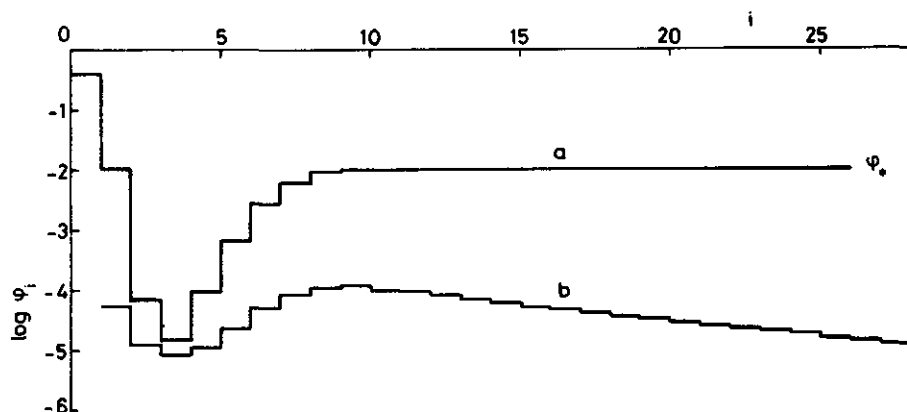


Figure 3.19. Total polymer volume fraction (a) and volume fraction of tails (b). $\chi = 0.5$, $\chi_s = 4$, $r = 1000$, $\alpha = 1$, in the absence of electrolyte, $\sigma_0 = -0.1 e/a_0$, $a_0 = 1 \text{ nm}^2$, $r_0 = 1 \text{ nm}$.

3.6.3.2 INFLUENCE OF THE DEBYE-HÜCKEL LINEARIZATION

In the Debye-Hückel approximation the potential is linearly proportional to the charge, whereas in the Gouy-Chapman double layer picture the potential levels off with increasing charge. Therefore the use of the Debye-Hückel approximation will overestimate the potential and hence underestimate the amount adsorbed. Over the whole region the Debye-Hückel polymer concentration profile (figure 3.16) is below that obtained with the Gouy-Chapman approach. Under the conditions indicated in figure 3.16 the Debye-

Hückel approximation gives only 42% of the amount adsorbed as predicted by the complete Poisson-Boltzmann equation. The difference in adsorbed amount that the two theories produce, depends strongly on the potential in the first layer ψ_1 . As long as this potential remains below $2 kT/e$, the Debye-Hückel approximation corresponds with the full Poisson-Boltzmann equation. In the Debye-Hückel approximation, both ϕ_1 and ψ_1 are almost proportional to χ_s . By contrast, in a Gouy-Chapman double layer the potential levels off at high χ_s whereas the adsorbed amount continues to rise (figure 3.20).

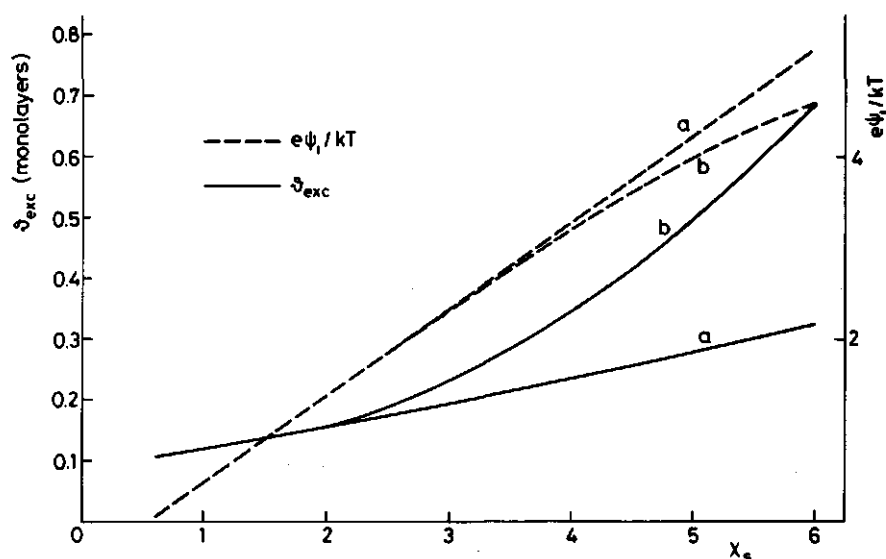


Figure 3.20. Potential in the first layer (----) and excess adsorbed amount (—) as a function of the non-electrostatic adsorption energy for the Debye-Hückel (a) and the Gouy-Chapman approach (b). $\chi = 0.5$, $\phi_* = 10^{-4}$, $r = 100$, $\alpha = 1$, $c_s = 0.01$ M, $\sigma_0 = -0.1$ e/a₀, a₀ = 1 nm², r₀ = 1 nm.

3.6.3.3 COMPARISON WITH HESSELINK'S THEORY

It is difficult to compare our theory with that of Hesselink^{3,4} directly. Hesselink used Hoeve's treatment for uncharged polymers,

assuming a fixed polymer concentration in the loop layer, which was obtained from the theory of Overbeek and Hermans⁸ for polyelectrolytes in solution. So the influence of the surface on the polyelectrolyte conformation is neglected. The concentration in the loop layer is taken identical to that in the bulk coils and hence no change in the free energy of mixing occurs for the loop layer during the adsorption process. In this respect the theory is inconsistent because it does give such a contribution. The assumption of a fixed loop layer concentration is the greatest difference between our theory and Hesselink's. Both theories have other approximations in common:

- a. The assumption that electrostatic and non-electrostatic effects are separable.
- b. The smearing out of charges parallel to the surface.
- c. The neglect of chain stiffness effects.
- d. The neglect of the influence of the potential on the dielectric constant and degree of dissociation.
- e. The neglect of the volume that is excluded for the small ions by the polymer and the small ions present.

Hesselink only gives results for the Debye-Hückel approximation. His choice of χ_s (< 1) justifies this assumption, but this was not explicitly stated. Especially those results which refer to the conformation of the adsorbed layer are very different from ours. Compared with the situation of uncharged polymers we predict a high fraction p of segments attached to the surface. At not too high salt concentrations (< 0.2 M) p exceeds 95%. The adsorbed layer is very thin. By contrast, Hesselink's theory gives nearly the same p for charged and uncharged polymers. He computes very extended adsorbed layers up to the micrometer range, although he states that such values might be overestimated. Between the two theories a number of trends concerning the total amount adsorbed are usually similar. This does not mean much, as regards discrimination between the two approaches, since most of them can also be anticipated intuitively. Examples of such trends are:

- a. Polyelectrolyte adsorption increases when the surface is charged oppositely to the polyelectrolyte and decreases by a charge of the same sign.

- b. The adsorption increases by salt addition when the nonionic adsorption energy is the driving force for adsorption, but it decreases when the driving force is of electrostatic origin (figure 3.21).

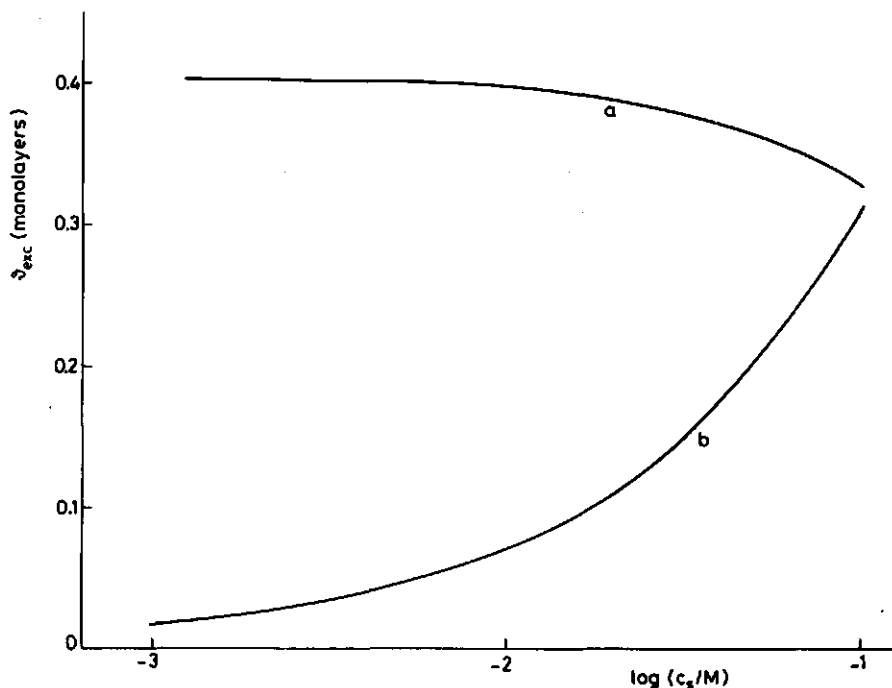


Figure 3.21. Excess adsorbed amount as a function of the indifferent electrolyte concentration. a: electrostatic driving force of adsorption ($\chi_s = 0$, $\sigma_0 = -0.4 \text{ e/a}_0$); b: non-electrostatic driving force of adsorption ($\chi_s = 2$, uncharged surface). $\chi = 0.5$, $\phi_* = 10^{-4}$, $r = 1000$, $\alpha = 1$, $a_0 = 1 \text{ nm}^2$, $r_0 = 1 \text{ nm}$.

3.6.4 CONCLUDING REMARKS

The conformation of adsorbed polyelectrolytes is strongly influenced by the polymer charge. The mutual repulsion between segments inhibits to a large extent the formation of loops and tails. When a non-electrostatic adsorption energy is present, charge reversal of the double layer takes place. As a potential of the

same sign as that of the polymer builds up, segments not directly attached to the surface are repelled from the surface and dips in the polymer volume fraction profile can occur. Thus very flat adsorbed layers are found.

Because loops and tails play a minor role when polyelectrolyte adsorption is concerned, the Roe theory of polymer adsorption gives results similar to those of the Scheutjens-Fleer theory.

The Debye-Hückel approximation yields overestimated potentials. So lower amounts adsorbed are obtained than in the case of the application of the full Poisson-Boltzmann equation. At low potentials ($< 2 \text{ kT/e}$) the differences are of minor importance.

3.7 REFERENCES

- 1 F.Th. Hesselink, in "Adsorption from Solution at the Solid/Liquid Interface" (C.H. Rochester and G.D. Parfitt, Eds.), Academic Press, London, 1983.
- 2 Th. Odijk and A.C. Houwaart, J. Polymer Sci, Polymer Phys. Ed. 16, 627 (1978).
- 3 F.Th. Hesselink, J. Electroanal. Chem. Interfacial Electrochem. 37, 317 (1972).
- 4 F.Th. Hesselink, J. Colloid Interface Sci. 60, 448 (1977).
- 5 C.A.J. Hoeve, J. Chem. Phys. 44, 1505 (1966).
- 6 C.A.J. Hoeve, J. Polymer Sci. C 30, 361 (1970).
- 7 C.A.J. Hoeve, J. Polymer Sci. C 31, 1 (1971).
- 8 J.J. Hermans and J.Th.G. Overbeek, Rec. Trav. Chim. 67, 761 (1948).
- 9 A. Silberberg, in "Ions in Macromolecular and Biological Systems (Colston Papers no. 29)" (D.H. Everett and B. Vincent, Eds.), Sciencetechnica, Bristol, 1978, p. 1.
- 10 R.-J. Roe, J. Chem. Phys. 60, 4192 (1974).
- 11 J.M.H.M. Scheutjens and G.J. Fleer, J. Phys. Chem. 83, 1619 (1979).
- 12 D.E. Brooks, J. Colloid Interface Sci. 43, 687 (1973).
- 13 J. Papenhuizen and H.A. van der Schee, to be published.
- 14 A. Katchalski, Pure Appl. Chem. 26, 227 (1971).

- 15 W.J.H.M. Möller, G.A.J. van Os and J.Th.G. Overbeek, Trans. Faraday Soc. 57, 325 (1961).
- 16 S. Levine and G. Neale, J. Colloid Interface Sci. 49, 330 (1974)
- 17 F.H. Stillinger, J. Chem. Phys. 35, 1584 (1961).
- 18 E.J.W. Verwey and J.Th.G. Overbeek, "Theory of the Stability of Lyophobic Colloids", Elsevier, Amsterdam, New York, 1948, p. 51.
- 19 Ibidem, p. 63.
- 20 P.J. Flory, "Principles of Polymer Chemistry", Ch. XII, Cornell University Press, Ithaca, New York, 1953.
- 21 Ibidem, Ch. XIII.
- 22 A. Silberberg, J. Colloid Interface Sci. 38, 217 (1972).
- 23 F.W. Klaarenbeek, Thesis, State University, Utrecht (1946).
- 24 J.Th.G. Overbeek, Progress Biophysics Biophys. Chem. 6, 57 (1956).
- 25 J.Th.G. Overbeek, in "Colloid Science" (H.R. Kruyt, Ed.), Vol. I, Elsevier, Amsterdam, New York, 1952, p. 191-193.

Appendix 3A THE POTENTIAL DISTRIBUTION ORIGINATING FROM SPACE CHARGES

In section 3.3 we described the potential distribution originating from polyelectrolyte charge which was assumed to be present concentrated in plane charges through the centre of the lattice layers. Instead of plane charges we can also assume the polymer charge to be smeared out within each lattice layer to form homogeneous space charges. Again, analytical expressions can be given for the Debye-Hückel case, whereas using the Gouy-Chapman approach we will have to rely on numerical procedures.

In the plane charge model the polyelectrolyte charges give rise to a discontinuity in the field strength. In the solution of the Poisson-Boltzmann equation they are accounted for via the boundary conditions at the positions of the plane charges. Uniform space charges within each layer give discontinuities in the second derivative of the potential at the boundaries of the lattice layers, but the potential and field strength are continuous throughout the system. The polyelectrolyte charges are accounted via an extra term in the Poisson-Boltzmann equation.

For the derivation of the potential distribution in the Debye-Hückel approximation it suffices again to solve the Poisson-Boltzmann equation for one homogeneous space charge in an isolated lattice layer. In section 3.3.2 we found that the potential near an interface is obtained as a contribution of charge and image-charge. Using this result we only have to find the symmetrical potential distribution originating from a space charge in an infinitely large salt solution. This situation is illustrated by figure 3A.1. Because of the symmetry the Poisson-Boltzmann equation is to be solved in two domains, (i) the polymer charge containing space from x_i to $x_i + r_o/2$, and (ii) the indifferent electrolyte solution, where $x > x_i + r_o/2$. In analogy to eq. 3.62 we define the space charge ρ_i within the lattice layer:

$$\rho_i = z\alpha e\phi_i/a_o r_o \quad (3A.1)$$

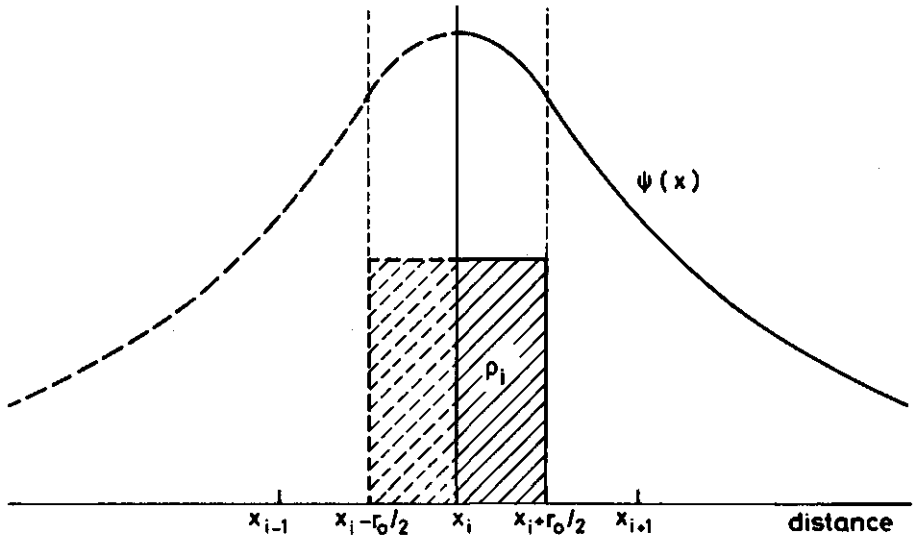


Figure 3A.1. Potential $\psi(x)$ and polyelectrolyte space charge (shaded) around an isolated lattice layer containing polyelectrolyte. Because of symmetry around x_i the dashed part of the figure is not needed to describe the system.

The Poisson-Boltzmann equation reads

$$\frac{d^2\psi(x)}{dx^2} = -\frac{e}{\epsilon} \left[\bar{n}_+ \exp(-e\psi(x)/kT) - \bar{n}_- \exp(e\psi(x)/kT) + \rho/e \right] \quad (3A.2)$$

where ρ is the polyelectrolyte charge. Within layer i the value of ρ is equal to ρ_i , outside the layer ρ is zero. The ion concentrations \bar{n}_+ and \bar{n}_- are both equal to the indifferent electrolyte concentration at infinite distance from x_i . The Debye-Hückel approximation yields

$$\frac{d^2\psi(x)}{dx^2} = \kappa^2 \left(\psi(x) - \frac{\rho}{\epsilon\kappa^2} \right) \quad (3A.3)$$

with κ defined as in eq. 3.6. The general solution of eq. 3A.3

is

$$\psi(x) = C_1 \exp(-\kappa x) + C_2 \exp(\kappa x) + \frac{\rho}{\epsilon \kappa^2} \quad (3A.4)$$

The boundary conditions are:

- (i) Because of the symmetry the field strength is zero at x_i .
- (ii) At $x_i + r_0/2$ both the potential and the field strength are continuous.
- (iii) At infinity the potential approaches zero and the field strength is given by

$$\frac{d\psi(x)}{dx} = -\kappa\psi(x) \quad (3A.5)$$

Elimination of C_1 and C_2 in the two domains leads to

- (i) within the lattice layer i:

$$\psi(x) = \frac{\rho_i}{\epsilon \kappa^2} \left[1 - \exp(-\kappa r_0/2) \cosh(\kappa|x - x_i|) \right] \quad (3A.6)$$

- and (ii) outside lattice layer i:

$$\psi(x) = \frac{\rho_i}{\epsilon \kappa^2} \sinh(\kappa r_0/2) \exp(-\kappa|x - x_i|) \quad (3A.7)$$

In the polymer adsorption part of the theory we use the potentials at the centres of the lattice layers, ψ_i , again. Here an inconsistency develops as the space charge feels the local potential. This approximation results in an overestimation of the contribution to the potential ψ_i of the charge in layer i, and an underestimation of all other contributions. The contribution of the charge ρ_i to the potential ψ_i is:

$$\psi_i = \frac{\rho_i}{\epsilon \kappa^2} \left[1 - \exp(-\kappa r_0/2) \right] \quad (3A.8)$$

The contribution of ρ_i to the potential ψ_j at all layers j ($j \neq i$) is

$$\psi_j = \frac{\rho_i}{\epsilon \kappa} \sinh(\kappa r_0/2) \exp(-\kappa |x_j - x_i|) \quad (3A.9)$$

The potential distribution originating from a given polyelectrolyte concentration profile is obtained as a sum of all contributions of all layers and their image charges.

For the Gouy-Chapman approach it is convenient to define the potential at an infinite distance from the surface as zero. Outside the M layers taken in the iteration procedure we assume the Debye-Hückel approximation to be valid. The homogeneous electro-neutral bulk solution does not contribute to the field strength at layer M . The Poisson-Boltzmann equation can be solved numerically within each layer by using a sixth order Runge-Kutte integration. The boundary conditions are

(i) at layer M we have

$$\frac{d\psi(x)}{dx} = -\kappa\psi(x) \quad (3A.5)$$

(ii) at the layer boundaries the potentials and the field strength are continuous.

(iii) at the surface of the adsorbent the field strength is determined by the surface charge:

$$\left(\frac{d\psi(x)}{dx}\right)_{x=0} = -\frac{\sigma_0}{\epsilon} \quad (3A.10)$$

Figure 3A.2 gives a comparison of the adsorbed amount between the space and the plane charge model. The lower the salt concentration the better the accordance between both models. Using the Debye-Hückel approximation this can be seen readily. We have to realize that $\rho_i r_0$ is equivalent to σ_i . When the linearization of $\exp(-\kappa r_0/2)$ can be applied, eq. 3A.8 reduces to the first term

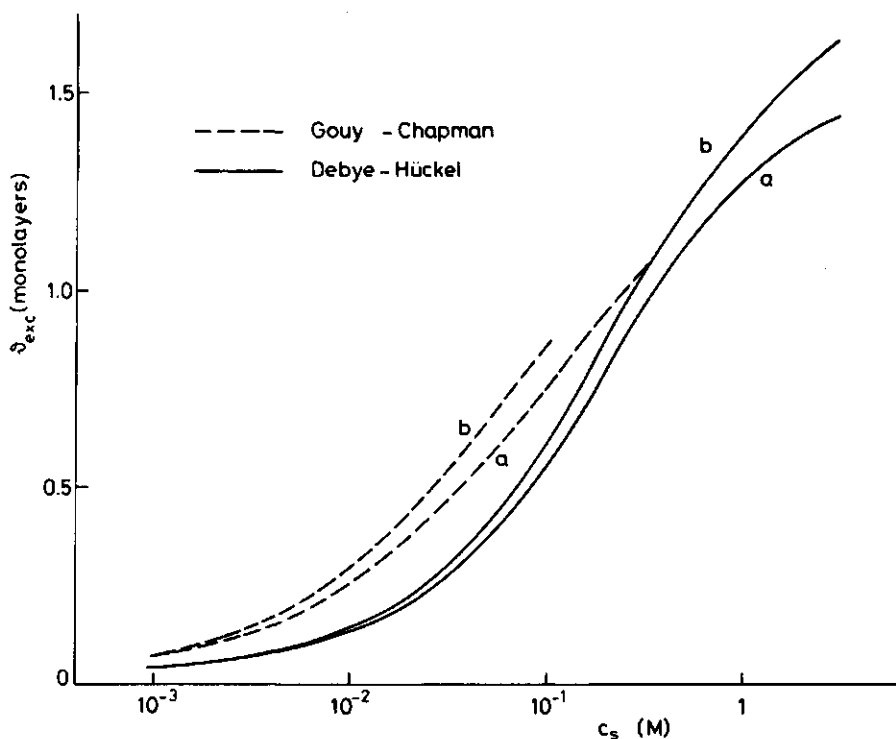


Figure 3A.2. Adsorbed amount as a function of the electrolyte concentration for the plane charge (a) and the space charge (b) model. Absence of surface charge, $\chi = 0.5$, $\chi_s = 4$, $\phi_* = 10^{-4}$, $r = 200$, $\alpha = 1$, $a_o = 1 \text{ nm}^2$, $r_o = 1 \text{ nm}$.

of 3.18. Eq. 3A.9 also reduces to the first term of 3.18 for $x = x_1$. At high salt concentrations lower potentials are obtained by means of the space charge model, as some shielding already occurs within each layer. Because of the lower potentials higher adsorbed amounts are found. The differences between the results of the two models are minor at all salt concentration in both the Debye-Hückel and the Gouy-Chapman approach. Because of computational problems no Gouy-Chapman results are available at very high salt concentrations. The Debye-Hückel results remain similar for both models even at three molar electrolyte. The shielding length κ^{-1} is then only 0.175 times the lattice layer thickness, so most of the polymer charge is compensated within each layer.

4 SYNTHETICALLY DEFINED OLIGOMERS OF L-LYSINE AS MODEL COMPOUNDS IN ADSORPTION STUDIES*

4.1 INTRODUCTION

It is now well recognized, that it is very important to have available homodisperse polymers in studies on polymer adsorption. The shape of the adsorption isotherm, one of the most easily accessible characteristics of polymer adsorption, depends strongly on the heterodispersity¹. The exchange of shorter chains for longer ones whilst increasing the polymer concentration causes the adsorption to increase, whereas adsorption theories for homodisperse polymers predict a distinct plateau value^{2,3,4}. Conversely, adsorption isotherms of homodisperse polymers of high molecular weight give little information about the adsorption process, since the plateau value is virtually independent of the polymer concentration and is already reached at extremely low concentrations. Oligomeric compounds have a lower affinity for the sorbent than polymers and will therefore give more information from the slope of the adsorption isotherm.

In this study the synthesis of defined oligomers of L-lysine is reported. From theoretical² as well as from practical studies⁵ the free ends of adsorbed chains appear to contribute strongly to the properties of the adsorbed layer. Therefore the structure of the end groups of the polymer should not differ too much from the chain groups. The latter consist of a peptide bond and an aliphatic chain containing an amino group, and such components were chosen as end groups. The carboxyl end of the peptide chain was converted into the N-methylamide and an ϵ -aminocaproyl group was attached to the terminal α -nitrogen.

Homodisperse oligomers of L-lysine have been prepared previ-

* Published in coauthorship with G.I. Tesser in Colloid Polymer Sci. 261, 461 (1983) except for some minor modifications.

ously. Waley and Watson⁶ synthesized sequences containing four residues, using classical methods. Yaron et al.⁷ separated homodisperse oligo-L-lysines from a mixture obtained from the partial hydrolysis of poly-L-lysine by means of ion exchange chromatography. It is difficult to convert specifically the α -amino group of an oligo-L-lysine peptide into the ϵ -aminocaproyl group, therefore classical methods were used.

Yaron et al.⁸ have reported that the optical rotation of fully charged oligo-L-lysines depends strongly on chain length. They ascribe this behaviour to end effects and give support to the proposal that fully charged poly-L-lysine possesses the random coil conformation (cf. ref.^{9,10}), whereas others¹¹⁻¹⁴ claim a cooperative structure, e.g. a 3_1 helix¹¹⁻¹³. Optical rotation measurements on oligo-L-lysines and their ϵ -tert.butyloxycarbonyl (Boc)-derivatives with suppressed end effects, should provide additional information.

Monomeric lysine is not suitable for direct comparison with poly-L-lysine since its behaviour is determined to a large extent by its dipolar nature; ϵ -aminocaproic acid N-methylamide was considered to be a better choice.

4.2 EXPERIMENTAL

General procedures

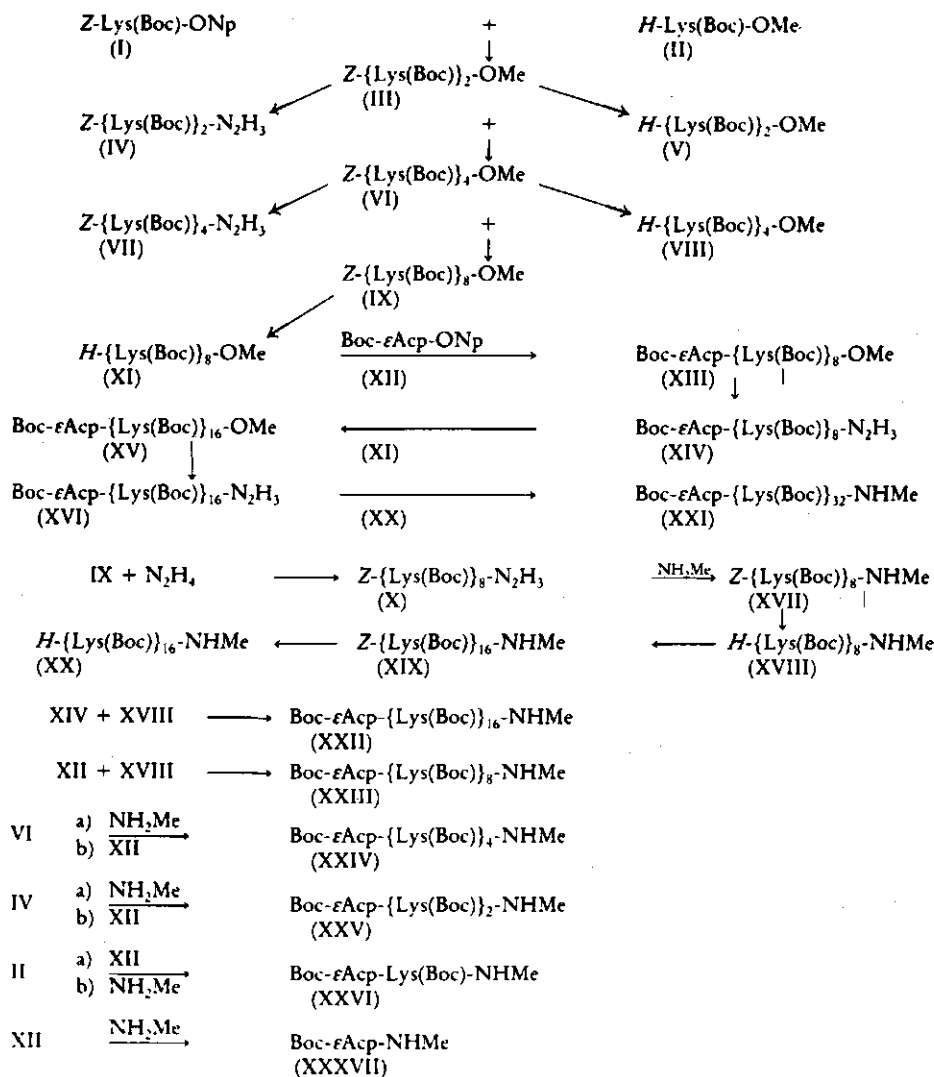
Reaction progression was monitored by thin-layer chromatography using Merck silicagel plates. R_F values are given for the following systems: A, chloroform: methanol = 9:1, and B, chloroform: methanol: acetic acid = 95:30:3.

Optical rotations were measured with an automatic polarimeter (Perkin Elmer 241). Acetic acid was used as the solvent unless otherwise stated. NMR-spectra were recorded with a Bruker 90 MHz spectrometer, operating in the Fourier Transform mode. Melting points were determined in open capillaries, using a Tottoli apparatus.

Synthetic procedures

The synthesis of peptide chains of considerable length is readily achieved by coupling peptide derivatives of the same length

using standard methods of peptide synthesis. In the synthesis of oligopeptide derivatives the solubility of the reaction components can be a limiting factor. It is difficult to anticipate up to what length oligomers of N^{ϵ} -tert.butyloxycarbonyl-L-lysine would remain



Scheme 4.1 Outline of the synthesis*

* Reprinted with permission of Steinkopff Verlag, Darmstadt.

tractable, therefore the appropriate end group was introduced at the octapeptide stage of the synthesis. The outline of the synthesis is given in scheme 4.1*.

In the description of the synthesis of compound VI all standard reactions which lead from the protected aminoesters (I and II) to the protected tetrapeptide ester (VI) are given as an example for the synthesis of longer oligomers. Hydrazides were obtained by the hydrazinolysis of the corresponding methyl esters, using excess hydrazine hydrate with methanol as the solvent. They serve as starting materials for the preparation of azides, which are required as non-racemizing acylating agents. The hydrazides were converted to azides by reaction with NO^+ ions which, in turn were produced *in situ* by the interaction of *tert.*butyl nitrite with H^+ ions at low temperature (-10°C) in a water-free medium. This procedure is known as the Honzl and Rudinger modification of the Curtius method^{16,17}.

α -amino compounds were obtained from the corresponding benzyl-oxy carbonyl (Z) compounds by hydrogenation in the presence of Pd-catalyst. Free amines of more than eight residues were purified by chromatography on silicagel with system B as the eluant.

*Tert.*butyloxycarbonyl- ϵ -aminocaproyl (Boc- ϵ Acp) groups were introduced by the reaction of the corresponding *p*-nitrophenyl ester¹⁸ with α -amino compounds¹⁹. *N*-methylenamides were prepared by aminolysis of the *p*-nitrophenyl ester (XII), the methyl esters (VI) and Boc- ϵ Acp-Lys(Boc)-OMe, and the acyl azide obtained from IV and X.

Sequences shorter than tetramers were purified by washing an extract in ethylacetate with aqueous solutions of sodium carbonate, potassium hydrogen sulfate and sodium chloride respectively. After drying (sodium sulfate) and evaporation of the solvent the products were recrystallized.

Tetramers and longer chain products were precipitated from a solution in dimethylformamide (DMF) by the addition of water and were purified by repeated precipitation in a similar manner.

Deprotection of the peptide derivatives was performed by treatment with 6 M aqueous hydrochloric acid. The solutions did not beco

* Abbreviations are in accordance with the IUPAC-recommendations¹⁵.

clear; they were diluted with *tert.*butanol to remove hydrochloric acid and this resulted in complete dissolution. The solutions were evaporated in vacuo and the deprotected products were lyophilized twice from acetic acid.

Boc- ϵ Acp-NHMe was deblocked by dissolving the compound in ethyl acetate that was 4 M with respect to hydrogen chloride; the HCl-salt crystallized directly from the solution.

H-Lys(Boc)-OMe·HCl (II)

This compound was synthesized by the method of Panneman²⁰. The procedure was modified in such a way, that an excess Boc-azide was used. Thus, *tert.*butyloxycarbonyl azide (0.65 mole) was added to a suspension of L-lysine methyl ester dihydrochloride (93 g, 0.39 mole) in ethyl acetate (100 ml). This was followed by triethylamine (168 ml, 1.2 moles). The reaction mixture was stirred overnight. The precipitated triethylammonium chloride and unreacted L-lysine methyl ester dihydrochloride were removed by filtration, and the filtrate was acidified with hydrogen chloride in ethyl acetate to remove excess of triethylamine and to precipitate the product. The latter was dissolved in hot dioxane, triethylammonium chloride was removed by filtration and cooling yielded the title compound (45 g, 39%) m.p. 150-153 °C, $[\alpha]_D^{22} = +18^\circ$ (c = 2.08 in methanol) (Lit.^{20,21}: m.p. 158-159 °C, $[\alpha]_D^{22} = +19^\circ$ (c = 1.09 methanol)).

Z-Lys(Boc)-Lys(Boc)-OMe (III)

Z-Lys(Boc)-ONP²¹ (56.7 g, 0.11 mole) and H-Lys(Boc)-OMe·HCl (37.7 g, 0.13 mole) were dissolved in dimethylformamide (200 ml) containing triethylamine (17.6 ml, 0.13 mole). After 15 h at room temperature triethylammonium chloride was removed by filtration and the solvent was evaporated in vacuo. The oily residue was dissolved in ethyl acetate and the extract was washed with 10% aqueous sodium carbonate until the yellow colour disappeared. Unreacted H-Lys(Boc)-OMe was then removed by washing with 1 M aqueous potassium hydrogen sulfate. After washing with water to remove traces of acid the extract was dried over sodium sulfate and the solvent was evaporated in vacuo.

The dipeptide derivative crystallized from ether/petroleum ether and was recrystallized from 99% ether and 1% methanol. Yield 63.8 g (93%), m.p. 69-73 °C, $[\alpha]_D^{22} = -4.8^\circ$ ($c = 1.15$ in acetone), $= -6^\circ$ ($c = 1.00$ in acetic acid), $R_F = 0.60$ (A), $= 0.79$ (B), (lit.²¹: m.p. 78-84 °C, $[\alpha]_D^{22} = -5.3 \pm 1^\circ$ ($c = 2.006$ in acetone)).

Z-Lys(Boc)-Lys(Boc)-NH₂ (IV)

The dipeptide ester III (10% solution in methanol) was treated with hydrazine hydrate (5 equiv.). After 20 h at room temperature the reaction mixture was concentrated *in vacuo* to about one fifth of the original volume and diluted with an equal volume of water, which induced the product to crystallize. Recrystallization from methanol: water (1:1) gave the hydrazide IV in 92% yield.

H-Lys(Boc)-Lys(Boc)-OMe (V)

Compound III (0.625 g, 1 mmole) was dissolved in methanol (12.5 ml) and subjected to catalytic hydrogenolysis. Almost 1 equivalent of hydrogen was absorbed within 15 min. The catalyst was removed by filtration and the filtrate concentrated *in vacuo* to the thick, almost colourless oil. Thin layer chromatography did not indicate the presence of any III and the crude product was used immediately in the following stage.

Z-Lys(Boc)-Lys(Boc)-Lys(Boc)-(Lys(Boc)-OMe (VI)

The hydrazide IV (0.621 g, 1 mmole) in DMF (10 ml) was cooled to -25 °C and the solution was treated with ethylacetate (1 ml) containing dry hydrogen chloride (2.77 M). There was a slight evolution of heat causing the temperature to rise to about -15 °C. At this temperature, *tert.*butyl nitrite (0.137 ml, 1.2 mmole) was added and stirring was continued for 30 min. The reaction mixture was subsequently neutralized by the addition of diisopropylethylamine (0.46 ml, 2.77 mmole) and added to freshly prepared V, dissolved in DMF (1 ml). The reaction mixture was stored in the refrigerator for 48 h, concentrated *in vacuo* and processed as indicated.

4.3 RESULTS AND DISCUSSION

Peptide sequences up to a length of 33 aminoacyl residues (inclusive the N-terminal ϵ -aminocaproyl residue) were synthesized by the condensation of acyl azides obtained from hydrazides (table 4-1) and free amino components of the same length, obtained by hydrogenation (Pd-Carbon) of the corresponding benzyloxycarbonyl compounds. In this way sequences of double length are obtained readily (table 4-2). This procedure is limited by the fact that at a certain stage the separation of the product from unreacted precursor becomes difficult. In the above this happened when the peptide chain reached a length of 33 amino acids. This component could not be obtained so pure as the other oligomers. The prepared N-methylamides are presented in table 4-3. The compounds listed in table 4-4 were formed following the introduction of the ϵ -aminocaproyl group.

In the NMR-spectra of deblocked tetra- and longer peptides were no signals that were not attributable to the oligomer but the CH_3 -peak of acetic acid originating from the lyophilization procedure. The integral intensity ratio of the ϵ -methylene and the N-methyl group were compared (table 4-5); they were in agreement with the calculated values within experimental error.

The optical rotations of the final products, before and after deblocking, are given in table 4-6. The optical rotations of the deblocked oligo-L-lysines increase strongly with chain length, confirming the observation of Yaron et al.⁸. In the case of the blocked peptide derivatives, however, there is hardly any change up to the octamer. The lower optical rotations of the longer oligopeptide derivatives can be ascribed to the formation of the α -helix, which has been reported previously for uncharged poly-L-lysine at high pH and for poly-L-Lys(Z)²². The experiments of Yaron et al.⁸ show the onset of α -helix formation at a length of about twelve aminoacyl residues. The pronounced increase in optical rotation with chain length of fully charged oligo-L-lysines indicates that a highly ordered structure exists, not only at high pH but also at neutral pH. The fact that this increase manifests itself with the second L-lysine residue, indicates that no specific interactions are involved with residues that are more distant along the chain.

Table 4-1 Hydrazides

Name	m. p. (°C)	c (%)	$[\alpha]_D^{22}$ (°)	RF_A	RF_B
Z-{Lys(Boc)} ₂ -N ₂ H ₃ (IV)	118-115	1.39	- 10.4	0.31	0.67
Z-{Lys(Boc)} ₄ -N ₂ H ₃ (VII)	175-178	0.87	- 16.2	0.27	0.68
Z-{Lys(Boc)} ₈ -N ₂ H ₃ (X)	223-230	1.00	- 17.5	0.36	0.68
Boc-εAcp-{Lys(Boc)} ₈ -N ₂ H ₃ (XIV)	> 260	1.10	- 17.9	0.30	0.68
Boc-εAcp-{Lys(Boc)} ₁₆ -N ₂ H ₃ (XVI)	> 260	1.12	- 12.4	0.31	0.69

Table 4-2 Products of azide condensations

Name	Precursors	m. p. (°C)	c (%)	$[\alpha]_D^{22}$ (°)	RF_A	RF_B
Z-{Lys(Boc)} ₄ -OMe (VI)	IV, V	120-122	1.02	- 15.3	0.50	0.80
Z-{Lys(Boc)} ₈ -OMe (IX)	VII, VIII	> 260	1.20	- 16.4	0.54	0.74
Z-{Lys(Boc)} ₁₆ -NHMe (XIX)	X, XVIII	> 260	1.01	- 14.6	0.40	0.73
Boc-εAcp- {Lys(Boc)} ₁₆ -OMe (XV)	XI, XIV	> 260	1.05	- 16.2	0.37	0.73
Boc-εAcp- {Lys(Boc)} ₁₆ -NHMe (XXII)	XIV, XVIII	> 260	1.01	- 11.6	0.34	0.72
Boc-εAcp- {Lys(Boc)} ₃₂ -NHMe (XXI)	XVI, XX	> 260	1.07	- 11.9	0.21	0.72

Table 4-3 N-methylamides

Name	Precursors	m. p. (°C)	c (%)	$[\alpha]_D^{22}$ (°)	RF_A	RF_B
Boc-εAcp-NHMe (XXVII)	XIII	119-121	-	-	0.36	0.73
Boc-εAcp-Lys(Boc)- NHMe (XXVI)		127-128	1.0	- 16.1	0.43	0.69
Z-{Lys(Boc)} ₄ -NHMe (VIa)	VI	169-179	1.32	- 16.8	0.45	0.73
Z-{Lys(Boc)} ₂ -NHMe (IVa)	IV	128-130	1.02	- 14.4	0.61	0.74
Z-{Lys(Boc)} ₈ -NHMe (XVII)	X	> 260	1.00	- 18.0	0.42	0.75

Table 4-4 Boc- ϵ Acp derivatives

Name	m. p. ($^{\circ}$ C)	c (%)	$[\alpha]_D^{22}$ ($^{\circ}$)	RF_A	RF_B
Boc- ϵ Acp-Lys(Boc)-OMe (IIa)	oil	-	-	-	-
Boc- ϵ Acp-{Lys(Boc)} ₂ -NHMe (XXV)	140-144	1.11	- 15.2	0.42	0.7
Boc- ϵ Acp-{Lys(Boc)} ₄ -NHMe (XXIV)	207-209	0.96	- 18.1	0.42	0.73
Boc- ϵ Acp-{Lys(Boc)} ₈ -NHMe (XXIII)	> 260	1.03	- 19.2	0.41	0.73
Boc- ϵ Acp-{Lys(Boc)} ₈ -OMe (XXII)	> 260	1.00	- 17.3	0.45	0.76

Table 4-5 NMR intensity ratios

ϵ Acp-Lys _n -NHMe. (n+1) HCl	$I_{\epsilon CH_2}/I_{N-CH_3}$	
	calc.	found*
n = 4	3.3	3.2
n = 8	6.0	6.24
n = 16	11.3	11.6

* Solvent D₂O.

Table 4-6 Optical rotation of Boc-ylated and deBoc-ylated final products

ϵ Acp-Lys _n -NHMe. (n+1) HCl	c* (%)	$[\alpha]_D^{22}$ ($^{\circ}$)
n = 1	0.9	- 10
n = 2	0.9	- 24
n = 4	0.5	- 37
n = 8	0.7	- 49
n = 16	0.7	- 58
n = 32	0.54	- 59
ϵ Acp-(Boc)-{Lys(Boc)} _n -NHMe	c** (%)	$[\alpha]_D^{22}$ ($^{\circ}$)
n = 1	1.0	- 16
n = 2	1.1	- 15
n = 4	0.96	- 18
n = 8	1.0	- 19
n = 16	1.0	- 12
n = 32	1.1	- 12

* solvent: water

** solvent: acetic acid

4.4 REFERENCES

- 1 M.A. Cohen Stuart, J.M.H.M. Scheutjens and G.J. Fleer, J. Polymer Sci., Polym. Phys. Ed. 18, 559 (1980).
- 2 J.M.H.M. Scheutjens and G.J. Fleer, J. Phys. Chem. 83, 1619 (1979).
- 3 A. Silberberg, J. Chem. Phys. 48, 2835 (1968).
- 4 C.A.J. Hoeve, J. Polymer Sci. C 30, 361 (1970); *ibid.* 34, 1 (1971).
- 5 J. Lyklema and T. van Vliet, Faraday Discuss. Chem. Soc. 65, 25 (1978).
- 6 S.G. Waley and J. Watson, J. Chem. Soc. 475 (1953).
- 7 A. Yaron, M.C. Otey, H.A. Sober, E. Katchalski, S. Ehrlich-Rogozinski and A. Berger, Biopolymers 11, 607 (1972).
- 8 A. Yaron, E. Katchalski, A. Berger, G.D. Fasman and H.A. Sober, Biopolymers 10, 1107 (1971).
- 9 D. Balasubramanian, Biopolymers 13, 407 (1974).
- 10 R.M. Eppard, G.E. Wheeler and M.A. Moscarello, Biopolymers 13, 359 (1974).
- 11 M.L. Tiffany and S. Krimm, Biopolymers 8, 347 (1969).
- 12 M.L. Tiffany and S. Krimm, Biopolymers 11, 2309 (1972).
- 13 W.A. Hiltner, A.J. Hopfinger and A.G. Walton, J. Am. Chem. Soc. 94, 4324 (1972).
- 14 P.C. Painter and M.M. Coleman, Biopolymers 17, 2475 (1978).
- 15 Amino acids, peptides and proteins, Vol. 2. Specialist periodical reports, The Chem. Soc., page 226 (1970).
- 16 J. Honzl and J. Rudinger, Coll. Czech. Chem. Commun. 26, 2333 (1961).
- 17 T. Curtius, Berichte 35, 3226 (1902).
- 18 G.I. Tesser and H.U. Fisch, R. Schwyzer, Helv. Chim. Acta 57, 1718 (1974).
- 19 M. Bodanski and V. du Vigneaud, J. Am. Chem. Soc. 81, 5688 (1959).
- 20 H.J. Panneman and F.H.A.A. van Bakel, Neth. patent nr. 12181 (1965).
- 21 R. Schwyzer and W. Rittel, Helv. Chim. Acta 44, 159 (1961).
- 22 J. Applequist and P. Doty, in "Polyaminoacids, Polypeptides and Proteins", (M.A. Stahmann Ed.), Univ. Wisconsin Press, Madison, p. 161 (1962).

5 ADSORPTION OF OLIGO- AND POLYPEPTIDES ON SILVER IODIDE, THEIR EFFECTS ON DOUBLE LAYER AND COLLOID STABILITY^x

5.1 INTRODUCTION

The stability of colloids, if due to the combined action of electrostatic and steric factors, is one of the more complex cases to describe. At the same time, it is of great practical importance.

One of the problems is that steric- and double layer interaction are not independent. Adsorbed polymers, even if uncharged, considerably modify the charge and potential distribution in an electrical double layer. Polymer adsorption is affected by the presence of a double layer, although this is a minor effect if the polymer is uncharged. With respect to the double layer, the main question is: how are the distributions of charge and potential and how do they change upon particle interaction? Concerning the polymer, the main problem is to establish its conformation in the adsorbed state (flat or expanded?, with or without tails? etc.) and the effect of this conformation on steric interaction.

Making a virtue of need, we have undertaken a systematic study of the modification of double layers on dispersed particles by the adsorption of molecules. From such studies, using available corresponding data for monomers, it was possible to obtain some insight in the segment distribution, for instance in the relatively simple case of poly(vinyl alcohol) (PVA) on silver iodide (Koopal and Lyklema¹, Lyklema²). In the present study, this work is extended to oligo- and polypeptides. As compared with PVA, these adsorbates introduce three new features:

^x Part of this chapter has been published in coauthorship with J. Lyklema in "The Effect of Polymers on Dispersion Properties" (T.F. Tadros, Ed.), Academic Press, London, 1982, p. 82

(i) Depending on pH, they can bear a charge which affects their adsorption behaviour.

(ii) Under suitable conditions, some of them assume a helical conformation in bulk, and the interesting question is if this helical structure is retained in the adsorbed state.

(iii) Working with oligomers helps to bridge the gap between monomer and polymer adsorption. Monomers act primarily as modifier of the van der Waals attraction and double layer repulsion, whereas polymers confer their own additional stability factor, provided the adsorbed layer is sufficiently thick.

From the adsorption point of view, monomers usually adsorb in a monomolecular layer; the isotherms are often of the Langmuir or Freundlich type and in many cases desorption upon dilution is possible. In contradistinction, polymers tend to adsorb in thicker layers, the isotherms are of the high-affinity type, and desorption upon dilution is usually not observed. In all these respects, oligomers are expected to exhibit intermediate behaviour.

The emphasis of this chapter is on the adsorption of oligo- and polylysines on silver iodide, whereas some attention will be given to a number of additional adsorbates for comparison purposes. One of the great advantages of the chosen system is that the surface charge σ_0 on silver iodide, which is due to the adsorption of potential-determining ions (Ag^+ , I^-) is measurable and can be varied as a function of pAg . The proton titration charge of the polypeptide depends on pH but not on pAg . In other words, the charges of adsorbate and adsorbent can be separately measured. If a change of pH at fixed pAg leads to a change of σ_0 , this must be a capacitative effect due to the variation in the screening power of the peptide.

All double layer measurements are conducted in 10^{-1} M electrolyte to suppress the diffuse part of the double layer. Consequently, any information on the adsorption of the various substances obtained from double layer measurements only refers to that part of the molecule residing in the inner or Stern layer. In other words, in our double layer measurements we "see" only the train segments. On the other hand, the adsorbed amount is the sum of train-, loop- and tail contributions.

5.2 EXPERIMENTAL

5.2.1 MATERIALS

5.2.1.1 SILVER IODIDE

Silver iodide sols and suspensions were prepared by condensation from potassium iodide and silver nitrate solution as described by de Wit³. The specific area was determined using the methylene blue method as described by Koopal⁴. The determination of the specific area of silver iodide has been a bone of contention for several authors^{3,4,5,6}. The areas found by means of adsorption measurements for several adsorbates, from solution as well as from a gaseous phase, show a rather good correspondence. However, the area obtained from the double layer capacitance near the point of zero charge is usually 3 to 4 times larger. Koopal⁴ uses the "adsorption area" for his polymer adsorption studies and the "capacitance area" for his double layer experiments. This procedure was strongly criticized by de Keizer⁵, who indicated the inconsistency of Koopal's choice and recommended to choose the capacitance surface area in all cases. However, in that case no justice is done to polymer adsorption experiments. If we had used the large capacitance area, very low adsorbed amounts would have been calculated. This would have been in clear conflict with the experimentally always found thick adsorbed layers⁴ and would not have been able to account for the steric stabilization found with poly(vinyl alcohol) by Flier⁷ either. Therefore we used the adsorption surface area. Many of the less recent results of silver iodide double layer work, as compiled by Bijsterbosch and Lyklema⁸, were analyzed by using the capacitance surface area. As we chose the adsorption area some of their conclusions must be reenvisioned. For instance, their components of charge analysis shows the absence of specific adsorption near the point of zero charge, whereas using the adsorption area specific adsorption must be assumed.

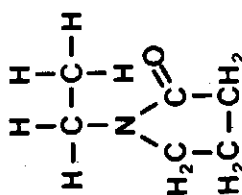
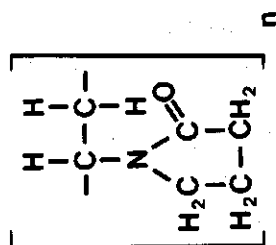
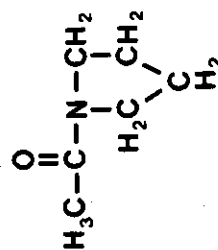
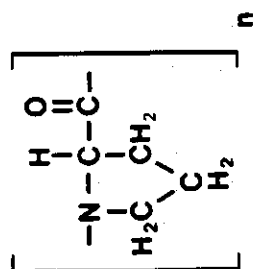
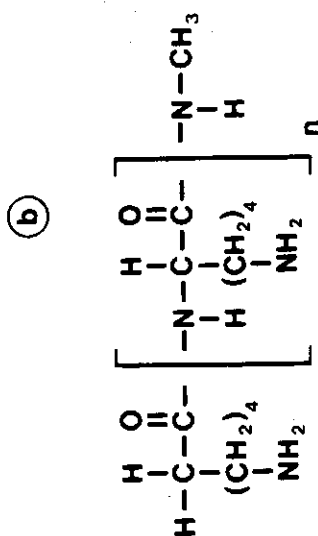
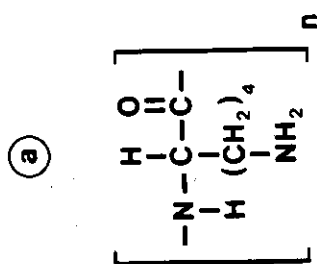
Table 5-1. Compounds used.

Name	Abbreviation	Structure formula +)	Conformation in solution	Degree of polymerisation (D.P.)	Manufacturer
poly-L-lysine		a	pH < 9 random coil pH > 9 α -helix	100 300 2000	Sigma (USA)
poly-DL-lysine		a	random coil	200	Sigma (USA)
ϵ -amino-caproyl-(L-lysyl) _n -N-methylamide	ϵ Acp-Lys _n -NHMe	b	pH < 9 random coil pH > 9 helix or random coil, depending on n	n = 0, 1, 2, 4, 8, 16, 32	x)
poly-L-proline		c	helical	60 500	Sigma (USA)
poly-DL-proline		c	random coil	+ 50	xx)
N-acetyl-pyrrolidine	NAP	d	-	-	ICN Pharmaceuticals Inc. (USA)
poly (vinyl pyrrolidone)	PVP	e	random coil	60, 6000	BASF (FRG)
N-ethyl-pyrrolidone	NEP	f	-	-	Aldridge (Belgium)

+) see below

x) Compounds were synthesized (Chapter 4)

xx) poly-DL-proline was synthesized (section 5.2.1.2.1).



5.2.1.2 ADSORBATES

The monomeric and polymeric compounds used in the adsorption studies are listed in table 5.1. The oligo-L-lysines were synthesized (see chapter 4). To suppress the influence of the end groups the α -amino end of the oligo-L-lysine peptides was blocked with the ϵ -aminocaproyl group, resembling the amino-terminated aliphatic chain of lysine. The carboxyl end was converted into the N-methyl amide, resembling the peptide entity. These compounds were obtained as chloride salts. The polylysines were purchased in the bromide form. To prevent interference with AgI these chloride and bromide ions were exchanged for fluoride or nitrate by precipitation with a slight excess of AgF or AgNO₃ respectively. The silver halogenide was removed by centrifugation. The excess Ag⁺ was removed by adding iodide till the pAg was about 8. Again silver iodide was removed by centrifugation. In this way stock solutions were obtained, which were diluted before use.

NAP and NEP were used for comparison with polyproline and PVP respectively. NEP was distilled prior to use. Poly-DL-proline was synthesized.

5.2.1.2.1 SYNTHESIS OF POLY-DL-PROLINE

Poly-DL-proline was obtained by polymerization of the DL-proline N-carboxyanhydride (DL-proline NCA).

DL-proline NCA

DL-proline NCA was synthesized, using the method developed by Randall⁹ for L-proline NCA, with slight modifications. To a suspension of DL-proline (5.7 g, 0.05 mole) in dry tetrahydrofuran (20 ml) a solution of 5.5 g phosgene in tetrahydrofuran (25 ml) was added. The mixture was stirred until a clear solution was obtained. The solution was degassed *in vacuo* at 35°C. Then the N-chloroformyl-DL-proline was cyclised to DL-proline NCA by adding triethylamine (6.37 ml, 0.045 mole). Triethylammonium chloride precipitated and was removed by filtration. The solvent was evaporated *in vacuo*. The oily residue was dissolved in ethyl acetate

(10 ml) and petroleum ether was added to such an amount that at -30°C no phase separation occurred. The DL-proline NCA crystallized and was recrystallized in the same way. M.p. 20°C , yield 2.3 g (33%).

Poly-DL-proline

DL-proline NCA (1.15 g, 8 mmole) was dissolved in dimethylformamide (50 ml). Diethylamine (16 μl , 0.16 mmole) was added to initiate the polymerization. The solution was allowed to stand overnight, after which it was concentrated *in vacuo*. The polymer was precipitated by successive addition of ether, diisopropyl ether and petroleum ether. Only the third fraction was strongly positive to the TDM (4,4'-tetramethyldiaminodiphenyl-methane) test¹⁰ on N-H groups, showing that a considerable amount of monomer or short polymer was present. The second fraction (0.4 g) was used for the adsorption experiments. The shape of the UV-peptide bond was the same as that of poly-L-proline. The polymeric character was also clear from the shape of the adsorption isotherm.

5.2.2 METHODS

5.2.2.1 SILVER IODIDE CHARGE POTENTIAL CURVES

The AgI-charge-potential curves were measured in an electrochemical cell, in which an AgI suspension was titrated with KI or AgNO_3 . I^- and Ag^+ concentrations were measured with AgI-ion-selective electrodes using a calomel electrode as the reference. The procedure has been described extensively elsewhere (Bijsterbosch¹¹, de Wit³, de Keizer⁵).

5.2.2.2 ELECTROPHORETIC MOBILITIES

Electrophoretic mobilities were measured with a Rank Bros. MKII microelectrophoresis apparatus. Samples were prepared as follows: to 0.9 ml sol ($380 \text{ m}^2/\text{l}$) 0.5 ml poly-L-lysine solution was added and shaken vigorously, using a Vortex whirler. The mixture was rotated end over end overnight. Of this mixture 1.25 ml was diluted

with 10^{-3} M nitric acid to 500 ml. The mobility of the sol particle was measured as described by Koopal⁴.

5.2.2.3 CRITICAL COAGULATION CONCENTRATIONS

Critical coagulation concentrations were determined by the kinetic method described by Reerink and Overbeek¹², using a Vitatron visible light colorimeter. Sols covered with polylysine were prepared as follows: 0.1 ml nitric acid (0.014 M) and 0.1 ml water were added to 1.1 ml sol (10.5 g/l, $145 \text{ m}^2/\text{l}$). To this mixture 0.1 ml polylysine solution (1400 mg/l) was added, corresponding to about twice the plateau value of the adsorption isotherm, to guarantee rapid adsorption and suppress flocculation during the adsorption process. After shaking vigorously the mixture was rotated overnight. The sol was then 1:50 diluted. This sol was left for two hours to allow flocs that might have been formed during the adsorption process to settle. The extinction of different samples varied about 10%, due to, for instance, differences in mixing rate. 1 ml of this sol was mixed with 0.5 ml potassium nitrate solution in the colorimeter and the change in extinction at 660 nm was recorded. Sols covered with PVP were prepared as follows: to 1 ml of sol (10.5 g/l, $145 \text{ m}^2/\text{l}$) the required amount of PVP was added. After vigorous shaking the sol was rotated overnight. 1 ml of this sol was diluted 1:25. Of this sol 0.5 ml was mixed with 1 ml of sodium sulphate solution in the colorimeter. This ratio was chosen to attain sufficiently high salt concentrations in the final mixture to ensure coagulation.

5.2.2.4 ADSORPTION MEASUREMENTS

Adsorption measurements were done through depletion methods. Most of the adsorptions of oligo- and polylysine were measured on suspensions, since it was difficult to obtain reproducible results on sols because of flocculation during the adsorption process. All adsorptions were measured at $\text{pH} \leq 3$. Under these conditions polylysine is fully charged. At neutral pH considerably more flocculation occurs when polylysine is added to the sol than at $\text{pH} = 3$.

In solution at pH = 7 polylysine is still highly charged. Apparently strong interactions are operative between only a few uncharged amino groups that are present and the silver iodide surface. At pH = 10 (maintained using an ammonia/ammonium nitrate buffer) high adsorptions are found (2 mg/m^2). At pH = 12 nearly all added polylysine is removed from the solution. This is an indication that phase separation takes place.

The amount of AgI-suspension present was determined by weighing after drying. Samples for adsorption isotherms were prepared as follows: to 0.9 ml sol ($380 \text{ m}^2/\text{l}$) or suspension ($\sim 300 \text{ g/l}$, $0.19 \text{ m}^2/\text{g}$) the desired amount of electrolyte was added, followed by the poly- or oligolysine. The suspensions had been brought to the desired surface charge before. Since the amount of charge on the surface was large with respect to the Ag^+ or I^- charge in solution, the surface charge remained virtually constant during the adsorption process, whereas the pAg changed. Adsorption took place at constant surface charge rather than at constant potential. The mixture was shaken vigorously and rotated overnight. Then the adsorbent was removed by centrifugation and the concentration of the adsorbate in the supernatant was determined. Adsorbed amounts of oligo- and polylysine are expressed as mg of neutral peptide per m^2 .

The electrolyte dependence of adsorption was determined using a series of short adsorption isotherms on suspension, consisting of three points in the low concentration part of the plateau region.

The influence of pAg on the adsorption was measured by titrating a silver iodide suspension in the presence of oligo- or polylysine. After half an hour of equilibration a sample of the supernatant was taken and the concentration of the adsorbate was determined.

Adsorption isotherms of polyproline and PVP were measured on sols. Here no flocculation occurred.

Concentrations of poly- and oligolysines

Concentrations of poly- and oligolysines were determined using a polyelectrolyte complex titration procedure, analogous to that described by Terayama¹³ and Horn¹⁴. Horn used this method for the titration of positively charged polyethylenimines. We used the same titrant, poly(vinyl sulphonate) and indicator, toluidine blue. In contradistinction to Horn, who used a spectrophotometer for the establishment of the equivalence point, we determined it

visually. A typical calibration curve is given in figure 5.1. For the reaction with polyethylenimine Horn found a nearly exact stoichiometric ratio. In our case the ratio of the numbers of vinylsulphonate per lysine residue varied from 0.8 to 1, depending on salt concentration and molecular weight.

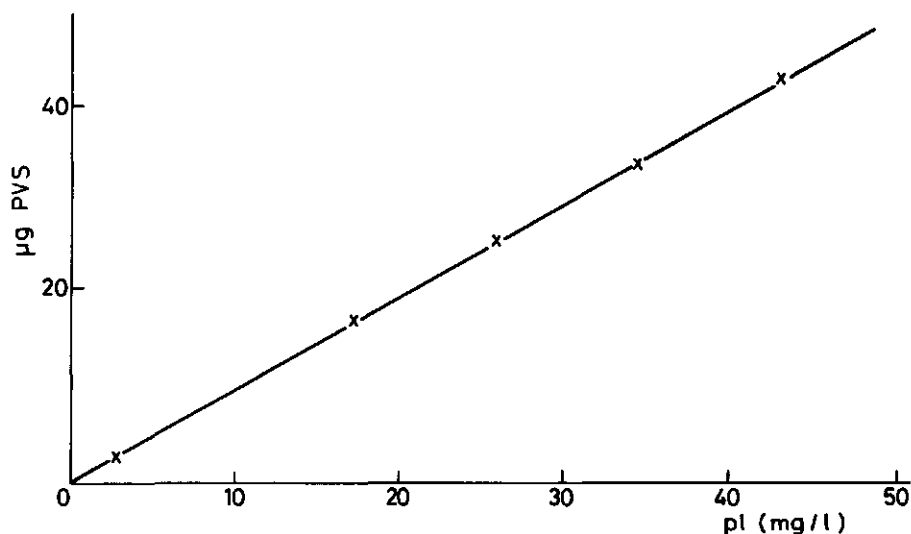


Figure 5.1. Calibration curve for the concentration determination of polylysine: amount of poly(vinyl sulphonate) (PVS) per ml of polylysine solution versus polylysine concentration (pl). Electrolyte 10^{-2} M KF; pH = 3; DP = 300.

For oligomers shorter than the pentamer the titrimetric concentration determination method does not work. Apparently sufficiently stable complexes are not formed. However, the adsorption for one point of the adsorption isotherm can be estimated. At a certain adsorbed amount the negative surface charge of the AgI sol is compensated by the positive charge of the substrate, leading to coagulation. The procedure was as follows: to 7.5 ml of an AgI sol ($48 \text{ m}^2/\text{l}$) at $\text{pI} = 4$ and $\text{pH} = 4$ aliquots ($50 \text{ }\mu\text{l}$) of adsorbate solution were added at intervals of fifteen seconds. When the equivalence point was reached the sol coagulated within fifteen seconds. Part of the adsorbate adsorbs on the silver iodide, the remainder is left in solution. To estimate the amount adsorbed the experiment was repeated with polylysine. As the equivalence point lies on the

rising part of the high affinity adsorption isotherm, all added polylysine adsorbs. The same amount adsorbed was taken for the oligomers at the coagulation concentration. The concentration of the adsorbate solution was chosen such that 20-60 aliquots of solutions had to be added.

The concentrations of polyproline and PVP

The concentrations of polyproline and PVP were measured from the absorbance from the peptide bond. Using a Beckmann 3600 spectrophotometer a residual molar extinction coefficient of $6260 \text{ dm}^3 \text{ mole}^{-1} \text{ cm}^{-1}$ was measured at 205 nm for poly-L-proline; for poly-DL-proline we found $5680 \text{ dm}^3 \text{ mole}^{-1} \text{ cm}^{-1}$. The residual molar extinction coefficient of PVP was $5850 \text{ dm}^3 \text{ mole}^{-1} \text{ cm}^{-1}$, which is slightly higher than the one reported by Cohen Stuart¹⁵, probably because of less stray light from a better spectrophotometer.

5.3 RESULTS AND DISCUSSION

5.3.1 POLY-L-LYSINE

The adsorption of this substance on AgI follows a simple pattern and allows a straightforward interpretation. Isotherms at low electrolyte concentration (10^{-2} M) are given in figure 5.2. They are

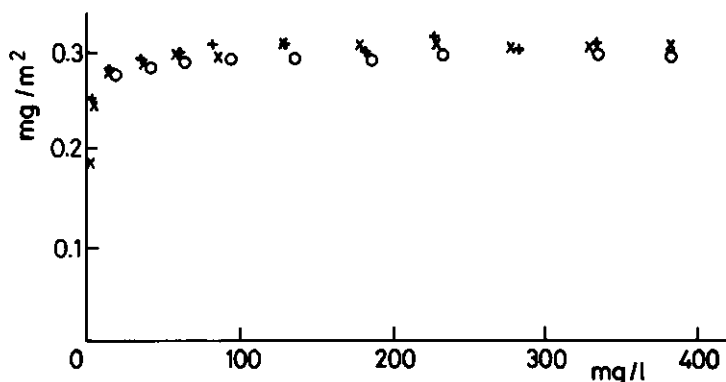


Figure 5.2. Adsorption of poly-lysines on silver iodide, x poly-L-lysine, DP = 300; o *idem*, DP = 2000; + poly-DL-lysine, DP = 250. $\sigma_0 = -0.03 \text{ C/m}^2$, electrolyte 10^{-2} M HNO_3 , $T = 293 \text{ K}$.

of the high affinity type, with a well-defined plateau of about 0.30 mg m^{-2} . This plateau is independent of molecular mass and not different from that for poly-DL-lysine. Insensitivity of plateau adsorption to molecular weight indicates adsorption in a flat conformation, *i.e.* with trains only.

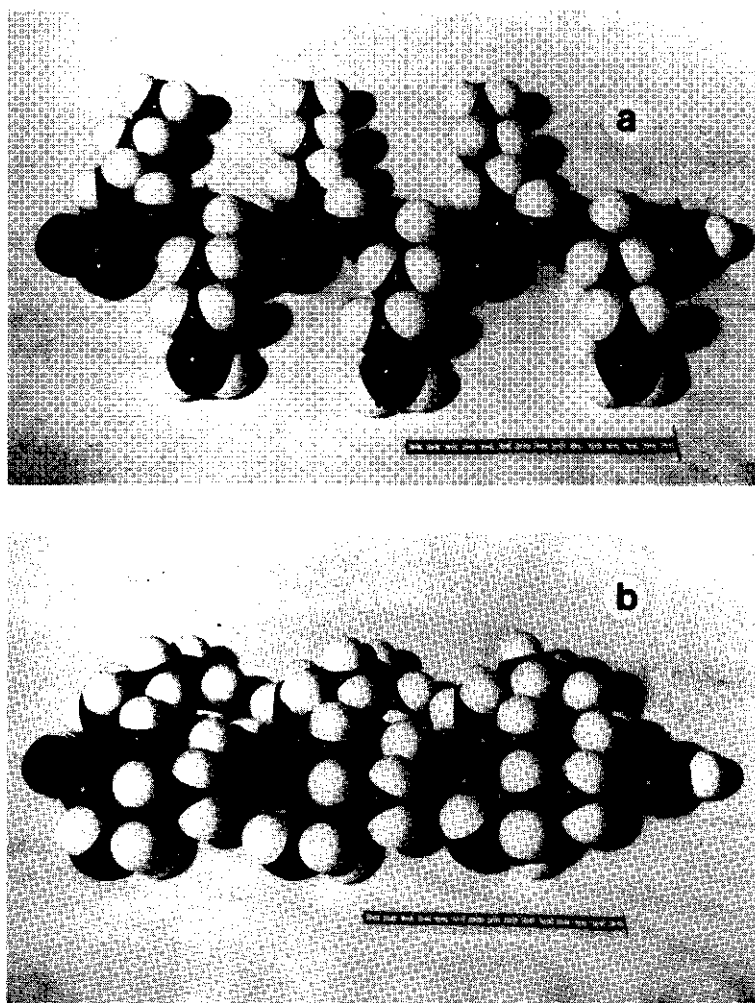


Figure 5.3. Stuart models of poly-L-lysine; a) extended configuration, b) compact configuration.

Figures 5.3 are Stuart models of poly-L-lysine. In the upper picture the molecule is fully extended, the lower one is the more compact configuration. Because of entropical reasons, an interme-

diate situation seems the most probable. Maximum monolayer coverage for these two configurations would amount to 0.41 and 0.61 mg m^{-2} , respectively. Comparison with the experimental value suggests that the molecule adsorbs in a rather extended fashion, i.e. with a relatively large contact area with the AgI.

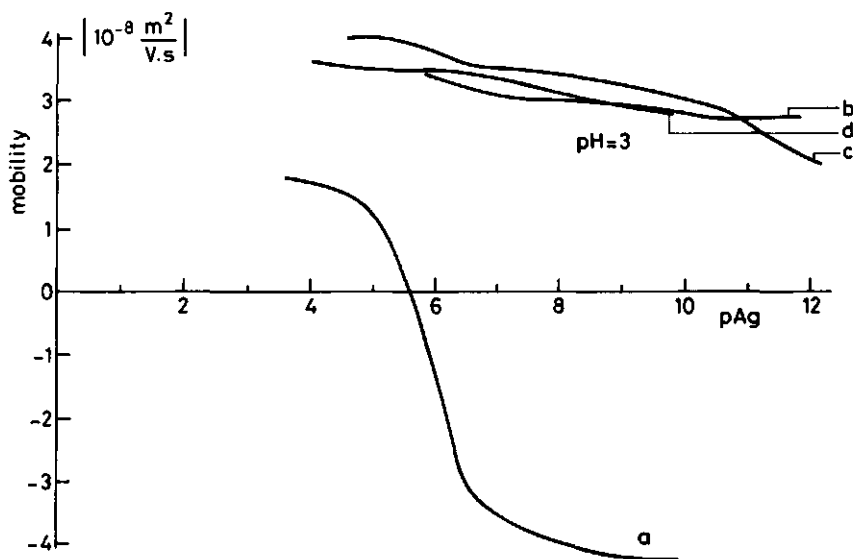


Figure 5.4. Electrophoretic mobility of AgI sol particles covered with poly-L-lysine at plateau adsorption; a) without poly-L-lysine, b) with poly-L-lysine, DP 100, c) idem, DP 300, d) idem, DP 2000. $T = 293 \text{ K}$, electrolyte 10^{-3} M HNO_3 .

Electrophoretic studies (figure 5.4) support this picture: mobility versus $p\text{Ag}$ curves in the presence of adsorbed poly-L-lysine are independent of molecular weight. If the molecules had adsorbed with loops and/or tails, the slipping plane would have moved outwards with increasing molecular weight, leading to a concomitant change of mobility.

The electrokinetic charge reversal occurring at $p\text{Ag} \gtrsim 6$ indicates superequivalent adsorption (more positive charge due to poly-lysine in the Stern layer than negative charge on the surface). The near-independence of the mobility of $p\text{Ag}$ evidences the complete screening of the surface charge by countercharge.

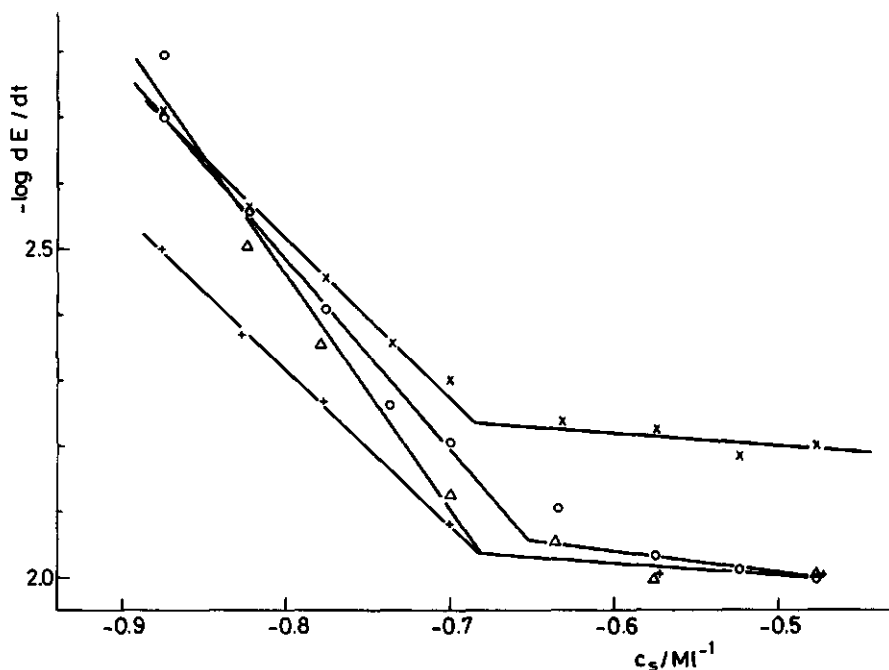


Figure 5.5. Stability curves for AgI sols covered with polylysines: rate of change of extinction E versus the logarithm of the indifferent electrolyte concentration (c_s). Electrolyte, KNO_3 ; pH = 3; Poly-L-lysine: +, DP = 100; Δ DP = 300; x, DP = 1000; Poly-DL-lysine: o, DP = 300.

Table 5-2. Critical coagulation concentrations (ccc) for poly-L-lysines (PLL) and poly-DL-lysine (PDLL).

compound	DP	ccc (mmole/l)
PLL	100	209
PLL	300	209
PLL	1000	207
PDLL	200	221

Stability and adsorption behaviour are closely related. Figure 5 presents the stability curves for some polylysines used. Table 5-2 gives the critical coagulation concentrations. No more than the electrophoretic mobilities do these concentrations vary systematically with chain length. Concentrations of about 200 mmole

are typical for electrostatic stabilization and interaction of the DLVO-type. If steric stability had occurred, much higher critical coagulation concentrations would have been found. The absence of steric stability confirms the absence of loops and tails. The stability of the sol was not particularly sensitive to lanthanum nitrate, supporting the charge reversal of the diffuse double layer part.

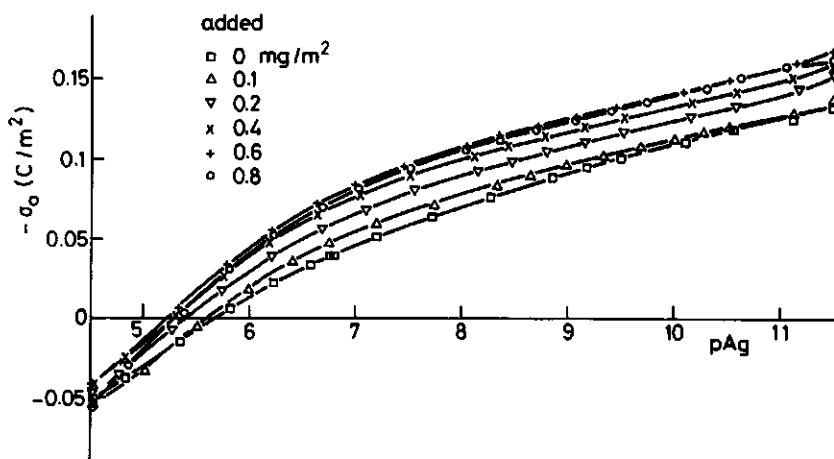


Figure 5.6. Surface charge on AgI particles in the presence of adsorbed poly-L-lysine. pH = 3, T = 293 K, electrolyte 10^{-1} M KNO_3 . The amount of polypeptide added is expressed per unit area of the adsorbent.

Charge-pAg curves for AgI in the presence of adsorbed high molecular weight poly-L-lysine at an electrolyte concentration of 10^{-1} M are given in figure 5.6. Qualitatively, the following three features are observed upon addition of the adsorptive:

- (i) the point of zero charge shifts to the left, i.e.: in a more positive direction;
- (ii) the slope of the curves changes;
- (iii) there is a tendency of the curves to converge to the left of the range of pAg that is experimentally accessible.

These three features, or variants of them, are usually also encountered for low molecular weight and high molecular weight uncharged adsorbates. Physically the interpretations are as follows.

Ad (i). The occurrence of superequivalent adsorption points to a non-electrostatic contribution to the interaction energy. Because of this, there is also some adsorption at the point of zero charge. The positively charged poly-L-lysine facilitates adsorption of I^- ions, hence a higher concentration of Ag^+ ions is needed to reach the new point of zero charge, i.e. this point shifts to the left.

Ad (ii). The slope of these curves or, for that matter, $-F\partial\sigma_0/RT\partial pAg$ is identical to the differential double layer capacitance, C . It is a measure of the extent of screening of the surface charge and determined by the adsorbate layer thickness (more precisely: by the Stern layer thickness δ , because in 10^{-1} M KNO_3 C is dominated by its non-diffuse part), its dielectric permittivity ϵ_s , and by specific adsorption. Without further information these three contributions cannot be unravelled. As a rule, C decreases upon adsorption of organic molecules, because (a) the Stern layer becomes thicker, (b) ϵ_s tends to decrease, and (c) specifically adsorbed ions are displaced. Poly-L-lysine does not follow this trend. Around the point of zero charge the capacitance clearly increases, whereas on negative surfaces (high pAg) C remains roughly constant. The increase of C in the pAg range 6-8 with respect to uncovered AgI is probably dominated by the specific adsorption of poly-L-lysine countercharge. The decrease of C with increasing pAg is perhaps attributable to dielectric saturation, as in the case of the absence of poly-L-lysine. It follows also from figure 5.6 that polymer dosage above 0.4 mg m^{-2} leads to no further change in σ_0 ; at this dosage the surface is apparently saturated. This amount added is in good agreement with the direct estimation of the monolayer capacity for a loosely packed adsorbed layer. At a salt concentration of $0.1 \text{ M } KNO_3$ the plateau value of the adsorption isotherm is 0.55 mg/m^2 , so a certain amount of the polyelectrolyte is not accommodated in direct contact with the surface but in loops and tails, the formation of which being less unfavourable than at low salt concentration due to the strong shielding.

Ad (iii). Polylysine being positively charged, it will be desorbed if the AgI surface is made sufficiently positive. If no peptide adsorbs, σ_0 becomes independent of the polymer dosage. Figure 5.6 suggests that this situation prevails at about 1 pAg unit to the left of the experimentally accessible range. This information

serves two purposes that we shall not pursue here: (1) it gives information on the binding strength, and (2) it allows the direct calculation of the adsorbed amount Γ_A through:

$$\Gamma_A(pAg) = -2.303 \frac{RT}{F} \int_{pAg_m}^{pAg} \left(\frac{\partial \sigma_0}{\partial \mu_A} \right)_{pAg, T} dpAg \quad (5.1)$$

where pAg_m is the pAg of the merging point². Eq. 5.1 follows from Gibbs' law. For tetraalkylammonium ions, Γ_A calculated in this way agrees within experimental error with directly measured data (De Keizer and Lyklema¹⁶). In our case this equation only supports the qualitative insight that the adsorption must increase with rising pAg . We obtain no quantitative results, since the region where the shape of the $\sigma_0(pAg)$ curves changes is the steep ascending part of the adsorption isotherms (fig. 5.2), where the concentrations of the polymer are vanishingly low. Hence, μ_A is not defined.

5.3.2 POLY-L-PROLINE, POLY-DL-PROLINE AND PYRROLIDONE DERIVATIVES

Before discussing other lysines it is useful to consider the counterpart of poly-L-lysine, namely poly-L-proline, which is uncharged in solution and forms a helix. It follows from our studies that the helix persists in the adsorbed state as we shall proceed to prove. Figures 5.7a and 5.7b give the $\sigma_0(pAg)$ curves for two molecular masses.

Again, the following features are observed:

- (i) the point of zero charge becomes more positive upon adsorption, and more strongly so than with poly-L-lysine;
- (ii) upon adsorption of the peptide the capacitance decreases throughout, due to the compounded action of counterion displacement by uncharged groups and a reduction of ϵ_s/δ .
- (iii) all curves pass through a very sharp common intersection point at $\sigma_0 = -5.2 \times 10^{-2} \text{ cm}^{-2}$ and $pAg = 7.55$. This is not a desorption point (as with poly-L-lysine) but an adsorption maximum as a function of pAg or σ_0 .

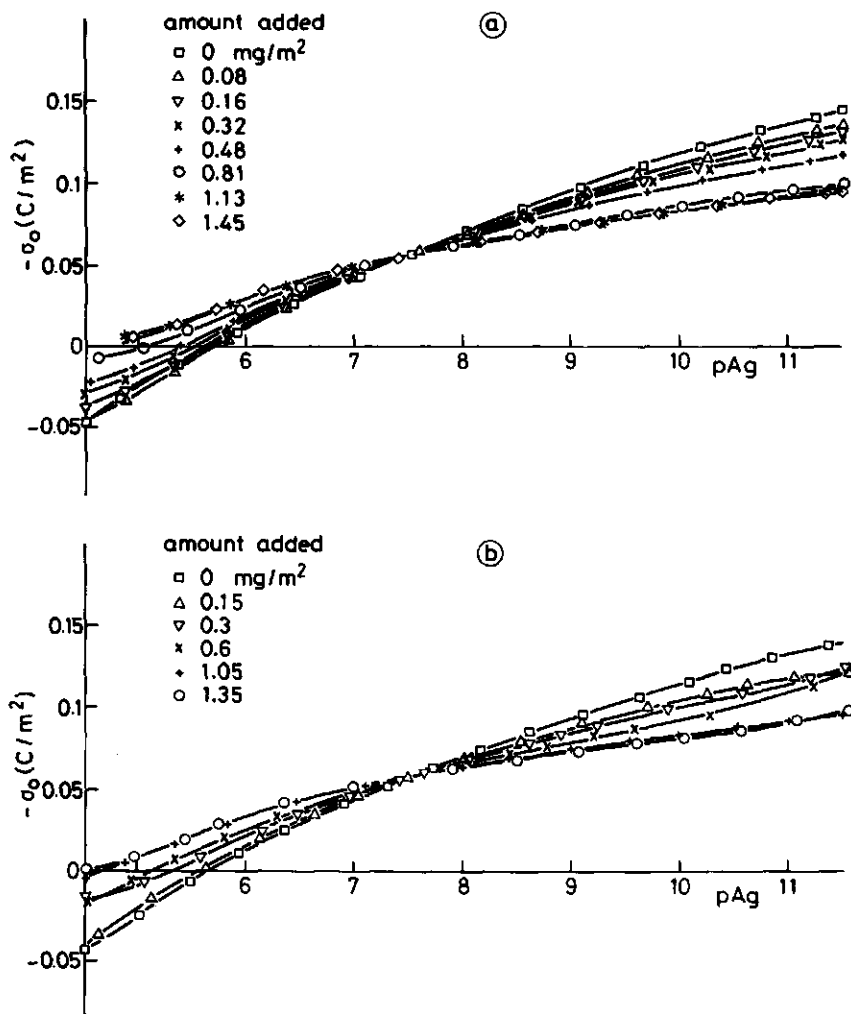


Figure 5.7. Surface charge on AgI particles in the presence of adsorbed poly-L-proline (a. DP = 60, b. DP = 500), pH = 6, T = 293 K, electrolyte 10^{-1} M KNO_3 .

The counterpart of equation 5.1 reads for this case:

$$\Gamma_A(\text{pAg}) - \Gamma_A(\text{pAg}_m) = 2.303 \frac{RT}{F} \int_{\text{pAg}_m}^{\text{pAg}} \left(\frac{\sigma_0}{\partial \mu_A} \right)_{\text{pAg}, T} d\text{pAg} \quad (5.2)$$

if pAg_m refers to the intersection point. It is easily verified that the righthand side of 5.2 is always negative, implying that $\Gamma_A(\text{pAg})$ is always lower than $\Gamma_A(\text{pAg}_m)$.

The explanation of the occurrence of this maximum is relatively subtle. Basically, competition occurs between water dipoles and segments of the polyproline. The dipole moment of water is relatively high, so that in strong Stern layer fields water is preferred over apolar or less polar groups or molecules. (The binding energy is $(\vec{\mu} \cdot \vec{E})$ plus quadrupole and polarisation contributions including lateral interactions). It follows that the water binding increases to the left and to the right, so that it must be a minimum somewhere near the centre. This minimum is obviously the maximum of the peptide adsorption.

Two features are clear (i) the unsurpassed sharpness of the common intersection point and (ii) its independence of molecular weight (compare fig. 5.7a and b). The former observation indicates that the mode of adsorption of the polypeptide is exactly the same from the first to the very last molecule, the latter one is evidence for the same mechanism irrespective of the length of the molecule. These considerations prove that poly-L-proline adsorbs as a rather rigid entity; this rigid entity might well be a helix.

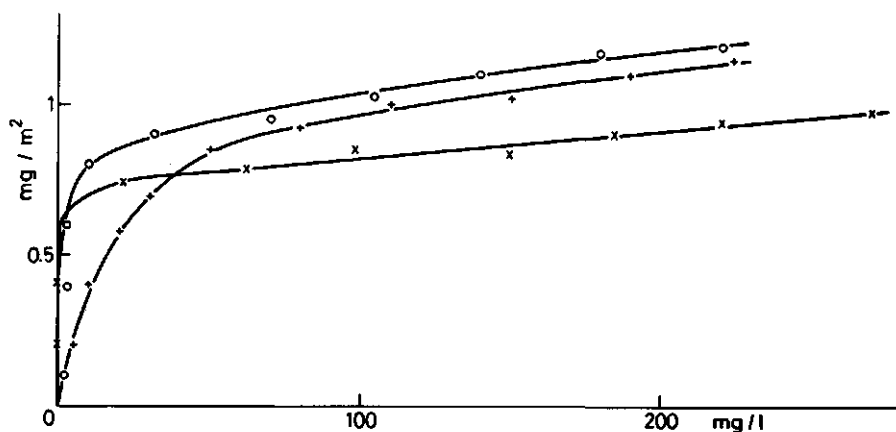


Figure 5.8. Adsorption isotherms for polyprolines on AgI. Poly-L-proline: x, DP = 60; o, DP = 500; Poly-DL-proline: +, DP \approx 50.

Additional information is obtained from the adsorption isotherm. Although the titration curves of AgI, covered with the longer and shorter polypeptide, do not differ, these two polymers have different plateau values of the adsorption isotherm (figure 5.8), viz. 1.1

and 0.9 mg/m^2 , respectively. Especially in the case of the longer polypeptide, the amount of adsorbed polymer continues to rise when no further change in the titration curves is observed anymore. It can be deduced that the molecule is not so stiff that no protruding tails or loops can occur, since part of the polymer is not accommodated in the Stern layer. This is also confirmed by the fact that an AgI sol can be stabilized sterically by adsorption of poly-L-proline.

It is instructive to compare poly-L-proline with poly-DL-proline because the latter molecule is not a helix but a random coil. Poly-DL-proline also shows high affinity adsorption, although the isotherm (figure 5.8) is more rounded than that of poly-L-proline. This effect might be attributed to the presence of non-adsorbing oligomers, originating from incomplete polymerization.

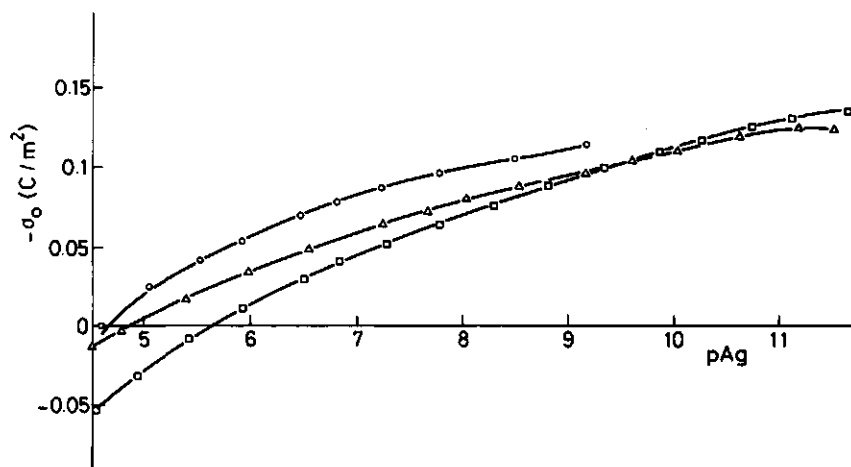


Figure 5.9. Surface charge on AgI particles in the presence of adsorbed poly-DL-proline (Δ) and NAP (∇); \square , blank. pH = 6; T = 293 K; electrolyte 0.1 M KNO_3 .

The $\sigma_0(\text{pAg})$ curves for poly-DL-proline and NAP are given in figure 5.9, where only saturation curves are presented (*i.e.* curves corresponding to the plateau adsorption). The curves for poly-L-proline and poly-DL-proline differ substantially, the most striking difference being the much more negative surface charge at the intersection point (*i.e.* the adsorption maximum) for the coiled modifi-

cation. At a highly negative surface charge the DL-product is less easily displaced by water dipoles. The place of the common intersection point does not only depend on the binding of water dipoles but also on that of the dipoles of the adsorbate and the changes in thickness and dielectric constant of the Stern layer upon adsorption. De Keizer⁵ derived a formula for the surface charge σ_m in the common intersection point, using a simple model of patchwise adsorption. The double layer is considered to consist of a covered and an uncovered part, each with its own potential difference across the Stern layer, originating from dipolar effects (χ_C^0 and χ_u respectively), its own Stern layer thickness (δ_C and δ_u respectively) and Stern layer relative dielectric permittivity (ϵ_C and ϵ_u respectively). χ_u is assumed to vary linearly with the surface charge. In the absence of adsorbate, there is a certain value of σ_O , σ_R , where the net dipolar contribution of the water molecules is zero. The value of χ_u at the point of zero charge is denoted χ_u^0 . According to de Keizer⁵) σ_m is given by

$$\sigma_m = \frac{\chi_u^0 - \chi_C^0}{\chi_u^0/\sigma_R - \delta_u/\epsilon_u + \delta_C/\epsilon_C} \quad (5.3)$$

It is difficult to unravel the influence of the various parameters in this equation. From several studies^{5,8,11} it was concluded that at the point of zero charge water molecules are oriented with their negative sides to the surface, thus giving a negative contribution to χ^0 , which is estimated to be about -0.2 V. The adsorption of organic matter tends to increase the Stern layer thickness and to lower its dielectric constant. When the adsorbed organic molecules have no net dipole momentum, i.e. $\chi_C^0 = 0$, the surface charge for maximum adsorption is less negative than the charge of random water orientation, σ_R . When adsorbed molecules have a dipole pointing to the surface with the negative side, i.e. $\chi_C^0 < 0$, σ_m is still less negative.

Using a molecular model (fig. 5.10) we can see that in poly-L-proline the aliphatic rings are attached to the surface, in contradistinction to the more polar parts that remain inside the helix. Hence it is likely that hydrophobic bonding is responsible for the adsorption. The dipolar carbonyl group that is nearest to the

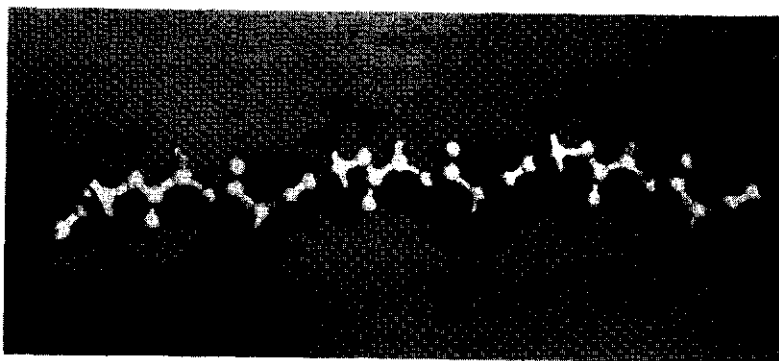


Figure 5.10. Model of helical poly-L-proline.

surface points to the surface with the negative oxygen atom. This carbonyl group dominates χ_C^O , since the dielectric constant in the region near the surface is lower than further away. So we expect a negative χ_C^O . In the case of NAP we expect the planar molecule to adsorb flat on the surface with no net dipole momentum perpendicular to the surface. Then χ_C^O is nearly zero. For poly-DL-proline it is difficult to indicate a most probable orientation, although one can imagine that the more flexible structure will allow the aliphatic ring to make more contact with the surface. A more flat orientation might give a less negative χ_C^O . Poly-DL-proline and NAP lower the slope of the $\sigma_0(\text{pAg})$ curve less than poly-L-proline does. Because of the strong shielding of the diffuse layer by the 0.1 M indifferent electrolyte, this slope is directly related to the Stern layer capacitance ϵ_C/δ_C , if changes with σ_0 in specific adsorption of counterions do not contribute. Both the less negative χ_C^O and the higher Stern layer capacitance point to a higher value of σ_m for poly-DL-proline and NAP, as is observed experimentally.

Since the segments are identical for the L- and DL-form, this observation can only mean that in the DL-product the chain is more flexible than it is in the L-modification. All this supports the view that poly-L-proline is a helix, in solution as well as in the adsorbed state, whereas poly-DL-proline is a random coil in both situations.

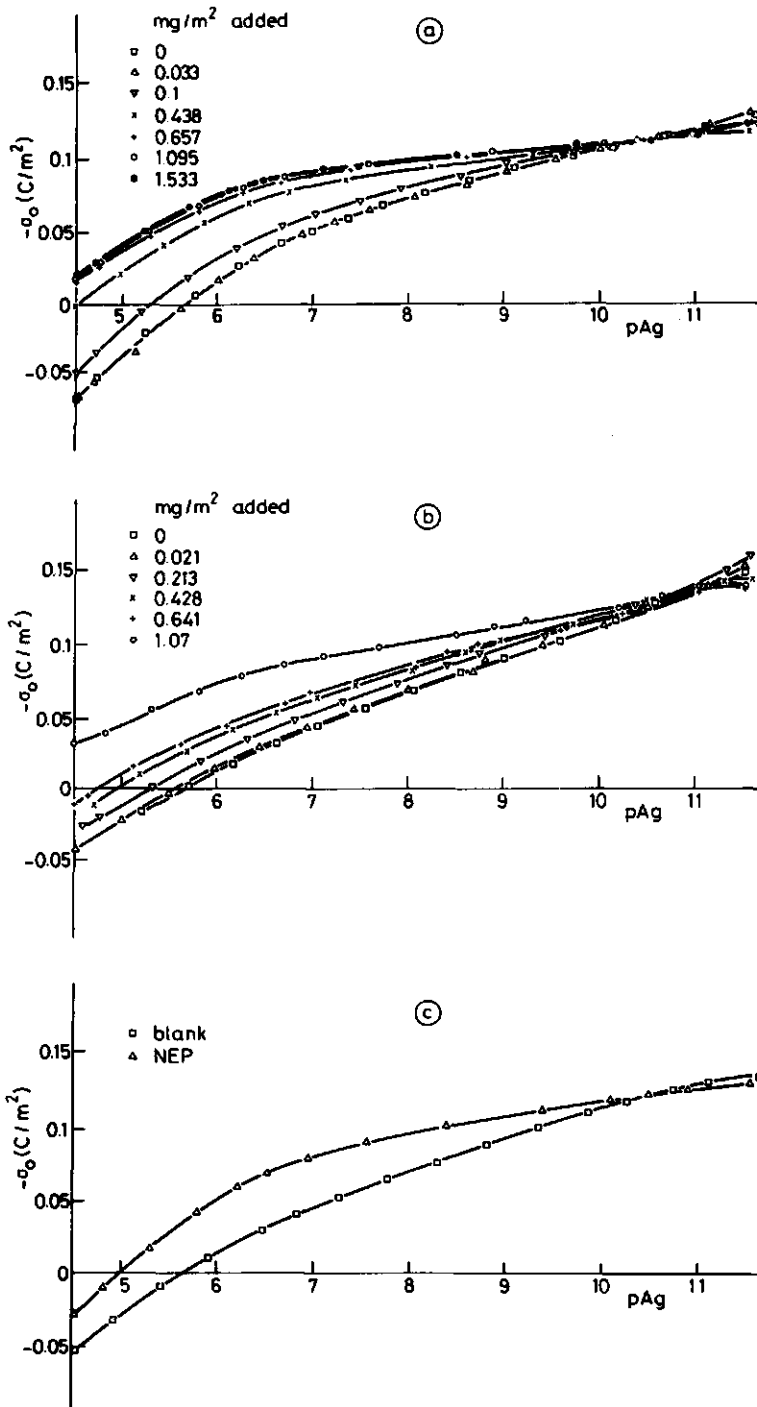


Figure 5.11. Surface charge of AgI particles in the presence of adsorbed PVP and NEP. PVP: a, DP = 60; b, DP = 6000. NEP: c. pH = 6; T = 293 K; electrolyte 0.1 M KNO_3 .

A number of observations with other adsorptives are in line with this. Qualitatively the $\sigma_0(\text{pAg})$ curve for poly(vinyl pyrrolidone) (figure 5.11) better resembles the one of poly-DL-proline than the curve of poly-L-proline. Quantitatively, PVP has a stronger influence on σ_0 than poly-DL-proline. The common intersection point of the lower molecular weight PVP (figure 5.11a) is much sharper than that of the longer polymer (figure 5.11b). This might be attributed to slower equilibration of the polymer conformation at the surface, which might lead to incomplete equilibration on the time scale of the experiment. It must be noted that at such high pAg values common intersection points are difficult to establish accurately. Figure 5.11c contains the $\sigma_0(\text{pAg})$ curve for N-ethyl pyrrolidone. This substance mimicks the monomer of PVP. Again a qualitatively similar curve is obtained, although a much higher capacitance is observed near the point of zero charge. High capacitances are often observed when desorption or reorientation occurs. In view of these considerations, the experiments indicate that with increasing positive charge the monomers reorient (or even desorb?), whereas the polymer segments cannot adjust themselves because of steric restrictions.

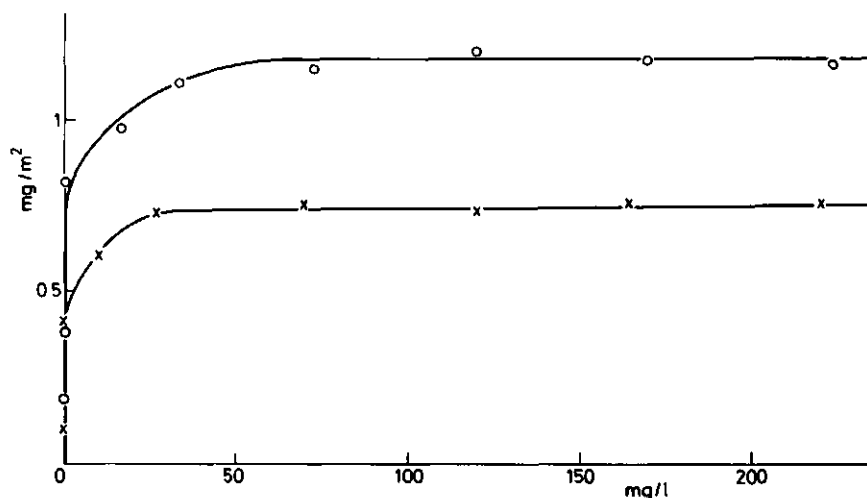


Figure 5.12. Adsorption isotherms for PVP on AgI. x, DP = 60; o, DP = 6000.

We also see with PVP that long and short polymers have about the same maximum change of the $\sigma_o(pAg)$ curve with respect to the blank curve, whereas they have different plateau values of the adsorption isotherm (figure 5.12). Again, increasing amounts of polymer with increasing chain length indicate accommodation in loops and tails. This feature is also reflected in stability data. Silver iodide covered with high molecular weight PVP in the plateau region of the adsorption

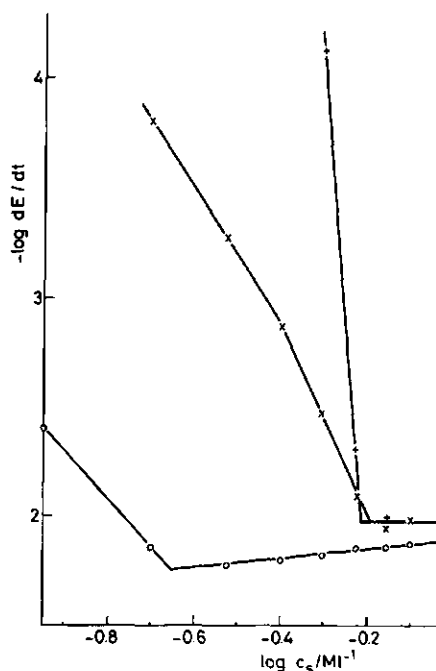


Figure 5.13. Stability curves for AgI sols covered with PVP. Electrolyte (c_s), Na_2SO_4 . 10% excess PVP with respect to plateau value: o, DP = 60; x, DP = 6000. 500% excess PVP with respect to plateau value: +, DP = 6000.

Flory's work¹⁷ it can be derived that even for rather long chains polymer solutions can be stable at low concentrations above the critical χ . The coagulation at salt concentrations lower than the

tion isotherm cannot be coagulated by simple electrolytes in the concentration range, typical for DLVO-type electrostatic stabilization. At much higher salt concentrations the polymer can be salted out. For example, 0.56 M sodium sulphate solution is a θ -solvent (Flory parameter $\chi=0.5$). At higher salt concentrations phase separation occurs for infinitely long chains. Then the adsorbed layers collapse and stick together when two particles meet. In figure 5.13 we see stability curves for sols covered with PVP, which was added in 10% excess with respect to the plateau value of the adsorption isotherm. So in the solution the polymer concentration is very low. The coagulation rate increases with the Na_2SO_4 concentration over the whole salt concentration range. The maximum coagulation rate is obtained at salt concentrations somewhat higher than the value corresponding to $\chi = 0.5$. From

critical one can be understood from the fact, that the adsorbed amount increases when the solvent becomes poorer because of the increase of the salt concentration. Since only little polymer is present in solution, adsorbed chains will form bridges between particles and cause coagulation. At higher polymer concentration (ca. 100 ppm) additional adsorption takes place from solution and no coagulation occurs at Na_2SO_4 concentrations lower than 0.56 M. At high Na_2SO_4 concentrations the coagulation rate increases rapidly with the salt concentration. The low molecular weight PVP gives much less steric stabilization. Already at Na_2SO_4 concentrations much lower than the one corresponding to the critical χ , the maximum coagulation rate is reached. This concentration still considerably exceeds that predicted by the DLVO-theory.

5.3.3 POLY-L-LYSINE AND POLY-DL-LYSINE

The adsorption isotherms of these two compounds are very similar (figure 5.2), as would be anticipated from the fact that both polymers are known to be in the random coil conformation at acidic pH (Appelquist and Doty¹⁸). At negatively charged AgI the titration curves (figures 5.6 and 5.14a) also show the same behaviour. The same holds for the stability measurements (figure 5.5), which were also done at a high surface charge. The critical coagulation concentration for poly-DL-lysine was similar to that of poly-L-lysine.

However, near the point of zero charge we observe a difference: the curve of poly-DL-lysine does not merge with the curve of uncovered AgI. Apparently poly-DL-lysine has a lower tendency to desorb. Probably, this behaviour can be attributed to a higher flexibility of the poly-DL-lysine chain, which allows the hydrophobic parts of the molecule to come in contact with the surface when electrostatic interactions lose their power. That polymerization into an L-lysine chain confers some additional stiffness can also be inferred from optical rotation measurements of oligo-lysines (see section 4.3). Since all asymmetric carbon atoms have the same chemical environment, we expect nearly the same contribution to the optical rotation by each monomer unit.

The strong rise of the optical rotation with chain length shows that a certain structure builds up to lengths of more than ten residues.

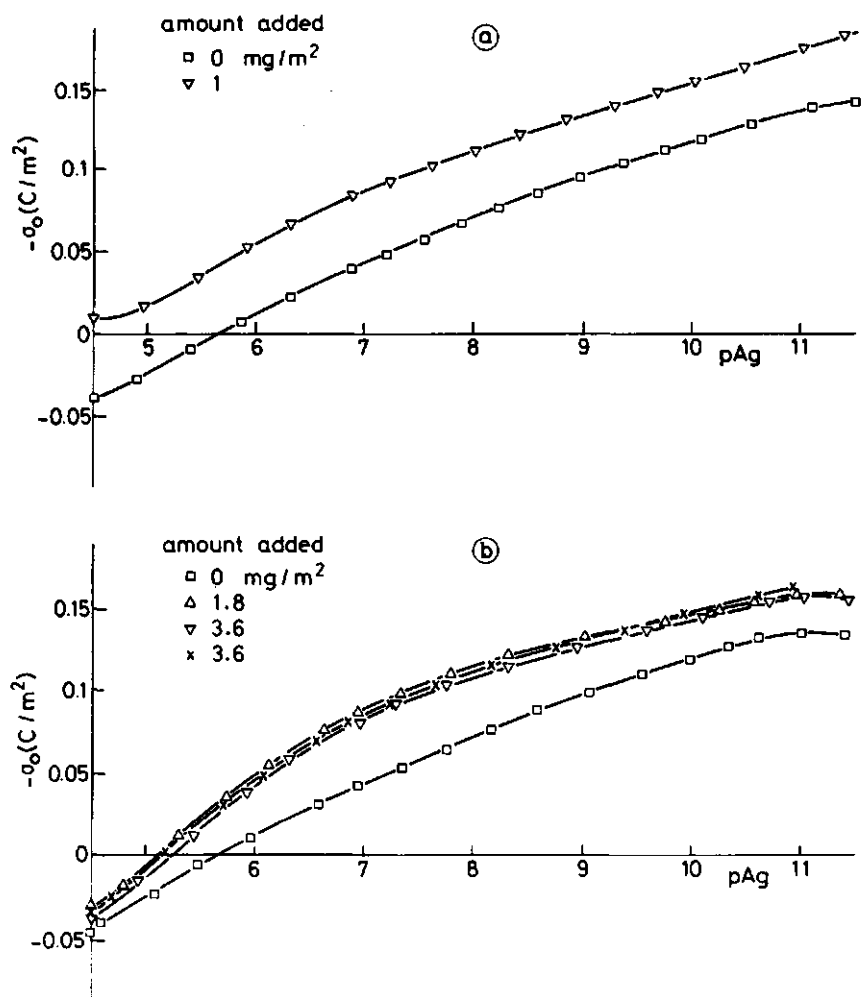


Figure 5.14. Surface charge on AgI particles in the presence of saturation adsorption of poly-DL-lysine of DP = 250 (a), and $\epsilon Acp-Lys_4-NHMe$ (b). pH = 3, T = 293 K, electrolyte 10^{-1} M KNO_3 .

5.3.4 OLIGO-L-LYSINE AND POLY-L-LYSINE

The AgI-titration curve of ϵ Acp-Lys₄-NHMe (figure 5.14b) is analogous to the one of poly-L-lysine, also showing desorption at a positive surface charge. The maximum deviation from the curve of the blank is also the same for both compounds. This indicates that the Stern layer is covered in the same fashion, *i.e.* again as a loosely packed monolayer. The plateau value of the adsorption isotherm (figure 5.15) for ϵ Acp-Lys₄-NHMe at highly charged AgI ($pI = 6$, $\sigma_0 = -0.15 \text{ C/m}^2$) is 0.42 mg/m^2 at a salt concentration of 0.1 M , corresponding to a loosely packed monolayer coverage. So we can conclude that also for oligomers at high salt concentrations nearly all adsorbed material is accommodated in the first layer. The octa- and hexadecamers, having plateau values of about 0.54 mg/m^2 , show an intermediate behaviour. The shapes of the adsorption isotherms of the oligomers are of the high affinity type like those of the polymers under these conditions.

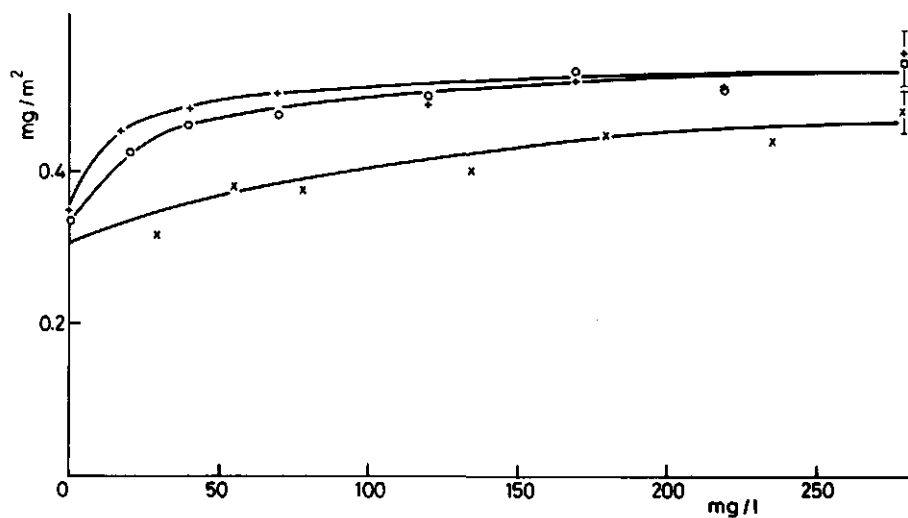


Figure 5.15. Adsorption isotherms for oligo-L-lysines on AgI. ϵ Acp-Lys_n-NHMe: x, $n = 4$; o, $n = 8$; +, $n = 16$. Electrolyte 0.1 M HNO_3 ; $\sigma_0 = -0.15 \text{ C/m}^2$. Accuracy as indicated.

For the very short oligomers we could not measure adsorption isotherms, because these compounds do not form stable enough complexes with poly(vinyl sulphonate). Another concentration determination method, via the UV-absorption of the peptide bond is not accurate enough to establish small adsorbed amounts in the presence of high bulk concentrations. As these oligomers are so short, the tendency to adsorb is low and high concentrations are needed to get adsorption. For these compounds we only can determine that concentration that gives such an adsorbed amount that just compensates the surface charge. This adsorbed amount was estimated by performing the same experiment with poly-L-lysine. Here the charge equivalence takes place at negligibly low polyelectrolyte concentration. Hence, all added adsorbate can be considered as adsorbed. As the double layer experiments do not show differences between the structure of the adsorbed layer of poly-L-lysine and the pentamer, the same adsorbed amount at the equivalence point is assumed for the short oligomers as is found for poly-L-lysine. The results are compiled in table 5-3.

Table 5-3. Adsorption data at the charge equivalence point for oligo- and poly-L-lysine.

compound n	ϵ Acp-Lys _n -NHMe			poly-L-lysine DP = 300
	0	1	2	
concentration of adsorbate solution (mg/l)	4000	168	56	43
amount of adsorbate added (mg)	11.5	0.49	0.089	0.038
amount of adsorbate adsorbed (mg/m ²)	0.1 ^x	0.1 ^x	0.1 ^x	0.1
concentration after adsorption (mg/l)	1100	43	5.6	-

x Data taken from the experiment with poly-L-lysine.

Longer chains show lower bulk concentrations, which cause adsorbed amounts compensating the surface charge. As flat adsorption occurs, nearly all segments of the adsorbed molecules are in contact with

the surface. Thus the non-electrical free energy of adsorption varies linearly with the chain length. Especially with very short chains each added segment gives a considerable contribution to the affinity to the surface.

5.3.4.1 INFLUENCE OF THE ELECTROLYTE CONCENTRATION

Since electrostatic interactions play an important role in the adsorption of poly- and oligo-L-lysines, a considerable influence of the electrolyte concentration is expected. For several lengths of the polymer adsorption data are presented in figure 5.16. For all lengths the adsorption increases with ionic strength. This trend is to be anticipated, because the electrostatic repulsion between segments tends to lower the adsorption and electrolytes

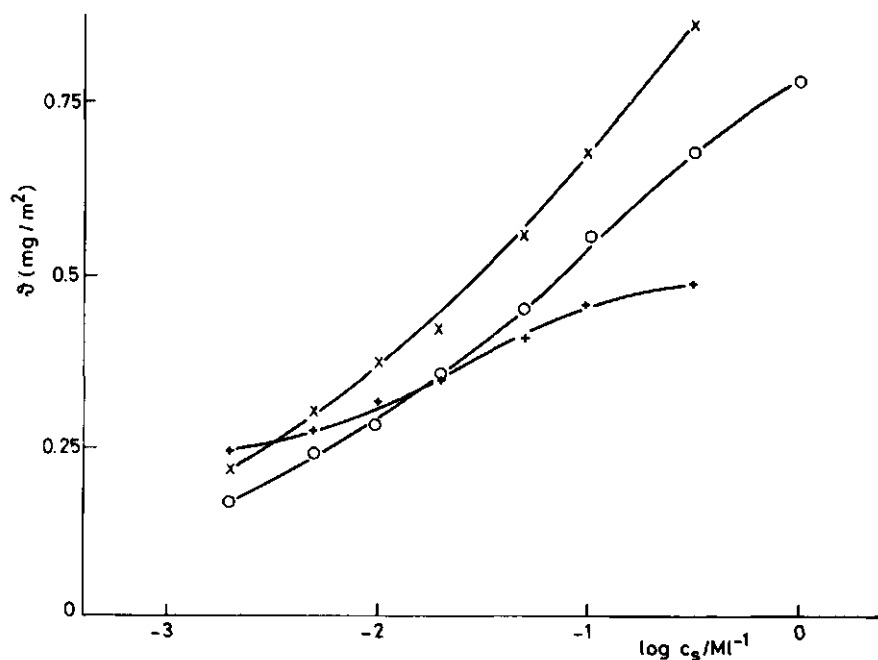


Figure 5.16. Dependence of adsorption of poly- and oligo-L-lysine on AgI on the indifferent electrolyte (HNO_3) concentration (c_s). $\sigma_0 \approx -0.1 \text{ C}/\text{m}^2$; poly-L-lysine: x, DP = 2000; o, DP = 300; $\epsilon\text{Acp-Lys}_{16}\text{-NHMe}$, +.

reduce this repulsion. The isotherms of the two polymeric compounds closely resemble each other. Especially at a high electrolyte concentration the adsorption of the longer polymer is higher. Because of the then occurring strong shielding formation of loops and tails becomes less unfavourable. The adsorption of the oligomer rises less because here no long loops and tails can be formed.

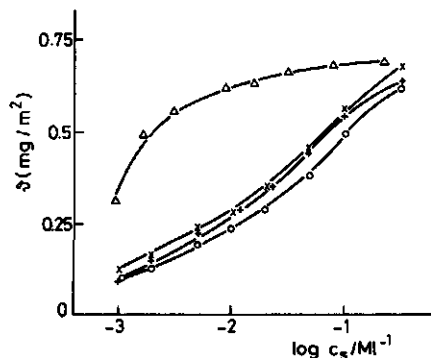


Figure 5.17. Dependence of adsorption of poly-L-lysine on the salt concentration for several electrolytes. x, HNO_3 ; o, $\text{KF} + 10^{-4} \text{ M HNO}_3$; +, $\text{KNO}_3 + 10^{-3} \text{ M HNO}_3$; Δ , H_2SO_4 .
 $\text{DP} = 300$; $\sigma_0 \approx -0.1 \text{ C/m}^2$.

By using different kinds of electrolytes it is possible to see whether the salt effect is a non-specific double layer effect or whether it is due to some specific interaction. Figure 5.17 shows the adsorption of poly-L-lysine in the presence of different electrolytes. Interchanging monovalent ions gives no change in curves within experimental error. Apparently double layer effects can mostly account for the increase in adsorption. However, the divalent ion sulphate leads to substantially higher adsorption, especially at low electrolyte concentrations. Strong interactions between this ion and the

positive ϵ -aminogroup of the lysyl residue are the probable cause of this behaviour.

5.3.4.2 INFLUENCE OF THE SURFACE CHARGE

Since a positive surface charge repels the positive poly-L-lysine and a negative surface attracts the polymer, a dependence of the adsorption on the surface charge is expected. Figure 5.18 gives the dependence of the adsorption on pAg at several electrolyte concentrations. In all cases the adsorption increases with rising pAg. At a low salt concentration there is virtually no adsorption at

positive AgI, because of the strong electrostatic repulsion. At a high electrolyte concentration this repulsion is reduced. Then adsorption also occurs at low pAg.

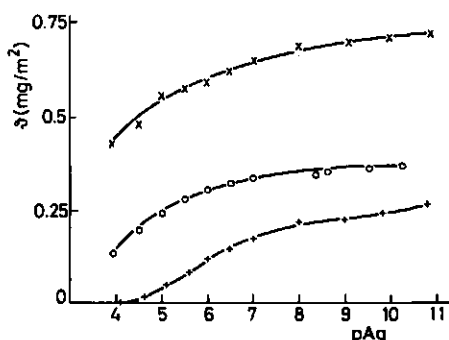


Figure 5.18. Dependence of adsorption of poly-L-lysine (DP = 2000) on pAg. Electrolyte (HNO₃): x, 0.1 M; o, 0.01 M; +, 0.001 M.

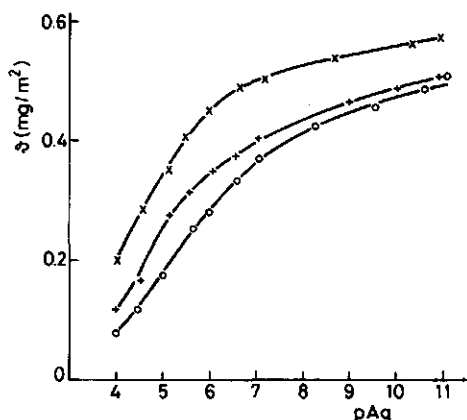


Figure 5.19. Dependence of adsorption of ϵ Acp-Lys₁₆-NHMe on pAg. Electrolyte (HNO₃): x, 0.1 M; +, 0.01 M; o, 5.10^{-4} M.

A similar picture is obtained in the case of the heptadecapeptide (figure 5.19). Here the adsorbed amount at a high surface charge and electrolyte concentration does not much exceed the amount at low ionic strength, since only short loops and tails can form.

To see whether the dependence of the adsorption on the surface charge is reversible, this experiment was also performed by changing the pAg from a high to a low value for the heptadeca- and pentamer (figure 5.20). Both oligomers show hysteresis, the longer one more so than the shorter one. We also measured the time dependence of adsorption and desorption by adding AgNO₃ in one portion to a sample equilibrated at pAg = 12 till pAg = 4. Then the tetra peptide was fully desorbed within one hour. During this period the heptadecapeptide was also desorbed to a large extent. Within one hour the adsorbed amount decreased from 0.48 to 0.06 mg/m². Then the adsorption remained constant within experimental error on a time scale of days. The same desorption experiment was done for poly-L-lysine (figure 5.21).

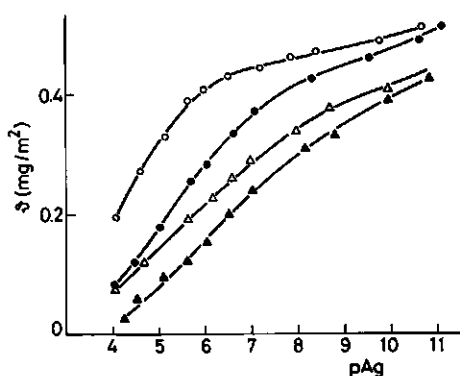


Figure 5.20. Adsorption and desorption of oligo-L-lysines as a function of pAg . Filled symbols: adsorption; open symbols: desorption. $\epsilon Acp-Lys_n-NHMe$: \circ , $n = 16$; Δ , $n = 4$. Electrolyte, 0.001 M HNO_3 .

After a rapid decrease during the first few hours the desorption slowed down, but even after a few days some desorption still occurred. The level of the adsorbed amount was then much higher than that of the heptadecapeptide after the same amount of time. There seems to be no sharp distinction between the behaviour of the poly- and the oligopeptide; rather a gradual transition is observed. These experiments give no conclusive evidence whether equilibrium in desorption experiments for the polypeptide is reached very slowly or whether the adsorption is really irreversible. The gradual

transition in the behaviour of short to long chains is an argument in favour of slow equilibration.

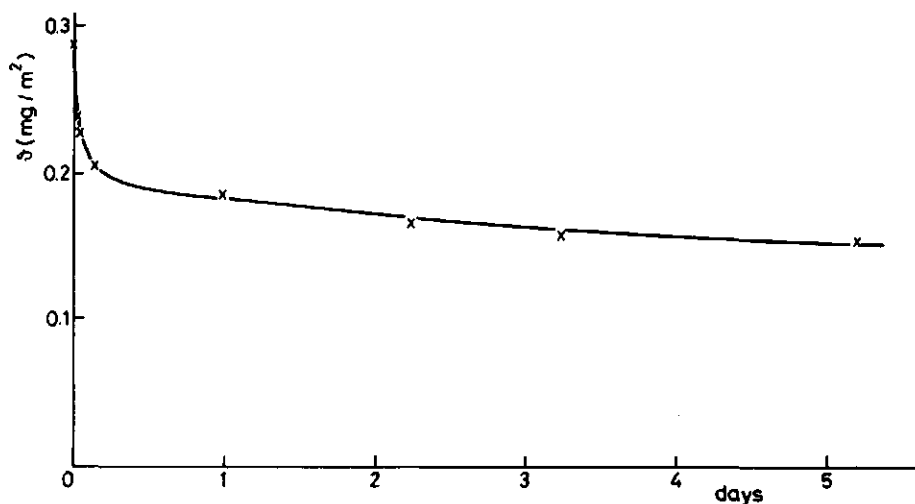


Figure 5.21. Desorption as a function of time of poly-L-lysine (DP = 2000) due to addition of $AgNO_3$. Electrolyte, 0.001 M HNO_3 .

5.4 CONCLUDING REMARKS

In this study double layer experiments prove to be good instruments to obtain insight into adsorption processes. Charge-potential curves appear to be sensitive to changes in the structure of the adsorbed layer. For instance, the helical shape of poly-L-proline adsorbed on AgI could be inferred. Combination of these measurements with other colloid-chemical and/or surface-chemical techniques like electrophoresis, coagulation kinetics and adsorption isotherms yielded a rather complete picture of the adsorption behaviour of oligo- and polylysine which, under the chosen conditions ($\text{pH} < 3$) can be considered models for highly charged polyelectrolytes. These compounds have some features in common with uncharged polymers like the high affinity-type isotherms and the increasing affinity with increasing chain length. The main difference is that, due to the electrostatic repulsion between segments, it is not favourable to form loops and tails like uncharged polymers do. Hence adsorbed amounts do not greatly exceed that of a monolayer. As a consequence adsorption of this polyelectrolyte will not lead to steric stabilisation.

5.5 REFERENCES

- 1 L.K. Koopal and J. Lyklema, Faraday Discuss. Chem. Soc. 59, 230 (1975).
- 2 J. Lyklema, Pure Appl. Chem. 46, 149 (1976).
- 3 J.N. de Wit, Thesis, Agricultural University, Wageningen (1975)
- 4 L.K. Koopal, Thesis, Agricultural University, Wageningen (1978)
- 5 A. de Keizer, Thesis, Agricultural University, Wageningen (1981)
- 6 H.J. van den Hul, Thesis, State University, Utrecht (1966).
- 7 G.J. Fleer, Thesis, Agricultural University, Wageningen (1971).
- 8 B.H. Bijsterbosch and J. Lyklema, Advan. Colloid Interface Sci. 147 (1978).
- 9 A.A. Randall, J. Chem. Soc. 374 (1962).
- 10 E. von Aix, M. Faupel and M. Brugger, J. Chromatogr. 120, 224 (1976).
- 11 B.H. Bijsterbosch, Thesis, State University, Utrecht (1965).

- 12 H. Reerink and J.Th.G. Overbeek, Discuss. Faraday Soc. 18, 74 (1954).
- 13 H. Terayama, J. Polymer Sci. 8, 243 (1952).
- 14 D. Horn, in "Polymeric Amines and Ammonium Salts" (E.J. Goethals, Ed.), Pergamon Press, Oxford, New York, 1980, p. 333.
- 15 M.A. Cohen Stuart, Thesis, Agricultural University, Wageningen (1978).
- 16 A. de Keizer and J. Lyklema. J. Colloid Interface Sci. 75, 171 (1980).
- 17 P.J. Flory, "Principles of Polymer Chemistry", Ch. XIII, Cornell University Press, Ithaca, New York, 1953.
- 18 J. Applequist and P. Doty, in "Polyaminoacids, Polypeptides and Proteins" (M.A. Stahmann, Ed.), Univ. Wisconsin Press, Madison, 1962, p. 161.

6 COMPARISON BETWEEN EXPERIMENTAL WORK AND THEORETICAL RESULTS

6.1 COMPARISON WITH LITERATURE DATA

It is not yet possible to apply the theory developed in the third chapter to many results published in literature quantitatively, because only few studies deal with polyelectrolyte adsorption in sufficient detail and under sufficiently characterised conditions. Hence, it is impossible to estimate the parameters used in the present theory from those results in a discriminative way. However, some general trends can be dealt with.

One of the most notable features of our theory is the independence of the adsorption of the molecular weight. This is at variance with Hesselink's theory¹, which predicts a dependence similar to that of Hoeve's theory. Horn² measured the adsorption of polyethylenimines on polystyrene latex. Neither for the adsorption nor for the electrophoretic mobility he found molecular weight dependence at low pH values, where this polyelectrolyte is highly charged. He concluded that flat adsorption occurs. Williams et al.³ found the same for the adsorption of highly charged poly-(carboxymethyl cellulose) to barium sulphate. At high ionic strength they find a considerable part of the adsorbed material, up to 25%, in loops and tails, where our theory gives only a few percent. As is usually observed for uncharged polymers, the adsorption rises with chain length at pH = 2, when the carboxyl groups are uncharged. Mabire et al.⁴ investigated the adsorption of polyelectrolytes on silica and did not find any molecular weight dependence either. In the studies mentioned above adsorbed amounts do not greatly exceed monolayer coverage. This also backs up our model of flat adsorption. In the case of the adsorption of poly-L-lysine and poly-L-glutamic acid at the mercury electrode surface Pavlovic and Miller⁵ also claim that monolayer adsorption takes place. Flat adsorption can also be inferred from the fact that no steric stabilization has been reported. For example, Böhm⁶ could not stabilize oil/water emul-

sions with highly charged poly(methacrylic acid) and poly(acrylic acid), whereas low charged polymer gave much higher adsorptions and stabilization.

In conclusion we might say that these literature data are in general agreement with our prediction.

6.2 CHOICE OF THE PARAMETERS

In our study we are able to assign values to most of the parameters used, based on model assumptions. So only few parameters are left to be fit to experimental results.

6.2.1 COORDINATION NUMBER OF THE LATTICE

Our model uses a lattice where segments and solvent molecules are each placed on a site. Several lattice types are possible, e.g. a hexagonal or a cubic one. Following Roe⁷ and Scheutjens and Fleer⁸ we chose a hexagonal lattice, where the coordination number is twelve. It has been shown that the results are insensitive to this parameter⁸.

6.2.2 THE AREA OF A LATTICE SITE a_0 AND THE DISTANCE BETWEEN THE LATTICE LAYERS r_0

The parameters used in the polymer adsorption theories of Roe⁷ and Scheutjens⁸ are essentially dimensionless. However, to relate such theories to experimental results and to electric quantities like the unit charge, the system has to be scaled. From the specific volume⁹ of the lysyl group, 0.82 ml/g, and its molecular weight 128, the volume of a lysyl residue is found as 0.17 nm³. Choosing the lattice cell to be isotropic, a_0 is 0.3 nm² and r_0 is 0.55 nm. This leads to a saturated monolayer coverage of 0.67 mg/m² based on lysyl residues.

6.2.3 THE DEGREE OF DISSOCIATION

In studies on the behaviour of polyelectrolytes in solution attention has been paid to a phenomenon called counterion condensation. For an infinite, straight chain in a dilute solution Manning¹⁰ derived that the line charge density never exceeds e/β , where β is the Bjerrum length, defined as

$$\beta = (e^2/\epsilon kT)^{-1/2} \quad (6.1)$$

For aqueous solutions $\beta = 0.71$ nm. Smearing out charges in planes involves the assumption that charges are further away from each other than the segment length. So the role of counterion condensation will be underestimated. As a correction we assigned such an effective value to α , that the line charge on a poly-lysine chain did not exceed e/β . Although the condition of an infinite, straight line charge is contradictory with the flexible polymer concept, especially so in the adsorbed layer, where we have no dilute solution either, we assume this theory approximately applicable. In our system the charges are 0.55 nm apart. Counterion condensation is therefore assumed to occur, to such an extent that the effective line charge density is e/β . The effective α is then 0.78. As is the case with the free small ions, we assume the condensation counterions to fit volumelessly into the lattice.

In the case of the monomer the residues are of course not connected at a distance of 0.55 nm, so here no counterion condensation will occur. Hence, α can be set 1.

6.2.4 THE FLORY-HUGGINS SOLVENT QUALITY PARAMETER

This parameter contains the excess interaction energy originating from direct contacts between solvent and segment. As only direct contacts are involved, the χ -parameter is not suitable to describe long range electrostatic interactions. Hence, only non-electrostatic interactions are included in the χ -parameter. The usual methods to obtain χ (e.g. viscosimetry and osmometry) are based on theories in which electrical interactions are absent. As

the charge on the chains influences the viscosimetric and osmotic behaviour, these methods cannot be applied here. Such kind of experiments cannot be done with uncharged poly-L-lysine at high pH either, because phase separation or precipitation will occur then. From this effect it can be concluded that χ exceeds 0.5, the critical value for infinitely long chains. Although the critical χ -value for oligomers is greater than 0.5, the fact that oligomers show no phase separation at any concentration at pH = 12, indicates that χ will not be very high.

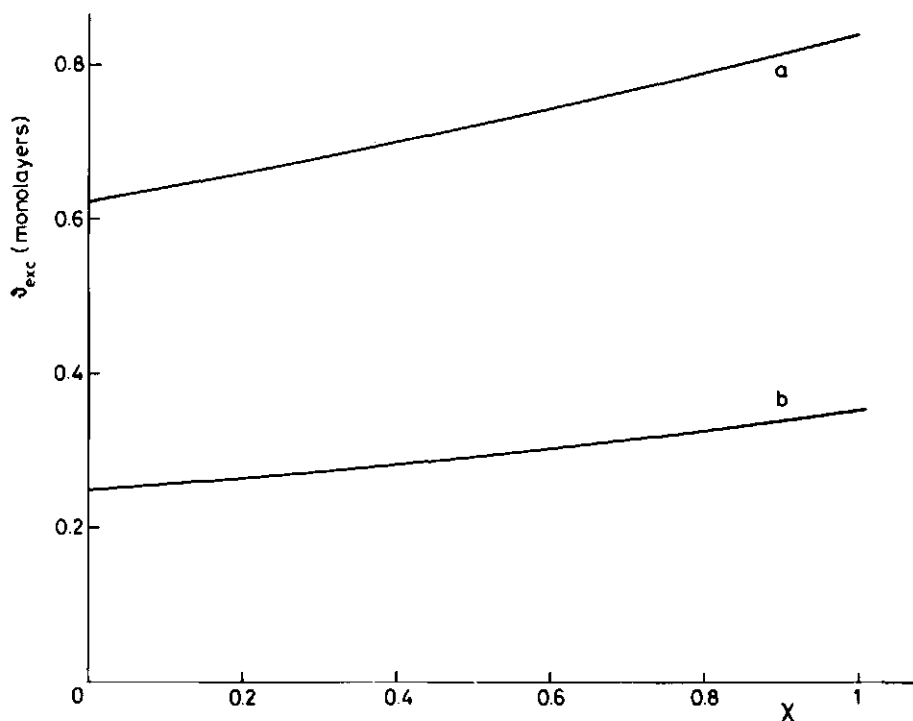


Figure 6.1. Theoretical dependence of the amount adsorbed on the solvent quality parameter χ . a: electrolyte 0.1 M; b: electrolyte 0.01 M. $\chi_s = 4.85$, $\phi_* = 10^{-5}$, $r = 300$, $\alpha = 0.78$, $r_O = 0.55$ nm, uncharged adsorbent.

The theoretical adsorption isotherms are not very sensitive to the value of χ chosen. A typical plot of the χ -dependence is given in figure 6.1. The adsorption varies by not more than 30% over the range of χ from 0 to 1.

For charged polylysine we chose $\chi = 0.6$, slightly exceeding 0.5, assuming that the non-electrostatic interaction energy of the solvent with the polymer is not greatly affected by the field strength due to the charge of the lysyl group.

6.2.5 THE NON-ELECTRICAL FREE ENERGY OF ADSORPTION PARAMETER χ_s

To estimate the value of χ_s we used data obtained from coagulation experiments with the monomer and the short oligomers (see table 5-3). At bulk concentrations where coagulation of the sols takes place, the potential outside the adsorbed layer is very low. We adjusted the χ_s -parameter in such a way, that at the experimentally determined adsorbate concentration the theoretical potential outside the first layer was very low. The concentrations (mg/l) were converted into the volume fractions using the specific volume of poly-L-lysine. Table 6-1 presents the values found for χ_s .

Table 6-1. χ_s values yielding theoretical coagulation conditions for silver iodide sols covered with $\epsilon\text{Acp-Lys}_n\text{-NHMe}$.

n	0	1	2
ϕ_*	9.1×10^{-4}	3.5×10^{-5}	4.6×10^{-6}
χ_s	5.4	4.9	4.2

Throughout our calculations we used the arithmetic average of the values in table 6-1, being 4.85. Cohen Stuart¹¹, who studied the adsorption of poly(vinyl pyrrolidone) on silica from water and dioxane, obtained a value for χ_s also based on studies with small molecules. His χ_s -values are subject to considerable scatter, more than in our case, probably because he used monomeric compounds of more variable structure.

6.3 RESULTS AND DISCUSSION

Some general features of the polyelectrolyte adsorption theory are readily recognized in the adsorption characteristics of polylysine on silver iodide (chapter 5). Most striking are both the independence of the adsorption of the molecular weight for long chains and the flat adsorbed layers with little contribution of loops and tails. Both theory and experiments show isotherms with a very distinct plateau value. A more quantitative comparison will now be given for the adsorption isotherms of the oligomers, the dependence on the electrolyte concentration and on the surface charge.

6.3.1 ADSORPTION ISOTHERMS

Calculated adsorption isotherms and experimental points for oligomers are given in figure 6.2. For oligomers shorter than

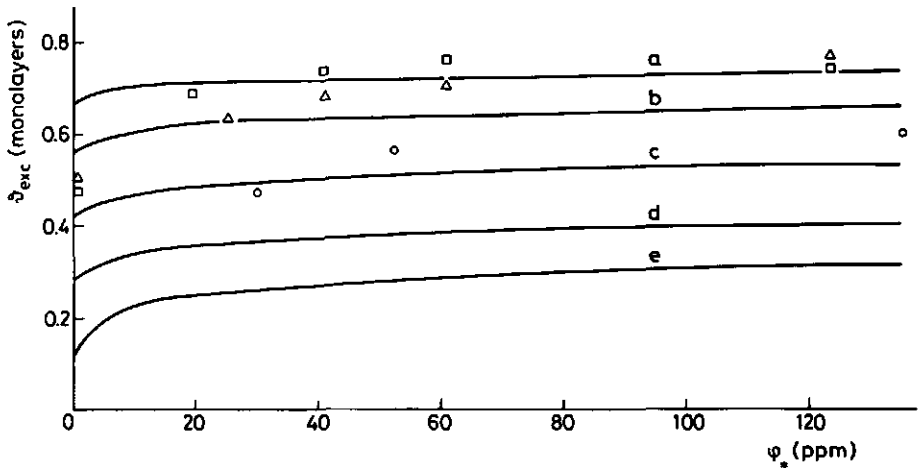


Figure 6.2. Theoretical adsorption isotherms and experimental points. \square , a: $r = 17$; Δ , b: $r = 9$; o , c: $r = 5$; d: $r = 3$; e: $r = 2$. $\chi = 0.6$, $\chi_s = 4.85$, $\alpha = 0.78$, electrolyte 0.1 M HNO_3 , $\sigma_o = -0.22 \text{ e}/a_o$, $r_o = 0.55 \text{ nm}$.

$r = 5$ no experimental isotherms can be measured, because then the concentration determination method fails. Both theory and experiments give high affinity adsorption. The theoretical curves have lower slopes in the plateau region of the isotherm with increasing chain length. This effect is not visible within the experimental error of the measured isotherms. Otherwise, the calculated and measured amounts adsorbed show a very good agreement.

6.3.2 DEPENDENCE ON ELECTROLYTE CONCENTRATION

Since electrical interactions are strongly dependent on the concentration of indifferent electrolyte, the salt concentration is an important variable in the evaluation of the theory. Results are given in figure 6.3. The general trend is similar for theory

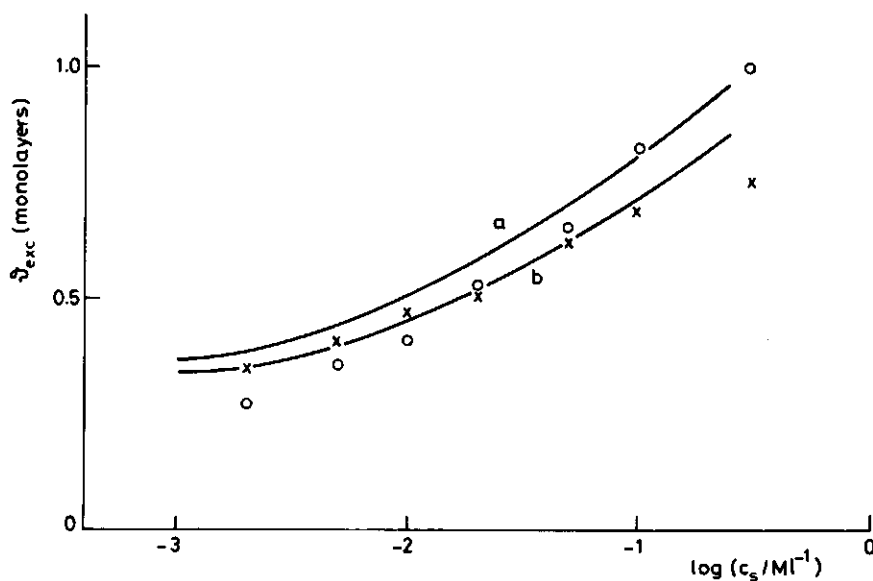


Figure 6.3. Dependence of the amount adsorbed on the indifferent electrolyte (HNO_3) concentration (c_s). Drawn curves: theoretical values: a, $r = 300$; b, $r = 17$. Experimental points: o, $r = 300$; x, $r = 17$. $\chi = 0.6$, $\chi_s = 4.85$, $\phi_* = 10^{-4}$, $\alpha = 0.78$, $\sigma_o = -0.22$ e/ a_o , $r_o = 0.55$ nm.

and experiments. Especially for the oligomer the quantitative agreement is also good. The lower experimental adsorbed amounts of poly-L-lysine at low ionic strength might be attributed to uncertainty in surface charge, which is difficult to control in small samples. The theory predicts a slightly stronger increase of adsorption with rising electrolyte concentration for the polymer than for the oligomer, but in practice this difference is much greater. A reason can be, that at high salt concentrations more loops and tails are formed than is predicted by theory. In chapter 5 we concluded that at 0.1 M electrolyte concentration part of the poly-L-lysine adsorbed is present in loops and tails. The underestimation of the amount adsorbed in the outer layers may be due to the approximation, that charges are smeared out in planes. As a consequence, the potential in each plane is uniform. Actually this is not true. Between two charges the potential is lower than at the place of the charges. Segments brought to the surface in the charging process tend to go to the places with a lower potential, i.e. to those between the charges. So higher adsorbed amounts will be found than calculated. This argument also holds for the first layer, but here the same error is made in the procedure of estimating χ_s . In literature about the use of the Poisson-Boltzmann equation^{12,13} this problem is often described as the difference between the mean potential and the potential of the mean force.

6.3.3 INFLUENCE OF THE SURFACE CHARGE

From the dependence of the adsorption on the pAg (figure 5.18) and the $\sigma_0(\text{pAg})$ curve (figure 5.6) the adsorption of poly-L-lysine as a function of the surface charge can be constructed in the case of 0.1 M electrolyte (figure 6.4). Since we have no $\sigma_0(\text{pAg})$ curves at other salt concentrations, this procedure cannot be applied there.

For bare silver iodide Lijklema¹⁴ showed that $\sigma_0(\text{pAg})$ curves at low electrolyte concentrations can be constructed from the 0.1 M curve and the diffuse double layer capacitance. From the 0.1 M curve the Stern layer capacitance C_s is found by neglecting the diffuse contribution. The diffuse double layer capacitance C_d is obtained from the surface charge by neglecting specific adsorption. The total

capacitance C is then found using

$$C^{-1} = C_s^{-1} + C_d^{-1} \quad (6.2)$$

The σ_0 (pAg) curve is then calculated by integration of the capacitance. Curves obtained in this way coincide with curves measured experimentally.

We devised an analogous method to construct σ_0 (pAg) curves at lower electrolyte concentrations than 0.1 M. However, we cannot assume the absence of specific adsorption, because of the high charge of poly-L-lysine which is present in the Stern layer. We will estimate the diffuse double layer capacitance from electrophoresis experiments. At 10^{-3} M HNO_3 we have electrophoretic mobilities at our disposal (figure 5.4). Using the computer programme of O'Brien and White¹⁵ these mobilities were converted into ζ -potentials. Their programme is based on the work of Wiersema et al.¹⁶ and Overbeek et al.¹⁷, but gives better convergence of the iteration procedure. The diffuse layer potential ψ_d is assumed to be equal to the ζ -potential. This approximation is reasonable, since poly-L-lysine is adsorbed as a flat layer. C_d is then obtained using eq. 6.3 (see, for instance, Bijsterbosch and Lyklema¹⁴):

$$C_d = \epsilon \kappa \cosh(ze\psi_d/2kT) \quad (6.3)$$

Values for ψ_d at 0.01 M electrolyte were estimated by interpolation between the ψ_d -value at 0.001 M and that at 0.1 M. For the latter a low value, $1 \text{ kT}/e$, was chosen arbitrarily. The interpolation was performed assuming ψ_d to vary linearly with $\sqrt{c_s}$, as has been reported before in some cases¹⁸. The value of C_s was assumed to be the same at all salt concentrations and was estimated using the σ_0 (pAg) curve at 0.1 M electrolyte. This curve gives the total capacitance C , which, in 0.1 M electrolyte, is dominated by C_s . The value of C obtained this way was combined with the C_d -value at low potential to give C_s (see eq. 6.2). C_d does not vary strongly with ψ_d at low potential. We used $\psi_d = 1 \text{ kT}/e$ arbitrarily.

Integration of the capacitance gives only relative surface charges. The point of zero charge in the presence of poly-L-lysine shifts to lower pAg as compared with the blank curve, which has

the same point of zero charge at all electrolyte concentrations ($pAg = 5.65$). Therefore we made the $\sigma_0(pAg)$ curves for poly-L-lysine at lower ionic strength cross the axis between the point of zero charge of the 0.1 M curve of covered AgI and that of bare AgI. Figure 6.5 presents the set of curves thus obtained. From these curves and the dependence of the adsorption on the pAg the $\delta(\sigma_0)$ curves for 0.01 and 0.001 M electrolyte in figure 6.4 are derived.

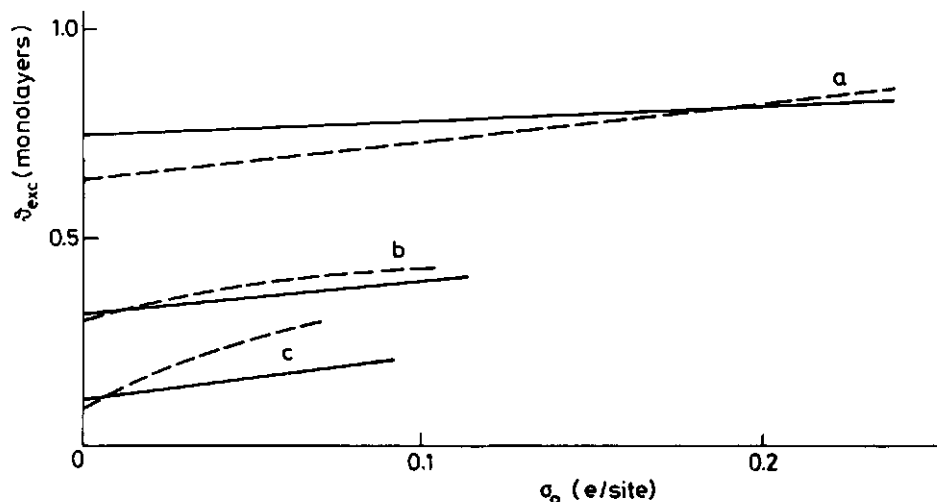


Figure 6.4. Dependence on the surface charge of the amount adsorbed. Electrolyte 0.1 M (a), 0.01 M (b) and 0.001 M. Experimental curves obtained by combining figures 5.18 and 6.5. $\chi = 0.6$, $\chi_s = 4.85$, $\phi_* = 10^{-4}$, $r = 300$, $\alpha = 0.78$, $r_0 = 0.55$ nm.

Qualitatively the same picture emerges from the theoretically and the experimentally obtained curves. Both are nearly linear and the effect of σ_0 is relatively stronger at lower salt concentrations. Quantitatively, the experimentally acquired curves have higher slopes, especially the curve for 0.001 M electrolyte. At lower electrolyte concentrations the experimentally obtained curves are also less linear, but tend to level off at higher surface charges. As can be seen from figure 6.5 the maximum attainable surface charges at low ionic strength are lower than at 0.1 M electrolyte. The quantitative difference is difficult to explain.

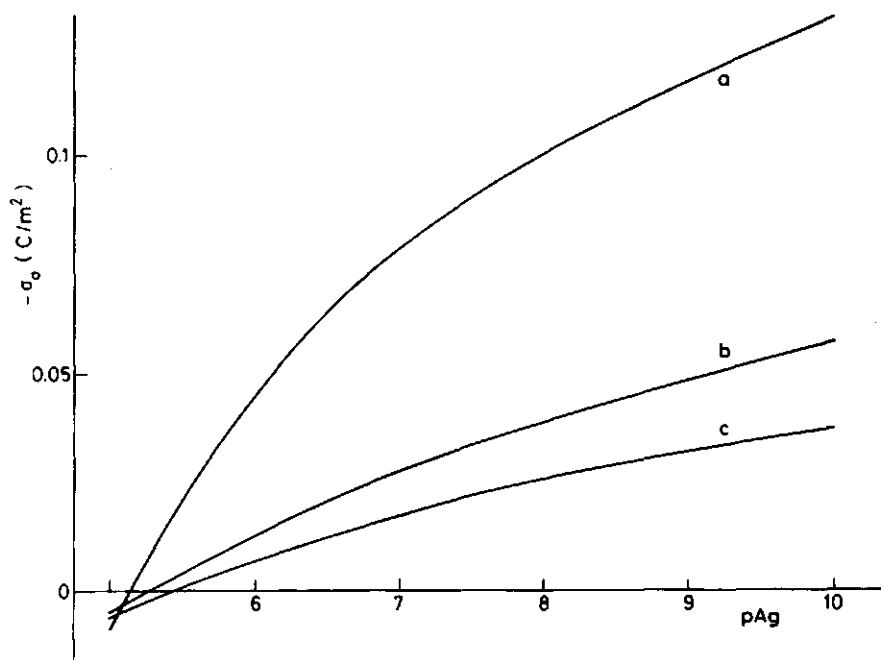


Figure 6.5. Surface charge on silver iodide covered with poly-L-lysine. a: electrolyte 0.1 M (experimental, see figure 5.6); b and c: calculated from a and the diffuse layer capacitance, electrolyte 0.01 M (b) and 0.001 M (c).

However, some problems can be indicated. There is a considerable uncertainty in the constructed $\sigma_0(\text{pAg})$ curves at low ionic strength. As our system is much more complex than the bare silver iodide system¹⁴, it is not sure that the capacity of the Stern layer in our case is the same at all ionic strengths. However, at low electrolyte concentration the total capacity of the double layer is predominantly determined by the diffuse double layer capacitance.

In the present theory only electrostatic changes due to variation of the surface charge are accounted for. From several investigations^{19,20} it has been concluded that surface properties, like the hydration state, specific adsorption and the local dielectric permittivity, vary with the surface charge. The influence of these changes on the adsorption is difficult to unravel.

6.4 CONCLUDING REMARKS AND SUGGESTIONS FOR FURTHER INVESTIGATIONS

Generally good agreement is found between theoretical and experimental results for the adsorption of oligomers and polymers of lysine. This is gratifying, considering that virtually a combination of two new types of theories had to be tested simultaneously. Theories of uncharged polymer adsorption, which are applicable to oligomers, i.e. the Roe and Scheutjens-Fleer theory, had not yet been subjected to experimental tests in the oligomer range. Incorporating electrostatic interactions in these theories, we cannot discriminate, whether differences between theoretical and experimental results stem from the polymer theory part or from the electrostatic part. If there is good accordance between theory and practice, it must always be realized that errors in the two parts of the theory might compensate each other.

Two rather serious approximations work in the same direction. First, both theoretical parts invoke a smearing-out in each layer, the so-called mean field or Bragg-Williams approximation, which tends to overestimate the non-conformational free energy. For the electrostatic part this will be a more serious approximation than for the polymer part, because the potential shows much stronger variation within each layer than the solvent quality does. Second, the flexibility of the polymer chain is overestimated in the polymer adsorption theories, because backfolding is allowed. This is a relatively poorer approximation in the polyelectrolyte case, since it is well known, that polymer chains become much stiffer when they are charged²¹. We expect, that chain stiffness effects will especially be reflected in the behaviour of loops and tails. Since these are hardly present, we presume that in this respect the present treatment is satisfactory.

Another approximation in the non-electrostatic part of the theory is the assumption of equal size for both polymer segments and solvent molecules. A first start to solve this "bulkiness" problem has been made by Cohen Stuart¹¹. Difficulties arise especially in counting lattice-cell contacts. Because of the strong influence of electrostatic effects in our case, we assume this approximation to be rather unimportant here.

The influence of other approximations in the electrostatic part

of the theory is difficult to assess. The presence of highly charged matter very near to the surface changes the dielectric constant in that region. Specifically, adsorption of organic matter and high field strengths lower the dielectric constant. This lowering leads to higher potentials due to surface charge and adsorbed polyelectrolyte. Thus, if the dependence of the dielectric constant on ϕ is neglected, the adsorbed amount tends to be overestimated. This effect is partly compensated by the lowering of the effective degree of dissociation. A lower dielectric constant increases the counterion condensation and thus diminishes the build-up of high potentials.

Assuming the small ions to be point charges we will obtain too low potentials, because we overestimate their screening, especially in the layers very near to the surface, where the potentials are high. The neglect of the volume excluded by the polymer segments for the small ions works in the same direction. As in reality the small ions cannot enter into the volume occupied by the polymer segments, less volume is available for the electrolyte to perform its shielding action than we assume. However, model calculations of Brooks²² show that this assumption only leads to minor modification of the potential distribution.

We can conclude that there is a satisfying concordance between theory and experiment, although we must bear in mind that some serious approximations have been made and that also some experimental uncertainty exists.

Some theoretical improvements are rather easy to perform. As we have a numerical procedure at our disposal to integrate the Poisson-Boltzmann equation, modifications that only involve this equation can be incorporated readily. Such extensions are the dependence of the dielectric constant on the field strength and polymer volume fraction, the dependence of the degree of dissociation of the polyelectrolyte on the potential and polymer volume fraction, and the volume excluded for the small ions by the polymer and electrolyte.

More complex are modifications that take into account the chain stiffness and no longer accept the smearing out charges in layers parallel to the surface. In the polyelectrolyte case these approxi-

mations have a higher weight than with uncharged polymers. Ash et al.²³ worked out a polymer adsorption theory, that forbids backfolding of the chains. Their formalism can be extended to more chain stiffness than just forbidding backfolding. However, because of computational problems they could not handle chains longer than tetramers. These problems will increase, if more chain stiffness is accounted for.

The problems to evaluate the potential distribution in a polymer solvent lattice without applying the Bragg-Williams approximation are very great. Segments to be placed in a layer will preferably go to a place between two segments already in that layer. There they will feel a lower than averaged potential. A possible improvement of our theory might be the evaluation of the potential just between two segments, after distributing the segments equidistantly in each layer.

As specific adsorption of small ions and the surface charge depend on the adsorption of polyelectrolyte and confuse a clear picture, interesting experiments can be performed using an uncharged surface. When the theory is extended with a variable degree of dissociation, the dependence of the adsorption of poly-L-lysine on the pH must be correctly predicted. Silver iodide is not a suitable adsorbent for such studies, since chemical interactions seem to occur between the surface and uncharged amino groups. A possible suitable adsorbent might be a suspension of poly(methylene oxide) crystals, which have well-defined crystal plane surfaces bearing no charge. At high pH (~ 12) the synthesized oligomers are uncharged and can be used to test the theories of Roe and of Scheutjens and Fleer for uncharged polymers. Polylysine cannot be used at high pH, since precipitation (poly-L-lysine) or phase separation occurs (poly-DL-lysine). The pH and indifferent electrolyte concentration dependence of the phase separation of poly-DL-lysine might be used to test the theoretical work on this phenomenon in chapter

6.5 REFERENCES

- 1 F.Th. Hesselink, J. Colloid Interface Sci. 60, 448 (1977).
- 2 D. Horn, in "Polymeric Amines and Ammonium Salts" (E.J. Goet-

- hals, Ed.). Pergamon Press, Oxford, New York, 1980, p. 333.
- 3 P.A. Willems, R. Harrop, G.O. Phillips, L.D. Robb and G. Pass, in "The Effect of Polymers on Dispersion Properties" (T.F. Tadros, Ed.), Academic Press, London, 1982.
 - 4 F. Mabire et al., personal communication, Strasbourg (1981).
 - 5 O. Pavlovic and I.R. Miller, J. Polymer Sci. C 34, 181 (1971).
 - 6 J.Th.C. Böhm, Thesis, Agricultural University, Wageningen (1974).
 - 7 R.-J. Roe, J. Chem. Phys. 60, 4192 (1974).
 - 8 J.M.H.M. Scheutjens and G.J. Fleer, J. Phys. Chem. 83, 1619 (1979).
 - 9 J. Applegquist and P. Doty, in "Polyaminoacids, Polypeptides and Proteins" (M.A. Stahmann, Ed.), Univ. Wisconsin Press, Madison, 1962, p. 161.
 - 10 G.S. Manning, Quarterly Reviews of Biophysics 11, 179 (1978).
 - 11 M.A. Cohen Stuart, Thesis, Agricultural University, Wageningen (1980).
 - 12 J.Th.G. Overbeek, in "Colloid Science" (H.R. Kruyt, Ed.), Elsevier, Amsterdam, 1952, p. 129.
 - 13 D.A. McQuarrie, "Statistical Mechanics", Ch. XIII, Harper and Row, New York, London, 1976.
 - 14 J. Lijklema, Thesis, State University, Utrecht (1957).
 - 15 R.W. O'Brien and L.R. White, J. Chem. Soc Faraday II 74, 1607 (1978).
 - 16 P.H. Wiersema, A.L. Loeb and J.Th.G. Overbeek, J. Colloid Interface Sci. 22, 78 (1966).
 - 17 J.Th.G. Overbeek and P.H. Wiersema, in "Electrophoresis", Vol. II (M. Bier, Ed.), Academic Press, New York, London, 1966, p. 1.
 - 18 J. Lyklema, private communication.
 - 19 B.H. Bijsterbosch and J. Lyklema, Advan. Colloid Interface Sci. 9, 147 (1978).
 - 20 A. de Keizer and J. Lyklema, Can. J. Chem. 59, 1969 (1981).
 - 21 T. Odijk and A.C. Houwaart, J. Polymer Sci. Polymer Physics Ed. 16, 627 (1978).
 - 22 D.E. Brooks, J. Colloid Interface Sci. 43, 687 (1973).
 - 23 S.G. Ash, D.H. Everett and G.H. Findenegg, Trans. Faraday Soc. 66, 708 (1970).

LIST OF SYMBOLS

a_o	Area of lattice site
a_r, a_c	Affinity parameter of component with chain length r or number c , respectively
b	Integration constant (eq. 3.7)
C_1, C_2	Numerical constants
c_s	Indifferent electrolyte concentration (mole/l)
c	Component number
E	Field strength
e	Elementary charge
F	Faraday constant
$f(r), f_c$	Fraction of polymer with chain length r or component number c , respectively
Δf_{exch}	Free energy of exchanging a chain of r_1 segments for one of r_2 segments
ΔF_M	Free energy of mixing
$\Delta F_{M,el}$	Electrical part of the free energy of mixing
Δf_{el}	Electrical part of the free energy of mixing per lattice site
ΔF_{el}	Electrical free energy
i, j	Layer number
k	Boltzmann constant
M	Number of lattice layers, Volume to surface ratio expressed in number of monolayers
N_o, N_1	Number of solvent and polymer molecules respectively
\bar{n}_+, \bar{n}_-	Positive and negative ion concentration at the reference potential (number/m ³)
\bar{n}_o	Indifferent electrolyte concentration at the reference potential (number/m ³)
$n_+(x), n_-(x)$	Local concentration of positive and negative ions, respectively
P	Integral defined by eq. 2.28
P_c	Chain probability of component c
p_c	Probability to find component c in the adsorbed layer
P_*	Probability to find a component in the bulk solution

p	Fraction of segments of adsorbed molecules attached to the surface
p_r	Idem, for component with chain length r
q	Numerical constant (eq. 2.26 and 2.31)
R	Gas constant
r	Chain length
r_n, r_w	Number and weight averaged chain length, respectively
r_b	Critical chain length beyond which all polymer is adsorbed
r_{eq}	Chain length at which equal amounts of the component are adsorbed and in solution
s	Numerical constant (eq. 2.26 and 2.31)
T	Absolute temperature
v_o	Lattice site volume
x	Distance
z	Valency of polyelectrolyte
z_i	Valency of small ion i
α	Degree of dissociation
β	Bjerrum length
Γ_r	Adsorbed amount in mole/area of component with chain length r
$\Gamma^{(0)}, \Gamma^{(s)}$	Idem with respect to solvent and adsorbent, respectively
δ_u, δ_c	Thickness of bare and adsorbate covered Stern layer, respectively
$\epsilon, \epsilon_u, \epsilon_c$	Dielectric permittivity of diffuse double layer and of Stern layer without and with adsorbate, respectively
ζ	ζ -potential, i.e. the potential at the slipping plane
δ	Amount adsorbed, expressed in equivalent monolayers or mg/m^2
δ_{exc}	Idem, excess
δ_r	Idem of component with chain length r
δ_{sys}	Total amount of polymer present in the system expressed in equivalent monolayers
$\delta_{sys,r}, \delta_{sys,c}$	Idem of component with chain length r or number c , respectively
κ	Reciprocal double layer shielding length

λ	Charging parameter
λ_0, λ_1	Fraction of lattice contacts in the same and the neighbouring lattice layer, respectively
μ	Dipole moment, chemical potential
μ_0, μ_1	Chemical potential of the solvent and the polymer, respectively
$\mu_{0,el}, \mu_{1,el}$	Electrical part of the chemical potential of the solvent and the polymer, respectively
Ξ	Grand canonical partition function
ξ	Electrical part of the effective solvent quality
π	Surface pressure
ρ_i, ρ_*	Polyelectrolyte space charge density in layer i and in the homogeneous bulk solution, respectively
σ_0	Surface charge density
σ_i, σ_*	Plane charge density of layer i and of bulk solution layers, respectively
ϕ_i, ϕ_*	Polymer volume fraction of layer i and of the bulk solution, respectively
$\phi_{*,c}, \phi_{*,r}$	Bulk volume fraction of component c and of component with chain length r , respectively
ϕ_*^0	Solvent bulk volume fraction
$\phi_{*,cr}$	Critical bulk volume fraction
$\phi_{*,cr}^{(DH)}$	Idem, for the Debye-Hückel approximation
χ	Flory-Huggins solvent quality parameter
χ_{cr}	Idem, critical
χ_s	Non-conformational free energy of adsorption parameter
$\chi_{s,eff}$	Idem, effective
$\chi_{s,c}$	Idem, of component c
χ_u, χ_c	Potential difference due to oriented dipoles at a bare and an adsorbate covered surface, respectively
χ_u^0, χ_c^0	Idem, at the point of zero charge
$\psi(x), \psi(x, \lambda)$	Potential as a function of distance and of distance and charging parameter, respectively
ψ_i, ψ_*	Potential at the lattice centre of layer i and of a bulk solution layer, respectively
$\bar{\psi}_+, \bar{\psi}_-$	Potential where the positive and negative ions are at their stoichiometric concentration, respectively

A superscript plus sign indicates a reference state.

SUMMARY

The purpose of this study is the description of the behaviour of a model polyelectrolyte near a model interface.

Chapter 1 gives a general background and the outline of the investigations.

The chapters 2 and 3 comprise the theoretical parts. Chapter 2 considers the applicability of equilibrium thermodynamics to polymer adsorption, an important prerequisite. We focus our attention on the applicability of Gibbs' law to polymer adsorption. In many cases results from surface tension measurements do not obey the classically formulated Gibbs' law, which is based on equilibrium thermodynamics. Thus, the use of equilibrium thermodynamics was questioned. We show that it is important to take the hetero-dispersity of the polymers used in adsorption studies into account when Gibbs' law is applied. Although not all problems could be solved completely, this result encourages the use of equilibrium thermodynamics in the polyelectrolyte adsorption theory.

Chapter 3 describes the polyelectrolyte adsorption theory. Expressions are derived for the potential distribution in and the free energy of a double layer containing polyelectrolyte charge. In the case of the Debye-Hückel approximation of the Poisson-Boltzmann equation analytical expressions are obtained. When the full Poisson-Boltzmann equation is used, we have to rely on numerical procedures. The electrostatic interactions are incorporated in the phase equilibria theory of Flory and the Roe theory and the Scheutjens-Fleer theory of polymer adsorption. Electrostatic interactions strongly influence the conformation of the adsorbed polyelectrolyte. Because of the mutual repulsion of the charged segments the formation of loops and tails is strongly suppressed. Thus very flat adsorbed layers are predicted. For uncharged polymers the increase of the adsorption with chain length and polymer concentration mainly takes place in the loops and tails. As for polyelectrolytes, these are all but absent, their adsorption is nearly chain length-independent and the plateau value of the adsorption isotherms is much more constant than with uncharged polymers. Polyelectrolyte solutions are resilient against

phase separation in much poorer solvents than uncharged polymers, depending on chain charge density and indifferent electrolyte concentration.

The chapters 4 and 5 make up the experimental part. As the polyelectrolyte adsorption theory does not only apply to long polymer chains, but also to the adsorption of oligomers, it is important to test the theory for short chains, too.

Chapter 4 describes the synthesis of these oligomers. Repeated coupling of chains of equal length yields a series of two, four, eight, sixteen and thirty-two segments long. For this kind of coupling reactions peptides are suitable compounds, since standard methods of synthesis have been developed for the benefit of protein research. Using only one type of amino acid, L-lysine, we obtained poly-L-lysine type oligomers.

Chapter 5 presents characteristics for the adsorption of the model-polyelectrolyte poly-L-lysine on the model-colloid silver iodide. Several colloid chemical techniques can be applied to investigate this system both in the absence and in the presence of poly-L-lysine. We investigated adsorption isotherms, charge-potential curves, coagulation kinetics and electrophoretic mobilities. From the results the following picture of polyelectrolyte adsorption emerges:

- (i) At low ionic strength only a thin layer of adsorbed polyelectrolyte is formed.
- (ii) Under these conditions the adsorption is chain length independent, provided the chains are not too short.
- (iii) Because of the shielding of indifferent electrolyte some loops and tails are formed at high salt concentrations.
- (iv) Oligomer adsorption increases with chain length.

This picture is in agreement with the theoretical predictions of chapter 3.

Chapter 6 gives a quantitative comparison of the experimental and theoretical data. The quantitative agreement between theory and experiment is also satisfactory. This chapter also gives some suggestions for further improvement of the theory and for additional experimental tests.

SAMENVATTING

Het in dit proefschrift beschreven onderzoek heeft ten doel de adsorptie van een model polyelektroliet aan een model vaste stof oppervlak te beschrijven.

Polyelektrolieten zijn lange ketens bestaande uit eenheden die of aan elkaar gelijk zijn of van elkaar kunnen verschillen. Deze segmenten kunnen een elektrische lading hebben. De polyelektroliet ketens kunnen aan tal van oppervlakken adsorberen. De reden hiervan is, dat, ook al is de bindingsenergie van ieder segment met het oppervlak gering, de som van de bindingsenergieën van vele segmenten tegelijk een sterke aantrekking van de polyelektrolietketen tot het oppervlak tot gevolg heeft.

Adsorptie van polyelektrolieten speelt een belangrijke rol in de natuur en de technologie. Zo verhindert de geladen polymere suiker heparine, dat bloedcellen aan vaatwanden vasthechten en daarom heeft het een antithrombogene werking. Polyelektroliet wordt bij de zuivering van afvalwater gebruikt om zwevend slib te binden, zodat het beter bezinkt.

In de literatuur is tot nu toe veel meer aandacht geschonken aan de adsorptie van ongeladen polymeren dan aan die van polyelektrolieten. Een bevredigende theoretische beschrijving van de adsorptie van de laatste was tot nu toe niet voorhanden. In dit proefschrift wordt eerst de polyelektrolietadsorptie theoretisch beschreven. De theoretisch verkregen resultaten worden vergeleken met eigen experimenteel werk.

Hoofdstuk 2 en 3 vormen het theoretisch gedeelte. Hoofdstuk 2 gaat over de vraag of polymeer- en dus ook polyelektrolietadsorptie wel met thermodynamische modellen beschreven kan worden. Deze vraag is opgekomen, doordat een aantal experimentele resultaten, zoals die van oppervlaktespanningsmetingen, niet aan het theoretische beeld voldoet. Hoewel nog niet op alle problemen een afdoend antwoord is gevonden, blijkt het van belang te zijn dat er rekening mee wordt gehouden dat in de praktijk polymeren mengsels zijn waarin niet alle ketens even lang zijn. Als dit wordt gedaan blijkt toepassing van evenwichtsthermodynamica verantwoord.

Hoofdstuk 3 beschrijft de polyelektrolietadsorptie. Adsorptietheorieën voor ongeladen polymeren worden uitgebreid met elektrische

wisselwerkingen. De adsorptie van ongeladen polymeren kan goed beschreven worden met het trein-lus-staart model: sommige gedeelten van een geadsorbeerde keten bevinden zich vastgehecht aan het oppervlak--de treinen--en andere gedeelten tussen twee treinen--de lussen--, terwijl de uiteinden staarten kunnen vormen die in de oplossing uitsteken. De elektrische wisselwerkingen wijzigen dit beeld. De onderlinge afstoting tussen de ladingen op de segmenten maakt, dat de lus- en staartposities ongunstiger worden dan de treinposities, waar de onderlinge afstoting wordt gecompenseerd door de aantrekking van het oppervlak. Dit heeft tot gevolg, dat bij polyelektrolietadsorptie de geadsorbeerde hoeveelheid zelden meer bedraagt dan een enkele laag segmenten, terwijl bij ongeladen polymeren vaak meer dan één laag wordt gevonden. Deze onderlinge afstoting van segmenten van de polyelektrolietmoleculen kan zo sterk zijn, dat juist buiten de geadsorbeerde laag de polyelektrolietconcentratie veel lager kan zijn dan in de oplossing. Bij ongeladen polymeren neemt de geadsorbeerde hoeveelheid toe met de ketenlengte, omdat langere lussen en staarten kunnen worden gevormd. Bij polyelektrolieten is dit niet mogelijk, zodat de adsorptie bijna onafhankelijk van de ketenlengte is.

Hoofdstuk 4 en 5 vormen het experimentele gedeelte. Omdat de polyelektrolietadsorptietheorie niet alleen van toepassing is op lange polymeren, maar ook op die van korte ketens,--de zogenaamde oligomeren--, is het van belang ook voor oligomeren de theorie te testen. Hoofdstuk 4 beschrijft de bereiding van deze korte ketens. Dit gebeurt door het herhaaldelijk aan elkaar koppelen van ketens van gelijke lengte. Zo ontstaat een reeks van twee, vier, acht, zestien en tweeëndertig segmenten lang.

In hoofdstuk 5 worden de adsorptieexperimenten beschreven. Als model polyelektroliet is poly-L-lysine gebruikt, als model oppervlak dat van zilveriodide. De eigenschappen van deeltjes zilveriodide kunnen met verschillende methoden worden onderzocht. Uit de resultaten ontstaat het volgende beeld van de polyelektrolietadsorptie:

- i) Bij een lage zoutconcentratie wordt slechts een dunne laag geadsorbeerd polyelektroliet gevormd.
- ii) Onder deze omstandigheden is de adsorptie onafhankelijk van ketenlengte bij niet te korte ketens.

- iii) Omdat zout de ladingen van de ketens afschermt, worden bij hoge zoutconcentraties wel enige lussen en staarten gevormd en neemt de geadsorbeerde hoeveelheid dus toe.
- iv) Bij de oligomeren neemt de adsorptie altijd toe met de ketenlengte.

Dit beeld is in overeenstemming met de theoretische resultaten beschreven in hoofdstuk 3.

Hoofdstuk 6 geeft een kwantitatieve vergelijking van de experimenteel verkregen resultaten met de theoretisch berekende. Ook kwantitatief is de overeenkomst tussen theorie en experiment goed. In dit hoofdstuk staan ook suggesties voor verdere vervolmaking van de theorie en voor experimenten die nog scherpere test voor de theorie zijn.

CURRICULUM VITAE

Op 21 mei 1953 ben ik geboren te Utrecht. Daar behaalde ik in 1971 het diploma Gymnasium β aan het F.H. de Bruijne Lyceum. Aan de Rijksuniversiteit Utrecht begon ik aan de studie Scheikunde. Hierin legde ik in 1974 met lof het kandidaatsexamen S_3 af. De doctoraalstudie omvatte Analytische Chemie als hoofdvak, met massaspectrometrie als specialisatie en waterzuivering aan de Landbouwhogeschool Wageningen als bijvak. Na in 1976 met lof afgestudeerd te zijn, volgde ik de cursus didactiek en behaalde ik mijn onderwijsaantekening en het diploma MO-A Natuur- en Scheikunde.

In dienst van de organisatie voor Zuiver Wetenschappelijk Onderzoek was ik werkzaam bij de vakgroep Fysische en Kolloïdchemie van de Landbouwhogeschool te Wageningen. Daarna ben ik gedurende een half jaar part-time aan dezelfde vakgroep verbonden geweest in dienst van de Landbouwhogeschool.

Sinds 1982 ben ik werkzaam bij de Keuringsdienst van Waren te Zutphen.